2017

Bracing of Pectus Carinatum: A Quantitative Analysis

Bugajski, Tomasz

UNIVERSITY OF CALGARY

Bracing of Pectus Carinatum: A Quantitative Analysis

by

Tomasz Bugajski

A THESIS

SUBMITTED TO THE FACULTY OF GRADUATE STUDIES

IN PARTIAL FULFILMENT OF THE REQUIREMENTS FOR THE

DEGREE OF MASTER OF SCIENCE

GRADUATE PROGRAM IN BIOMEDICAL ENGINEERING

CALGARY, ALBERTA

JUNE, 2017

Abstract

Pectus Carinatum (PC) presents as an overgrowth of costal cartilages resulting in a sternal protrusion. Treatment of PC is performed with a pectus carinatum orthosis (PCO) that compresses the protrusion. Injuries may arise when this PCO is over-tightened. For the first time, a force measurement system (FMS) was constructed that measured PCO forces. The purpose of this study was to determine if participants could accurately attain their clinically prescribed force (CF) over time, and if the protrusion stiffness (PS) influences the participant-applied forces (PF) and correction rate (CR). Results demonstrated that most PFs (75%) exceeded their associated CF (0.46-5.01 lbs). Further investigation is required to determine clinical significance. PS had a positive relationship with PF, but no relationship with CR. Future studies focusing on improved displacement measurements would enhance the ability to quantify PS. Developing a FMS to provide real-time feedback should also be considered to improve PCO efficacy.

Preface

This study was approved by the Conjoint Health Research Ethics Board (Ethics ID: REB14-1759).

Parts of this thesis have been previously presented the following proceeding:

Bugajski, T., Murari, K., Lopushinsky, S., Schneider, M., Ronsky, J. Dynamic Bracing of Pectus Carinatum: A Pilot Study. *Annual Alberta Biomedical Engineering Conference*. Banff, Alberta, Canada, 2016 (Poster Presentation).

Acknowledgements

I would like to thank the following individuals for their crucial role and assistance in this thesis:

Dr. Janet Ronsky for being an amazing and supportive supervisor. Your confidence in me gave me the drive required to push forward through every obstacle. The seemingly endless amount of knowledge you contain - both academically and through experience - motivates me to keep learning and pursue difficult challenges.

Dr. Kartikeya Murari for his incredible work in the development of a system to measure our outcome variables. Your mentorship with circuitry and sensors was beyond helpful, and I could not have asked for a better (and patient) teacher.

Dr. Steven Lopushinsky for your outstanding assistance in organizing this thesis. Your help with recruitment of participants, as well as clarifying clinical applications of this research was invaluable.

Marc Schneider and Nancy Schneider for assisting in participant recruitment, and allowing me to use a treatment room for many months to collect data. More importantly, for operating a remarkable clinic that clearly understands the importance of clinician-researcher communication, allowing for efficient progress throughout the thesis.

Braceworks and MITACS for providing me with funding for the project.

Jacob Reichbart for assistance in the initial proposal stages of my thesis.

Dr. Kent Paulson for helping calibrate the force measurement systems. Only you could make eight hours of calibration a good time, especially since we had to do it twice.

Douglas Kondro for aiding in the development of the force measurement system.

Ion Robu for assisting me with the first force measurement system.

Dr. Tak Fung for helping me with the statistical methods.

My research group for being the most fun, easy going group a graduate student could ask for!

Dedication

I dedicate this thesis to my mother, father, and Alex.

Table of Contents

List of Tables

List of Figures, Illustrations, and Other Graphics

List of Symbols, Abbreviations, and Nomenclature

Symbol	Definition
3D	Three Dimensional
A1	Adapter 1
A2	Adapter 2
AP	Anterior-Posterior
BM	Body to manubrium ratio
BXM	Body + xiphoid process to manubrium ratio
CF	Clinically Prescribed Force
CPR	Cardiopulmonary Resuscitation
CS	Carbon Shell
CT	Computed Tomography
FE	Finite element
FM1	Force Measurement System 1
FM2	Force Measurement System 2
FM3	Force Measurement System 3
GEE	Generalized Estimating Equation
GUI	Graphic User Interface
HI	Haller Index
MTS	Material Testing System
n	Sample size
PC	Pectus Carinatum
PCO	Pectus Carinatum Orthosis
PE	Pectus Excavatum
PF	Participant-Applied Force
PS	Protrusion Stiffness
rANOVA	Repeated Measure Analysis of Variance
SA	Specific Aims
UCS	Unpadded Carbon Shell

Chapter One: Introduction

1.1 Background

Pectus Carinatum (PC) presents as an idiopathic overgrowth of the costal cartilages that results in a protrusion of the sternum (Figure 1-1) (Colozza & Bütter, 2013). It is the second most common chest wall deformity occurring in approximately 1 in every 500 to 1500 children (Cobben, Oostra, & van Dijk, 2014). PC can develop anytime between infancy to teenage years (Fonkalsrud, 2008). It is four times more common in males than females, and can present itself in two forms: chondrogladiolar (appearing on the body of the sternum) and chondromanubrial (appearing on the manubrium of the sternum) (Shamberger & Welch, 1987; Welch & Vos, 1973). Of the two forms, chondrogladiolar appears more often, arising in 92.3% to 95% of those with PC (Desmarais & Keller, 2013). These forms can be further classified as symmetrical or asymmetrical, depending if the apex of the protrusion forms centrally on the sternum or deviates from the center, respectively (Fonkalsrud, 2008; Shamberger & Welch, 1987). The cause of PC is unknown, but can be associated with certain genetic disorders or syndromes such as Marfan syndrome or Noonan syndrome (Golladay, 2003; R. T. Lee, Moorman, Schneider, & Sigalet, 2013). Additionally, 25% of PC cases are related to having an extended family member with a chest wall deformity (Fonkalsrud & Anselmo, 2004). PC primarily influences body image and may be associated with psychological issues as well (Davis & Weinstein, 2004). Embarrassment and avoidance of activities that may reveal the chest are a common occurrence in children with PC (Colozza & Bütter, 2013). Other complications include chest pain/tenderness, as well as breathing difficulties when performing minimal exercise (R. T. Lee et al., 2013). If the deformity is severe, chances of developing cardiopulmonary disarrangement exist (Cahill, Lees, & Robertson, 1984; Sigalet, Montgomery, & Harder, 2003). Previously, the primary course of action to reduce or remove the protrusion was invasive surgery (Lam & Taber, 1971). Long-term

effects of this surgery have been inconsistent, with some surgeries resulting in worsened cosmetic appearance and decreased chest wall plasticity (Lacquet, Morshuis, & Folgering, 1998).

Figure 1-1 - The protrusion on the chest wall associated with Pectus Carinatum.

Consequently, an alternative non-invasive procedure to correct the PC deformity has been created and has transitioned to become the primary course of treatment for PC.

A Pectus Carinatum Orthosis (PCO) is now in development in conjunction with Braceworks (Calgary, AB). This orthosis primarily consists of an aluminum bar, a pad, back and shoulder straps, and boa closures (Figure 1-2). The PCO is designed to provide a force to the underlying protrusion in the sternum via the pad (Kravarusic et al., 2006). The magnitude of the force is altered by turning the boa closures. The objective of this device is to provide sufficient force to remodel/correct the sternal protrusion. Over the course of treatment, the force applied by the PCO to the protrusion is manually adjusted by the patient. The goal is to maintain a force that is consistent with the clinically prescribed guidelines, otherwise known as the clinically prescribed force (CF). From anecdotal observation, if these guidelines are not followed there may be either insufficient or excessive forces applied to the protrusion, leading to lengthened treatment time or

injury, respectively. Injuries due to excessive forces include minor cases of pectus excavatum (PE [a depression of the chest wall]) or serious skin abrasions on the protrusion. This device has shown to decrease anterior-posterior (AP) depth (distance from front to back) of the torso significantly for those who successfully complete the bracing protocol (Colozza & Bütter, 2013). Many versions of PCOs have been developed by clinicians globally, however the PCO in this thesis is associated with a protocol named 'The Calgary Protocol' that supplies the patient with guidelines on the usage of the PCO (Kravarusic et al., 2006).

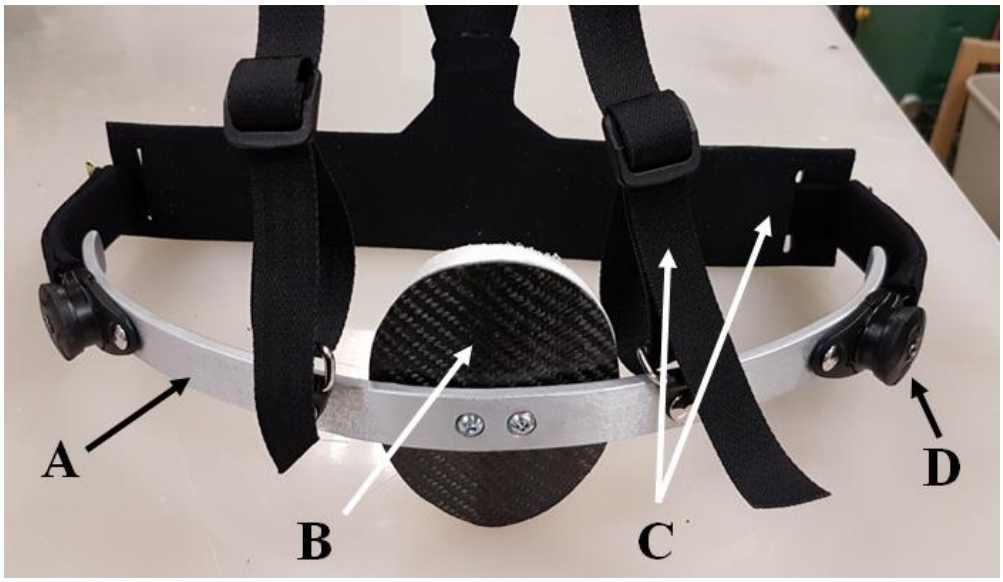

Figure 1-2 - The Pectus Carinatum Orthosis developed by Braceworks (Calgary, AB) and its major components: A) Aluminum bar, B) Pad, C) Straps (right arrow - back strap, left arrow - shoulder strap), and D) Boa closures.

1.2 Etiology of Pectus Carinatum

PC has no determined cause, however anatomical differences between healthy and PC individuals have been reported in literature. It is believed that the genesis of PE is due to growth complications of the costal cartilages, the medium of attachment for the ribs to the sternum (Cobben et al., 2014; Forman & Kent, 2014) (Figure 1-3). In response, theories of PC developing due to cartilage overgrowth have been suggested. Park et al. (2014) reported that the costal cartilages in the 4th-6th ribs were longer in PC subjects when compared to matched healthy controls. However, the corresponding ribs were shorter in PC subjects, thus forming equal overall rib plus cartilage length when compared to the controls (Park et al., 2014). These findings corroborate previous work performed by Haje et al. (1999) who also determined sternal differences in those diagnosed with PC. The body of the sternum was found to be under-grown, and contained complications in the fusion of the two joints between the manubrium, body, and xiphoid process of the sternum (Haje et al., 1999). This group speculated that the combination of the abnormal sternal and costal cartilage development resulted in unnatural forces, leading to the bowing of the chest wall (Haje et al., 1999). Furthermore, Guo et al. (2007) discovered that once children enter into adolescent years, the costal cartilages become less stiff. The reasons for this decrease in stiffness are still unknown, but could possibly be due to changes in the collagen structures. This decrease in costal cartilage stiffness when entering adolescence may be also contribute to the occurrence of PC during adolescent years.

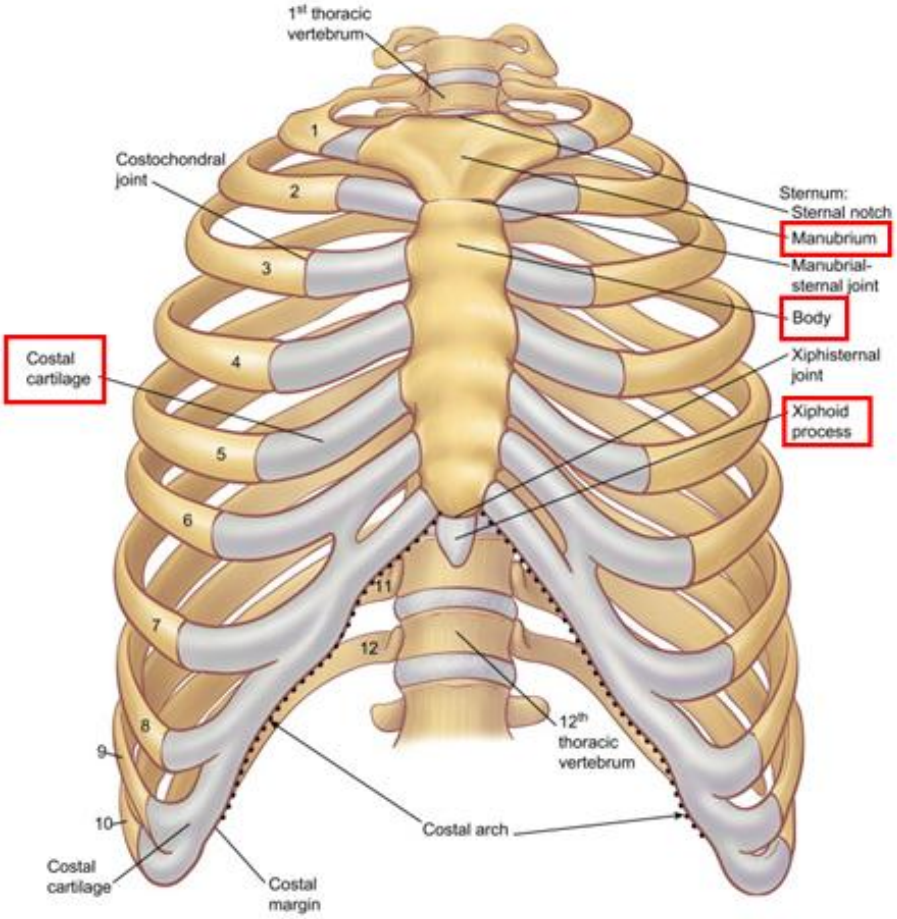

Figure 1-3 - The costal cartilages attaching the ribs (numbered) to the sternum. The three sections of the sternum are indicated (manubrium, body, and xiphoid process).[1]

1.3 The Calgary Protocol

The Calgary Protocol was created to provide guidelines to the patient on the length of time the PCO should be worn. Using a similar protocol to dental braces, the Calgary protocol for the PCO (Figure 1-4) involves two phases: the correction phase (~ 4-6 months) and maintenance phase (~18 months). The correction phase consists of a period of continuous wear (23 hours per day) of

[1] **Image reprinted from The Anatomy of the Ribs and the Sternum and Their Relationship to Chest wall Structure and Function, 17/4, Graeber, G.M. & Nazim, M., Thoracic Surgery Clinics, 473-489, Copyright 2007, with permission from Elsevier.**

the PCO by the patient until the protrusion is corrected (i.e. no longer visible). Afterwards the patient enters the maintenance phase where the PCO wearing time reduces to 8 hours per day, usually occurring at night. The maintenance phase is completed once estimated skeletal maturity is attained (Kravarusic et al., 2006). Multiple visits to the clinic occur during PCO treatment. The first is the fitting appointment, where the CF is determined and the patients learn how to wear the PCO properly. The CF is established primarily by the clinician. The CF is set at a level where the patient is unable to obtain a maximal inhalation but can still breathe comfortably. Patients are encouraged to provide feedback, to ensure the PCO feels comfortable when tightened. At the fitting appointment, the patient is instructed to manually adjust/tighten the PCO to the perceived CF when it has been removed or shifted during treatment. This force is referred to as the participant-applied force (PF). Patients revisit the clinic in two month intervals for their follow-up appointments to ensure the PCO still fits and functions correctly. The clinician may perform adjustments to the PCO during these follow-up appointments, as correction of the protrusion or growth of the patient may cause the PCO to become uncomfortable, or the apex of the protrusion may shift to a slightly different location.

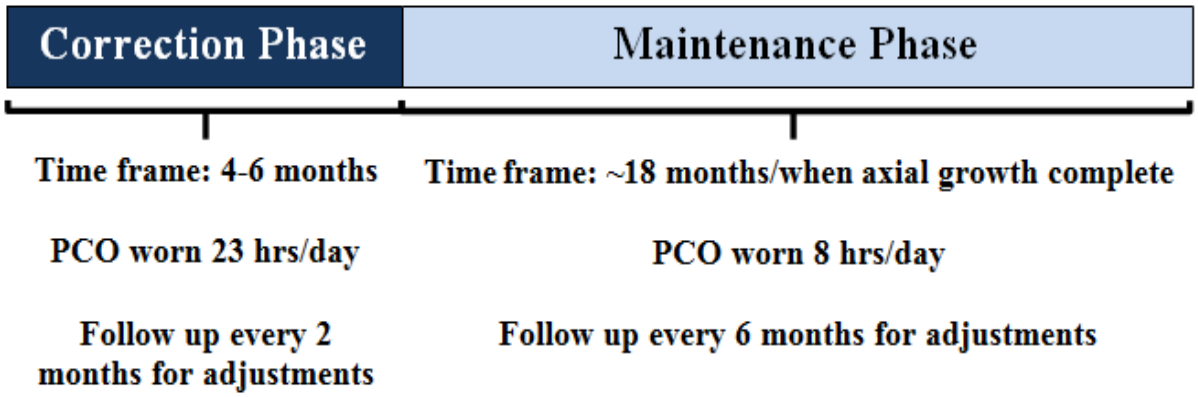

Figure 1-4 - The Calgary Protocol used by Braceworks (Calgary, AB) for patients with Pectus Carinatum.

1.3.1 Brace Construction

The PCO brace primarily consists of four components (Figure 1-2):

1) Aluminum bar - This is custom made to surround the patient's torso anteriorly. The bar is adjusted during treatment to ensure it does not make contact with the torso.
2) Pad - A carbon shell (CS) that is overlaid with two layers of foam for padding. The top layer of foam has a lower durometer value (less stiff) than the layer of foam underneath. The pad attaches to the aluminum bar via screws located at the apex of the protrusion, and contains a channel to allow fine adjustment of the positioning of the pad if necessary (Figure 1-5).
3) Straps - The back strap provides a flexible backing to the PCO for comfort. The shoulder straps allow the PCO to suspend the pad at the protrusion level.
4) Boa closures - These allow fine adjustment of the PF through turning of the dials. When turning the dials, the straps attached to them will shorten thus shifting the pad of the PCO towards the protrusion. The force can be released by pulling out the dials, and pushing the PCO away from the protrusion. Clicking the dials back in will allow them to provide a force to the protrusion once again.

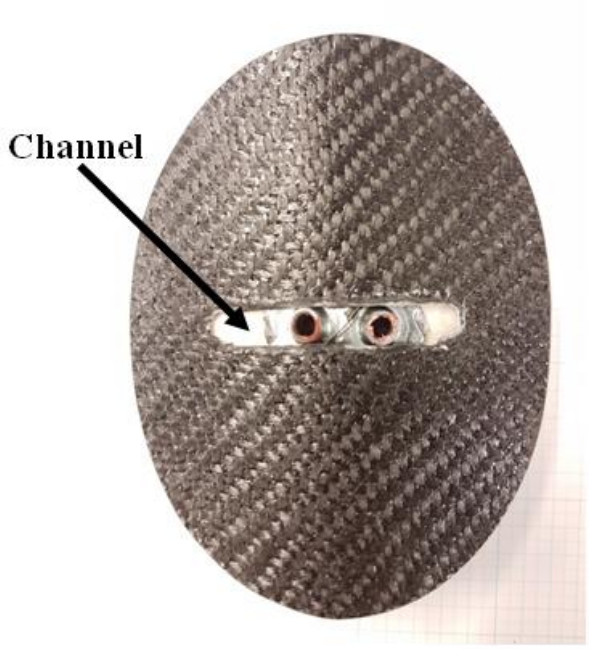

Figure 1-5 - Pad for the Pectus Carinatum Orthosis. The channel in the center allows for adjustment of the pad to ensure it lies on the apex of the protrusion.

1.3.2 Complications

The PCO has been shown to successfully treat PC (Colozza & Bütter, 2013; Kravarusic et al., 2006). Successful treatment is defined as obtaining a flat chest or when the protrusion is no longer visible (Colozza & Bütter, 2013). However, complications can arise within the protocol of the PCO - specifically the fitting appointment. When the clinician establishes the CF, the patient is left with their memory alone to recall the amount of force applied to their chest. This situation exists because there are no visual cues on the PCO to notify the patient of the magnitude of force. Consequently, clinicians have noted that patients may return to their follow-up appointments either under-tightening or over-tightening the PCO, leading to lengthened treatment time or injury. Additionally, the CF magnitude is unknown to the clinician and presumably differs between patients. This situation is the direct result of the clinician's method

of determining the CF. In applying the Calgary protocol, the clinician does not attempt to establish a consistent CF across all patients. Instead, each individual patient receives a CF that results in the same outcome - obtaining a breath that is "just short" of maximal inhalation. Therefore, physiological properties of the protrusion, such as the protrusion stiffness (PS), may influence the amount of force required to reach that outcome (Martinez-ferro, Fraire, & Bernard, 2008). The conventional use of the term "stiffness" involves characterizing the resistance (deformation or displacement) to an applied force of a homogenous object. However, because the protrusion is a heterogenous structure, the PS is defined here as a bulk equivalence stiffness, or the resistance of the protrusion to a given force. As the protrusion is a deformity caused by costal cartilage overgrowth, the PS may be influenced by age, subsequently affecting the amount of force applied by the PCO. Although rare, literature has reported that costal cartilage can become stiffer during adolescence, likely caused by calcification or ossification of cartilage tissues (Guo et al., 2007). Stiffening of the costal cartilages over the course of treatment may lead to different force magnitudes applied by the PCO. This situation may cause either excessive force production to obtain the same correctional displacement of the protrusion, or increase treatment time as the CF may not be sufficient to correct the deformity. The patient's age at the beginning of treatment may also influence the correction rate of the protrusion, as PCO forces have been shown to be influenced by the age of the patient (Martinez-ferro et al., 2008).

1.4 Knowledge Gaps

Scientific literature providing insight into the PCO methodology for correcting PC is scarce. Various research illustrates the success of the PCO bracing as an alternative to the surgical methods (e.g., Colozza & Bütter, 2013; Kravarusic et al., 2006; Martinez-ferro et al., 2016). Additional research demonstrates the use of three dimensional (3D) images to monitor the progress of PC during PCO treatment (e.g., Stephenson & Du Bois, 2008; Wong, Gorton,

Tashjian, Tirabassi, & Moriarty, 2014). However, no research has been reported on the forces applied by the PCO and how its purpose (to provide a corrective force to the protrusion) is influenced by the PS. Harrison et al. (2016), indicate that objective data is still required to further improve current assessment protocols, as well as the design and function of the PCO itself. This data can range from the cellular level (such as tissue responses to the PCO forces) to the type of force required to correct the protrusion (Harrison et al., 2016). Based on the current literature, one can only speculate on the relationships that exist between the force provided by the PCO and the characteristics of the protrusion. For example, beginning treatment at a later age has been shown to coincide with a larger CF (Martinez-ferro et al., 2008). This relationship has been attributed to the PS increasing with age (Desmarais & Keller, 2013). Therefore, one could contemplate that the PF would also be larger for those with a greater PS. Additionally, the same researchers determined that individuals in the older age groups had a longer treatment time (Martinez-ferro et al., 2008). Longer treatment times are associated with lower protrusion correction rates. In other words, the percent change in AP depth between two time points would be closer to 0% (i.e. no change). These longer treatment times at older age groups may also be related to the higher PS. To our knowledge, these are only speculations, as quantitative data relating the PCO and PS have not been reported. Clearly, in order to fully understand this condition as well as to advance treatment protocols, these relationships must be quantified.

1.5 Specific Aims & Hypotheses

There is a need to understand the forces applied by the PCO to ensure patients receive an optimal CF, and are able to maintain this CF over the course of treatment. Furthermore, the PS may influence the magnitude of these forces, as well as the correction rate of the protrusion. The overall goal of this research is to quantify the forces applied by the PCO, and to determine if the stiffness of the protrusion influences these forces and the correction of the protrusion.

Therefore, the following hypotheses were tested:

H1: There will be a difference between PF and CF at the initial fitting.

H1a: There will be a difference between PF and CF after one month of treatment.

H1b: There will be a difference between PF and CF after two months of treatment.

H2: PF will be different over time.

H3: A positive relationship will exist between PF and PS.

H4: A negative relationship will exist between correction rate (CR) and PS.

H5: PS will be different over time.

These hypotheses were tested through completing the following specific aims (SA):

SA1: Develop and validate a force measurement system to measure force applied by the PCO (CF and PF) and protrusion displacement simultaneously.

SA2: Determine relations between: CF and PF, PS and PF, and PS and CR.

SA3: Determine effect of time on PF and PS.

1.6 Expected Outcomes

The CF is anticipated to vary between individual participants. However, we expect the majority of participants to apply a PF that is significantly different from their CF over the course of two months. The PF will also be significantly different over time. In other words, the PF will either fluctuate (increase or decrease) over time, or consistently increase or decrease over time. PS is expected to demonstrate a similar result, containing a significant difference over time. Additionally, both the correction rate of the protrusion and PF will illustrate a similar result when compared to PS. As the overall participant PS increases, the correction rate will decrease (0% = no correction) and the overall PF for every participant will increase.

1.7 Significance

Clinical observation and qualitative analysis indicate that successful treatment with the PCO (by delivering a force to the site of the protrusion) reduces protrusion size effectively (Kravarusic et al., 2006). However, treatment efficacy varies with individual chest wall stiffness and patient compliance during the course of treatment (Harrison et al., 2016; Martinez-ferro et al., 2008). Quantitative analysis will advance our understanding of the PCO biomechanics and the variables influencing treatment efficacy throughout the bracing treatment duration. Additionally, initial experimental design should result in a high degree of confidence in the instrumentation and estimation of the dataset required for a larger scale data collection in the field.

The PCO device appears to be a viable non-invasive alternative to surgical intervention, in many cases. For appropriate candidates, out-patient treatment is less expensive than surgery. Analysis of quantitative data combined with clinical observation, will deliver an improved brace with reduced injuries, and provide clinicians with better assessment tools as well as standardized guidance for the treatment of PC.

1.8 Thesis Format

There are seven chapters in this thesis. Chapter 2 contains a literature review of all relevant literature surrounding PC, and external resources that provide rationale for the study findings. Chapters 3 and 4 are presented as sub-studies performed with two different force measurement systems. These chapters describe two force measurement systems developed to satisfy the first SA, which is to develop a system to measure the PCO forces and protrusion displacement simultaneously. Chapters 5 and 6 include the methods and results of the final force measurement system used in the study. Chapter 7 contains the discussion of our results, including the conclusions, limitations, and future recommendations. Appendix A outlines details of a third prototype force measurement system that was developed as part of this thesis but was not sufficient for the final version. The shortcoming of this prototype system are also presented.

Chapter Two: Literature Review

This chapter outlines relevant knowledge towards PC and its bracing treatment. The first section refers to the anatomical differences between healthy and PC individuals. Costal cartilage physiology is discussed specifying the composition of costal cartilages, physiological changes with age, and its material properties. Current literature in PC bracing is then summarized, outlining the different PC braces and the methodologies used for measuring the correction of the deformity. Subsequently, knowledge gaps that exist in PC bracing are presented and external resources available to provide rationale to the study's findings are outlined. The final section summarizes the chapter and explains the novelty and impact of the study.

2.1 Healthy versus Pectus Carinatum Anatomy

Development of the chest wall is a complex procedure and involves multiple pathways (Canavese & Dimeglio, 2013). Remarkably, the human body is able to consistently repeat this complicated procedure, producing chest walls with similar growth patterns and geometries. A study by Sandoz et al. (2013) collected CT scans for 48 normal participants with ages from 4 months to 15 years. The CT scans were used to produce 3D models of the ribs, costal cartilages, and sternum. From these models, a costal index was calculated (the costal cartilage length divided by the total costal length [cartilage + rib length]) . Additionally, sternum growth patterns were compared in 3D. It was found that at younger ages, the costal cartilages contribute a larger proportion of the total costal length (i.e. the costal cartilages shorten with aging) (Sandoz et al., 2013). This coincides with the general development of bones through endochondral ossification. In endochondral ossification, the cells within cartilage will gradually die leaving a cartilage matrix. This cartilage matrix allows for ossification to occur, thus producing bone (Mackie, Ahmed, Tatarczuch, Chen, & Mirams, 2008). During the development of the chest wall, the rib end of the costal cartilages will die, allowing for ossification and rib lengthening while aging.

Additionally, Sandoz et al. (2013) discovered that sternal growth patterns did not contain a correlation with age. Not every repetition of chest wall development follows the generic pathways. If any abnormalities arise during development, occurrence of chest wall deformities such as scoliosis or PC may result (Sandoz et al., 2013).

Two distinct anatomical differences are reported between healthy and PC individuals. The first difference is in the development of the sternum (Haje et al., 1999). Obtaining radiographs for 71 controls and 42 children with PC, this group aimed to produce evidence that sternal growth disturbances exist that contribute to PC (Haje et al., 1999). PC individuals were separated into their type of protrusion. These three main types include PC that can form on the manubrium of the sternum (chondromanubrial), body of the sternum (chondrogladiolar), and laterally on the chest wall (asymmetrical). These types were classified as superior (sample size [n] = 8), inferior (n = 22), and lateral (n = 12), respectively. Sternal indices were calculated for both groups by measuring the length of the manubrium, body, and body with the xiphoid process. Indices were created by calculating the ratio between the length of the body and manubrium (BM), and the ratio between the length of the body and xiphoid process with the manubrium (BXM) if the xiphoid process was fused to the body. For the controls, no fusion of the sternal joints was observed. This was also observed in individuals with inferior and lateral PC, but superior PC showed fusion between the body and xiphoid process. Controls were reported to have a BM of 2.16 (0.24) and a BXM of 2.73 (0.31). Superior and inferior PC had smaller indices, with a BXM of 1.68 (0.21) and BM of 1.83 (0.30), respectively. Lateral PC showed smaller indices as well (BM = 2.04 (0.24)), but not to the extent of superior and inferior PC. These smaller indices were speculated to be attributed to the sternum discontinuing its growth prematurely. As the costal

cartilages continue to grow, the sternum does not; causing disproportionality and abnormal forces to bow out the chest wall anteriorly (Haje et al., 1999).

The second discovery was regarding the length of the costal cartilages. Park (2013) first compared the length of the fourth, fifth, and sixth ribs and associated costal cartilages in 22 participants with asymmetrical PC. Obtaining 3D Computed Tomography (CT) scans, this study compared the length of the ribs, costal cartilages, and total length (ribs + cartilages) of both sides of the rib cage. No differences were found in all three outcome variables, with differences ranging from 0.086 mm to 2.36 mm. However, this study only compared the lengths within each individual and never considered comparisons of these values to normal individuals. Therefore, Park performed a similar study comparing the previously mentioned lengths between 26 individuals with PC and their matched controls (Park et al., 2014). The costal cartilage length was significantly longer in the PC group than the control group, with differences ranging from 5.6 mm to 8.5 mm. In addition, the ribs were significantly shorter in the PC group. Rib length differences ranged from 11.5 mm to 13.1 mm (Park et al., 2014). However, when taking into account the overall length of the costal cartilage and ribs, the majority of rib levels demonstrated no difference (ranges from 3.0 mm to 6.4 mm). The fourth rib level showed a difference in overall length (7.3 (15.4) mm). Therefore, the development of PC was speculated to not only be related to the overgrowth of costal cartilage, but also the undergrowth of the ribs (Park et al., 2014)

To summarize, the sternum in individuals with PC prematurely ceases growth (Haje et al., 1999). The growth of the costal cartilages, combined with the deficient length of the sternum, is speculated to create abnormal growth patterns causing the bowing of the chest wall found in PC. This mechanism was later supported by another study that found the costal cartilages are

overgrown (Park et al., 2014). These overgrown cartilages are also partnered with under grown ribs, potentially contributing to the development of PC.

2.2 Costal Cartilages

The ribs and sternum are bridged via costal cartilages. Being the primary connections of the ribcage, costal cartilages influence the distribution of applied forces to the chest wall (Forman & Kent, 2014). These forces can originate from internal tasks such as breathing, or external sources such as CPR compressions. The composition of the costal cartilages are primarily identified by three layers: 1) the perichondrium (outer layer), 2) hyaline cartilage (mid layer), and 3) areas of calcified cartilage (Forman & Kent, 2014). The component of costal cartilage that has a significant role in force distribution in the chest wall is the perichondrium, an external layer of closely bundled collagen fibres that have a tendon like appearance and surround the hyaline cartilage interior (Forman, del Pozo de Dios, Dalmases, & Kent, 2010). In human cadaveric testing of 22 third or fourth ribs, the perichondrium has shown to contribute approximately 50% of the stiffness in costal cartilage (Forman et al., 2010). Forces to mimic *in vivo* bending of the costal cartilages when the chest is compressed were applied to costal cartilages with and without a perichondrium layer. Specifically, the sternal end of the cartilage was displaced posteriorly to the rib end. Cartilages with the perichondrium required approximately 50% more force to obtain a specific displacement. Additionally, without the perichondrium the hyaline cartilage mid layer was unable to withstand higher tensile forces. Therefore, the perichondrium was speculated to resist the tensile forces while the hyaline cartilage interior bears the compressive forces (Forman et al., 2010).The ability of the perichondrium to resist tensile forces may be partially attributed to its tightly arranged fibres (Forman et al., 2010). The 50% stiffness contribution provided by the perichondrium may be affected by the amount of calcification contained. A cadaveric study on 11 human costal cartilage reported greater calcification in the perichondrium of individuals

over the age 40 years (Lau, Oyen, Kent, Murakami, & Torigaki, 2008). However, no differences in costal cartilage stiffness were found with age. An explanation for this may be derived from the methodology of this study. An indentation method was used to apply only compressive forces. However, this method does not resemble physiological forces (Lau et al., 2008). With the perichondrium acting to resist tensile forces, there may have been no force contribution from it. This would result in no difference in stiffness even though there was increased calcification of the perichondrium. Nonetheless, the authors suggested that the calcification of the perichondrium may influence the stiffness of the rib cage as a whole, rather than just the costal cartilages (Lau et al., 2008).

The costal calcifications appear in various shapes and sizes, containing similar properties to bone (Dearden, Bonucci, & Cuicchio, 1974; Rejtarová, Slízová, Smoranc, Rejtar, & Bukac, 2004). The size of these calcifications tend to increase with age (Forman & Kent, 2014). Costal cartilage calcifications have been classified into four types (Rejtarová et al., 2004):

1) Peripheral - Calcification occurs on edges of costal cartilage.
2) Central - Calcification occurs centrally inside the costal cartilage, can be in the form of globules or pyramidal.
3) Mixed - Calcification occurs both peripherally and centrally.
4) Indifferent - Calcification pattern with no specific pattern.

These types were created to sex differences in costal cartilage calcification. Females generally develop central calcifications (77%) while males develop peripheral calcifications (93%) (Rejtarová et al., 2004). These differences seem to have no contribution to mechanical properties of the costal cartilages. Guo et al. (2007) tested the tensile strength and stiffness of costal cartilages for 181 males and 86 females, at different age groups, *in situ*. Age groups were defined

as children (5-10 years), adolescent (11-17 years), and adults (18-25 years). Slopes of the stress-strain curves differed between age groups. Children had the steepest, while adolescents had the flattest and adults resided in the middle. Therefore, stiffness of the costal cartilage was found to decrease when entering adolescents, and began to increase when entering adulthood (Guo et al., 2007). Why the cartilage becomes less stiff when entering adolescence is still unknown, but could possibly be due to changes in the collagen structures of the cartilage (Guo et al., 2007). The increase in stiffness when entering adulthood is suspected to be from calcification of the costal cartilages, as calcification rarely occurs in adolescence and begins in later years (Guo et al., 2007). Moderate calcification may begin before the age of 40 years, but is common over the age of 50-60 years (Forman & Kent, 2014). No gender differences were seen in regards to costal cartilage stiffness (Guo et al., 2007). Furthermore, all age groups showed no difference in tensile strength between males and females. Therefore, calcification patterns may not have an influence on mechanical properties of the costal cartilage.

An increase in calcification of costal cartilage with age may potentially develop through chondrocyte apoptosis. Apoptosis of chondrocytes in articular cartilage has been reported to release apoptotic bodies that can cause many changes to the articular cartilages (Hashimoto et al., 1998). Apoptotic bodies can degrade the pericellular matrix surrounding the chondrocyte, allowing entrance into the interterritorial matrix within the cartilage (Hashimoto et al., 1998). Without any phagocytic cells present in the cartilage, these bodies are able to reside within the cartilage and increase the production of pyrophosphate (Hashimoto et al., 1998). Pyrophosphates provide an ideal environment for calcium crystals to form within the cartilage, thus causing calcification (Hashimoto et al., 1998). Aside from aging, a persistent pressure to articular cartilage has also been reported to produce chondrocyte apoptosis (Trias, 1961). Therefore, there

is a possibility that providing costal cartilages with persistent forces may result in chondrocyte apoptosis, thus creating calcification within the costal cartilages. These persistent forces, supplied by the PCO, may produce this effect later in treatment.

Costal cartilages have been found to represent characteristics of a linear viscoelastic material (Mattice, Lau, Oyen, & Went, 2006). Thus, the strain is linearly proportional to stress at any given time if under low magnitudes of stress (i.e. under the yield point or point of permanent deformation). For example, applying a stress (x) would result in the strain (y) at a specific time. If the stress was doubled (2x), the strain would also double (2y) at the same time point. However, this relationship must consider strain rates as costal cartilage stiffness may be strain rate dependent. A study using bovine articular cartilage determined that strain rate influences the magnitude of articular cartilage stiffness. Using an impacting indenter, Oloyede et al. (1992) determined that increasing strain rates by an order of 5 produced an almost linear increase in stiffness of articular cartilage from ~1 MPa to ~40 MPa. This in turn alters the relationship between stress and strain. However, a plateau effect was observed that allowed the cartilage stiffness to remain consistent at ~40 MPa with increased strain rate. This relationship between stiffness and strain was attributed to water inside the cartilage having the ability to displace at lower strain rates, allowing greater deformation. At higher strain rates, water may not have sufficient time to displace and thus remains inside the cartilage, causing it to become stiffer. Eventually, the strain rate increases to a point where the amount of water retained remains consistent, causing the plateau effect (Oloyede et al., 1992). These findings could potentially apply to costal cartilages, as both costal cartilage and articular cartilage are categorized as hyaline cartilage. Nonetheless, there are differences in stiffness magnitudes between costal cartilage and articular cartilage. Human costal cartilages stiffness values of 5-7 MPa have been

reported, which are relatively higher than articular cartilage (Lau et al., 2008). Laasanen et al. (2003) measured the stiffness of 25 bovine articular cartilages in unconfined compression. A constant strain rate of 2 mm/s was used. Stiffness of the bovine articular cartilage ranged from 0.3-1.5 MPa. The higher stiffness in costal cartilage may be due to its highly insoluble proteoglycans, and/or the lower water content in costal cartilages (Lau et al., 2008).

2.3 Current Literature in Pectus Carinatum

2.3.1 Bracing of Pectus Carinatum

Several braces exist that perform the same function; that is to provide a constant force to the protrusion (e.g. Ateş, Karakuş, Hakgüder, Olguner, & Akgür, 2013; Colozza & Bütter, 2013; Haje & Bowen, 1992; Kravarusic et al., 2006; R. T. Lee et al., 2013; S. Y. Lee, Lee, Jeon, Lee, & Lee, 2008; Lopez et al., 2013; Martinez-ferro et al., 2008). All braces have similar appearances, containing a bar and pad that lies anteriorly to the torso. What differs in these braces is the treatment. Majority of braces apply a force that is determined subjectively and according to the opinion of the clinician. Some studies suggest that the CF applied are sufficient to keep the brace stationary while being worn, or until the protrusion is flattened (Ateş et al., 2013; Haje & Bowen, 1992). Other braces are fastened by the clinician and given markings to notify the individual where to set the tightness if the brace is removed (S. Y. Lee et al., 2008). Only two braces were found to use a pressure system when determining the CF. With the first brace, the clinician applies the brace to their desired level (not exceeding 3 psi) using a pressure device for feedback (Lopez et al., 2013). With the second brace, the CF is decided on using a different pressure device with the criteria of applying the amount of pressure required to fully flatten/correct the protrusion (Martinez-ferro et al., 2008). These pressures could obtain magnitudes greater than 5 psi (Martinez-ferro et al., 2008). A more current study with the same

brace, reported that individuals requiring greater than 14 psi for correction are considered for surgery (Martinez-ferro et al., 2016).

The successes of these devices are dependent on the compliance of the patient. If the patient does not wear the brace consistently, the protrusion may not be corrected within the expected timeline, if at all (R. T. Lee et al., 2013). Therefore, Kang et al. (2014) suggested certain factors that would help influence the compliance of the patient. These factors included an initial success with the brace (correction of the protrusion occurring immediately) and aspects of comfort (Kang, Jung, Chung, Cho, & Lee, 2014). The comfort aspects consisted of both mental and physical categories. Physically, the brace could cause skin abrasions or torso pain if not fabricated or adjusted properly (Kang et al., 2014). Psychologically, if the brace is large and bulky the patient may have a sense of embarrassment (Kang et al., 2014). Lack of consideration of these factors may result in lack of patient compliance leading to increased correction times. Recently, there has been an attempt to measure patient compliance through the use of wireless sensors (Harrison et al., 2016). This approach could be ideal to accurately measure patient compliance to determine if these factors hold true.

2.3.2 Measures of Deformity

PC braces are reported to successfully correct the PC deformity (e.g. Colozza & Bütter, 2013; Kang et al., 2014; Martinez-ferro et al., 2008). However, no consensus exists when defining a corrected protrusion. The majority of literature defines "correction" as a qualitative outcome, relegating the determination to personal opinions. For example, some authors state the deformation is fully corrected when the chest is 'flattened' (Colozza & Bütter, 2013; Stephenson & Du Bois, 2008). Another example is using a subjective scale that rates the correction from 1 to 4 (Haje & Bowen, 1992). The appearance of the protrusion relative to its previous time point

determines if the protrusion worsened (rating of 1) or had remarkable improvement (rating of 4) (Haje & Bowen, 1992).

To quantify the amount of correction over time, simple instruments such as calipers have been used. In this approach calipers are aligned with the apex of the protrusion and a measurement of the AP depth is recorded. Colozza and Bütter (2013) used this method to detect differences in AP depth changes associated with PCO treatment between participant groups. The 20 participants who were compliant with the bracing protocol showed a greater change in AP depth (2.31 (1.17) cm) than the 2 non-compliant participants (0.64 (0.90) cm) (Colozza & Bütter, 2013). Other studies have used more advanced methods to quantify magnitude of correction such as 3D imaging (Wong et al., 2014). In this study a total of 50 participants underwent full body scans to calculate the Haller Index (HI). The HI was calculated as the largest transverse distance of the torso divided by the AP distance of the torso at the apex of the protrusion (Wong et al., 2014). The participants were divided into three groups based on whether they received a brace (no treatment group), wore the brace less than 12 hours a day (non-compliant group), and wore the brace more than 12 hours a day (compliant group). No significant changes in the HI were found for both the 'no treatment' group (2.5 (1.1) %) and the 'non-compliant' group (1.6 (0.99) %), but there were significant changes for the 'compliant' group (8.3 (1.0) %). These results show that 3D modeling of the torso, to calculate the HI, is a good indicator of PC correction (Wong et al., 2014). Additional indices such as an asymmetry index and an angle of sternal rotation, in addition to the HI, when using CT scans with radiographic markers have been proposed (Stephenson & Du Bois, 2008). The asymmetry index was calculated as the ratio between the inner AP diameter of the left and right thorax, while the angle of sternal rotation was measured at the point of greatest sternal rotation (Stephenson & Du Bois, 2008). Of these

indices, the HI and asymmetry index did not show any differences with those who completed bracing. However, the angle of sternal rotation did show significant changes (11.99 (5.6) deg vs. 5.53 (1.1) deg). The study sample size was small (n = 10), which could explain why the HI and asymmetry index were not different (Stephenson & Du Bois, 2008). These two studies are the only studies found in the extensive literature review conducted that depict correction of PC through 3D modelling. Although this advanced technology has the capabilities to offer a multitude of indices such as torso areas and center of volume, no studies reporting the use of this approach in PC correction monitoring were found. These indices may provide a standardized protocol for monitoring the progress and completion of protrusion correction.

2.4 Gaps in Pectus Carinatum Literature

There is a small amount of literature regarding the characteristics and properties of the chest wall in regards to PC and the PCO. Therefore, scientific literature and finding from related areas are reviewed to augment understanding and to supplement rationale for the proposed hypotheses and approaches.

2.4.1 Forces in Bracing

The magnitude of pressures applied by the PCO brace have been reported (Martinez-ferro et al., 2016, 2008). Both of these papers highlight a specific brace where the CF is determined by using a pressure device. The device is manually pushed onto the protrusion until it is "corrected". The user is notified of the amount of pressure required to obtain the specific correction. The largest amount of pressure that should be applied to the protrusion is suggested as 2.5 psi (Martinez-ferro et al., 2016). However, the pressures calculated with this device may originate from an average force, allowing excessive point forces to be masked. Unfortunately, the mathematics used to derive the pressures involved with this device, and the corresponding forces were not reported. Harrison et al. (2016) developed a system for measuring patient compliance remotely

by using an application compatible with a mobile phone. This application connected to temperature and pressure sensors on the pad of the brace that could log data outside of the clinic. Therefore, one could track the pressures of the brace throughout treatment. Unfortunately, only temperature data was illustrated and no pressure data was reported (Harrison et al., 2016). Because no forces have been reported, alternative approaches must be used to compare the amount of force applied to the thoracic region of the body.

A reasonable alternative for estimation of forces applied to the torso is scoliosis bracing as thoracic pads are used to provide a constant force to the thoracic region, similar to the PCO. Scoliosis braces have been reported to provide forces ranging from an average of 58.1 N to 66 N, translating to 13.0 lbs to 15 lbs, respectively (Chase, Bader, & Houghton, 1989; Van den Hout, Van Rhijn, Van den Munckhof, & Van Ooy, 2002). Additionally, these thoracic forces change with position. Mean forces while standing were 66 N (15 lbs), but significantly increased when sitting (92 N [21 lbs]) and when supine (96 N [22 lbs]). The mean forces significantly decreased when lying prone (50 N [11 lbs]). This large variation in forces with posture was speculated to result from the change in location of the thoracic pad when changing positions (Van den Hout et al., 2002). Forces provided by braces may also be influenced by the pain tolerance and pain threshold of the individual. According to Woodrow et al. (1972) the amount of pressure that an individual can withstand decreases with an increasing age. Although older individuals cannot tolerate pain as well as younger individuals, older individuals have been reported to have a higher pain threshold (Tucker, Andrew, Ogle, & Davison, 1989). Additionally, repetitive exposure to a specific environment can increase the pain tolerance to that environment. An example of this phenomena is athletes obtaining an increased pain tolerance to cold after receiving multiple cryokinetic training sessions (Carman & Knight, 1992). For the PCO, the

location of the pad may influence the amount of force applied. Additionally, patients beginning treatment at different ages may have different pain tolerances and thresholds. This could directly influence the magnitudes of forces provided by the PCO (either through positioning or tightness). Correction rates with scoliosis bracing have been influenced by multiple factors such as the geometry of the scoliotic curve, the stiffness of the curve, and patient compliance in wearing the brace (Van den Hout et al., 2002). Furthermore, while scoliosis braces can produce significant forces the deformity may be corrected at different rates due to these factors (Chase et al., 1989). Although the PCO is a different brace, several similar factors may be applicable to deformity correction rates. Both braces are used on a population of similar ages, and act to remodel a structure composed of bone, cartilage, and other soft tissues. Therefore, the geometry and stiffness of the protrusion may have an influence on the correction rate of the individual.

2.4.2 Stiffness of the Chest Wall

The stiffness of the protrusion is considered by some clinicians as a determining factor in assessing suitability for PC bracing. However, to date quantitative measures of protrusion stiffness are lacking. In the simplest approach called a manual compression test, the palm of a hand is used to press down on the protrusion. If partial or complete correction was observed during the manual compression test the protrusion was considered flexible and appropriate for treatment (Haje & Bowen, 1992; S. Y. Lee et al., 2008). Another study suggested that if the corrective pressure from the pressure device was greater than 14 psi, it was a stiff protrusion (Martinez-ferro et al., 2016). These measures are all subjective and only define the stiffness relatively. No literature was found that reported the quantitative values of the PS. However, studies on normal chest walls have been performed and can be used as a secondary resource. Research concerned with the validity of Cardiopulmonary Resuscitation (CPR) mannequins allows for the comparison of stiffness magnitudes of the chest wall. One study compared the

chest wall force-displacement curves between human participants and CPR mannequins (Gruben, Guerci, Halperin, Popel, & Tsitlik, 1993). For the human participants, stiffness of the chest wall had been seen to increase non-linearly as the displacement of the chest wall increased, and ranged from 5 kN/m to 40 kN/m (Gruben et al., 1993). The force and displacements of these participants were obtained using a custom made device for CPR applications. The device contained a handheld module that could measure compressive forces. The handheld module was attached to an arm (containing transducers) that could record its movements in three dimensions. Chest compressions were applied to the human participants with the handheld module. Movement of the arm was simultaneously recorded with the forces. The movement of the arm perpendicular to the chest wall was used for analysis to obtain a force-displacement curve. Finite element (FE) models of the thoracic cage have also been developed. Ruan et al. (2003) validated a FE model of the human thorax during a frontal impact simulation. Cadaveric tests were additionally performed to determine if the FE model was an accurate representation of these impacts. From the force-displacement curves, it can be estimated that the thorax stiffness of the cadaveric specimens were approximately between 300 kN/m to 400 kN/m (Ruan et al., 2003). Similar values have been reported in a FE model where chest wall stiffness was determined to be approximately 326 kN/m when exposed to a frontal impact (Kimpara et al., 2006). The velocities of the impacts in both studies were of high magnitude (~ 6 m/s), and may not accurately represent the loading rate of the PCO. However, the values in these studies provide a good indication of the range of PS that may be encountered.

2.5 Summary and Impact

Literature supports the strong need to understand the force produced by braces for PC (Harrison et al., 2016). However, there is currently a lack of devices to measure these forces and an absence of reported forces during treatment. Therefore, literature from related conditions must be

used to provide rationale in our findings such a scoliosis bracing. Furthermore, there is extremely limited understanding of the PS and the extent of influence the PS has on brace forces. Stiffness of the chest wall has only been reported for normal individuals and FE models to date. Therefore, this study aimed to develop a system with the capabilities of measuring the PCO forces and displacements simultaneously to achieve a calculation of PS. This was the first time that PC brace forces and PS would be reported in literature. In addition, this study aimed to follow a cohort over time to determine if any changes in PS influence PCO forces and correction rates, which has also not been previously reported.

Chapter Three: Force Measurement System 1

This chapter focuses on force measurement system 1 (FM1) developed to measure PCO forces, and the associated sub studies. The first section outlines the goal of this system, followed by the construction and calibration of the system. Multiple sub studies performed with the system are described in the next sections. A “CPR mannequin" study was performed with the system to determine what force ranges would be expected on a human participant. Results of the “CPR mannequin" study were then evaluated on human participants in a “mannequin validation" study. The “mannequin validation" study also tested the error detection required by the system. Finally, FM1 sensitivity was tested with forces applied in different scenarios, called the “load cell sensitivity" study.

3.1 Goal of Force Measurement System 1

The first study aim (SA1) involves developing a contact patch to measure the PCO forces applied to the protrusion. Therefore, the initial step was to determine the range and magnitude of expected PCO forces. Knowledge of the force ranges enabled specification of load cells with appropriate compensation for the normally distributed accuracy. While load cells may measure in a wide variety of ranges, they may not be fully accurate within that entire range. For any specific range the load cell measures, the most accurate measurements are typically obtained within the midrange. Therefore, a load cell was required that would contain a midrange within the proximity of the expected force magnitudes. In addition, a load cell that contained a measurement error that was smaller than the minimal PCO force changes was required. In other words, if PCO force changes were within the error range, these may be attributed to error of the load cell and not a difference in the PF.

3.2 Construction of Force Measurement System 1

FM1 was designed and constructed prior to this thesis. It consisted of an unpadded carbon shell (UCS) that was attached directly to the PCO itself. The UCS acted as one of two hard surfaces to restrain the load cell, the second hard surface being the carbon shell (CS) of the pad. Assembling FM1, the UCS was screwed into the aluminum bar of the PCO. The calibrated load cell (Omega® LCKD-50, 0-50 lbs) within FM1 was adhered centrally onto the UCS, below where the screws inserted (Figure 3-1 B). To attach the CS, the UCS contained a hole on the bottom that the CS would slot into via its extension piece (created specifically for this design) (Figure 3-1 A). The top was attached with a hook and loop fastener.

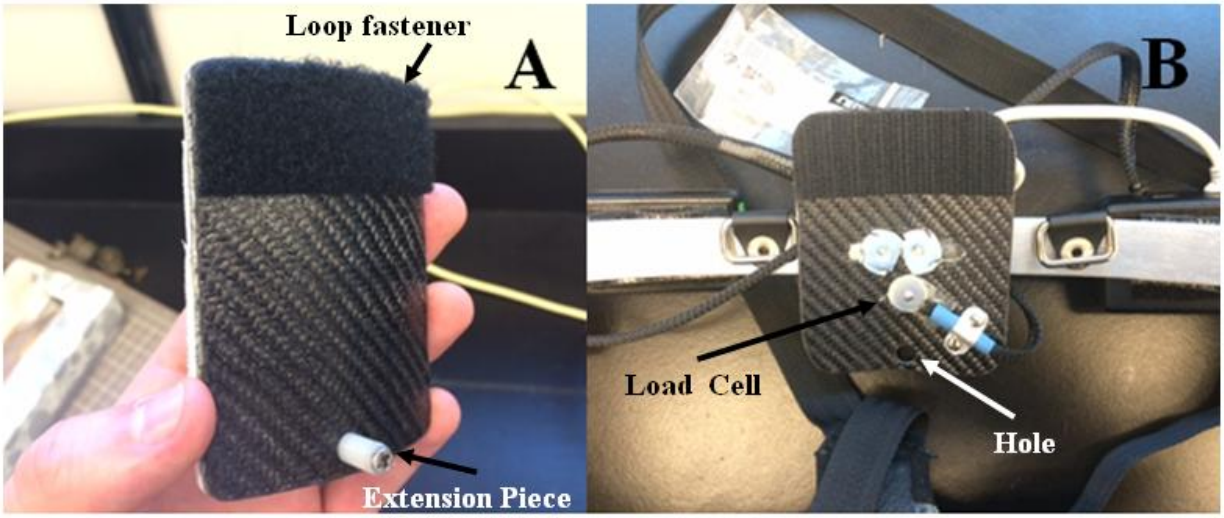

Figure 3-1 - A) The modified carbon shell (CS) of the pad, containing the loop fastener and extension piece that would slot into the unpadded carbon shell (UCS). B) The UCS containing the calibrated load cell. The hole for the extension piece on the CS can be seen below.

3.3 Calibration

No calibration was previously performed with the load cell of FM1. Therefore, there was no means of relating the load cell outputs to the magnitude of force applied. A calibration was performed to determine a relationship between the force applied to the load cell and its subsequent voltage output. The load cell design was of a sub-miniature type (~ 1 cm diameter) and contained a large force range. These specifications are uncommon in a load cell and require specific equipment to calibrate, as large forces applied across a 1 cm diameter is difficult to achieve. To accommodate these specifications, calibration of the load cell was performed in a Material Testing System (MTS [Bose® 3220-AT]) in Zymetrix® laboratories at the University of Calgary.

3.3.1 Protocol

The load cell was removed from the UCS and placed onto a metal plate inside the MTS. Forces were applied in a stepwise fashion ranging from 0 N to 220 N (0-50 lbs) in increments of 10 N. A 10 N increment was chosen to provide a data set of 23 points that represented the whole force range spectrum. For each force increment, data was collected for approximately 10 seconds. The data acquisition software provided with the load cell was limited to a sample rate of 1 Hz. Therefore, 10 seconds of data collection at each force increment provided enough data to calculate an average load cell output. Forces were applied at increasing and decreasing increments to test for any hysteresis in the load cell. A total of three trials of the entire sequence were performed. Data was averaged for each force increment, and then plotted on a line graph. A line of best fit having the largest R^2 value was overlaid onto the data to obtain a conversion equation. The conversion equation converted the load cell voltage outputs into a pound force. The calibration of FM1 showed a linear relationship with no signs of major hysteresis (Figure 3-2).

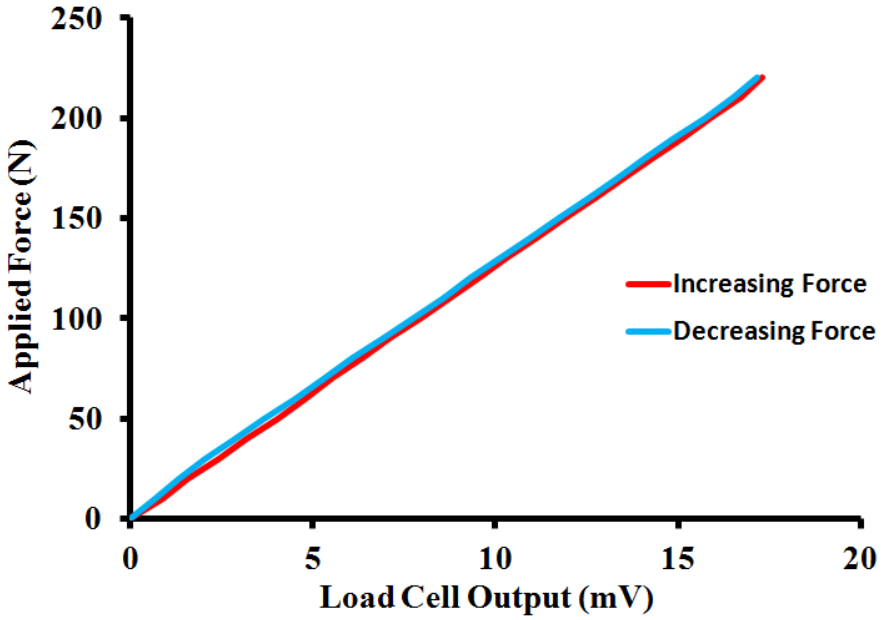

Figure 3-2 - Calibration of the load cell in FM1. Forces were produced in increasing increments, immediately followed by decreasing increments. No major hysteresis was seen, as shown by the overlap of the two lines.

3.4 CPR Mannequin Study

3.4.1 Methods

No human participants were recruited for this study to avoid any scheduling conflicts that may arise. Instead, a CPR mannequin was purchased to act as a surrogate patient with PC. CPR mannequins and humans have been reported to share similar chest wall mechanical properties (Gruben et al., 1993). A PCO with FM1 attached was fixed on the CPR mannequin by the clinician. The mannequin contained a fabricated protrusion on its chest to simulate PC. The clinician confirmed that the simulation felt similar to patients with PC. Each day (for three days), three sessions took place in which the clinician placed the PCO on the mannequin 5 times. The clinician would tighten the PCO to a magnitude that was representative of the CF of a patient. A

total of 45 trials were obtained throughout the three days. This allowed the investigation of intra-day and inter-day repeatability of the CF. On the last day, at the end of the third session, the clinician tightened the PCO on the mannequin to an approximate maximal PF (what the clinician believed to be the largest amount of force a patient had applied to their protrusion). The sequencing of this experimental protocol ensured all previous experimental data was obtained in case the PCO failed during maximal force testing. To determine the repeatability of the placement of the PCO, rulers were placed on the mannequin to act as fiducial markers (Figure 3-3). The rulers used were basic rulers that measured the position of the pad in millimeter accuracy. Both the mannequin and rulers were aligned perpendicularly and level to the table surface. Photographs of the PCO on the mannequin were taken after each trial using a digital camera. The camera was mounted on a tripod to guarantee no movement of the camera. Perpendicular alignment of the camera to the chest wall of the mannequin was ensured with the use of levels on the tripod. The ruler was removed during placement of the PCO in order to negate any guidance for the clinician. Position of the PCO was recorded as a vector in a two dimensional cartesian coordinate system.

Figure 3-3 - The cardiopulmonary resuscitation (CPR) mannequin with the fabricated protrusion and fiducial markers (rulers).

When collecting data, the CFs and clinician derived maximal PFs were recorded over five trials for 10 seconds using a laptop containing Omega® software provided with the load cell. The length of recording provided ten data points to obtain an average force, as data acquisition with the Omega® software was limited to a maximum of 1 Hz. Cartesian coordinates of the position vector were converted into magnitude using the Pythagorean theorem. Force and position data from the five trials in each session were averaged to obtain a mean and standard deviation. The maximum and minimum force values from the overall sessions were determined to obtain the range of forces. The CF and position data were plotted to obtain a trendline and its corresponding R^2 value to determine if a relationship exists between the two variables.

3.4.2 Purpose

The purpose of this study was to use FM1 to obtain preliminary measurements of the CF and maximal PF, and to determine if the position of the PCO changed. The change in PCO position

was measured as it may have influenced the magnitude of these forces. This assisted in the decision process of what force ranges the load cell would require, guaranteeing the mid-range fell within the proximity of the expected forces.

3.4.3 Results & Discussion

The CF magnitudes recorded from the CPR mannequin ranged from 4.79 to 7.69 lbs (Table 3-1). The average maximal PF was calculated to be 12.30 (0.42) lbs. The position of the PCO ranged from 20.60 to 21.06 cm (Table 3-1). There was a small variation in position within each day, ranging from 0.76 to 1.35 cm (Table 3-1). Furthermore, there was minimal effect of the PCO position on the CF, with $R^2 = 0.11$ (Figure 3-4).

Overall, the results of this pilot study indicate that FM1 was able to adequately measure both the range of the CFs and maximal PF applied by the PCO. The study revealed that these forces are likely within the range of 0 to 15 lbs. Therefore, a load cell capable of measuring ranges of 0 to 25 lbs was considered to be appropriate for this application. Additionally, it was expected that the CF and the PF for future studies would reside at approximately 4 to 8 lbs. The position of the PCO minimally influenced the magnitude of PCO forces applied to the CPR mannequin. Therefore, the position of the PCO was not controlled for in future studies.

Table 3-1 - The average (standard deviation) of the CF and PCO position at each day for all sessions.

Day	Session	Clinically Prescribed Force (lbs)	Position (cm)
1	1	5.40 (1.34)	20.91 (0.48)
	2	4.79 (1.00)	20.71 (0.52)
	3	5.27 (1.40)	20.68 (1.10)
	Average	**5.15 (1.26)**	**20.77 (0.76)**
2	1	6.46 (1.60)	20.97 (1.33)
	2	6.64 (0.82)	21.05 (0.73)
	3	6.01 (0.59)	21.01 (1.77)
	Average	**6.37 (1.09)**	**21.01 (1.35)**
3	1	6.99 (0.76)	20.60 (0.80)
	2	7.69 (0.75)	21.06 (1.11)
	3	7.20 (0.85)	20.81 (1.21)
	Average	**7.29 (0.79)**	**20.82 (1.05)**

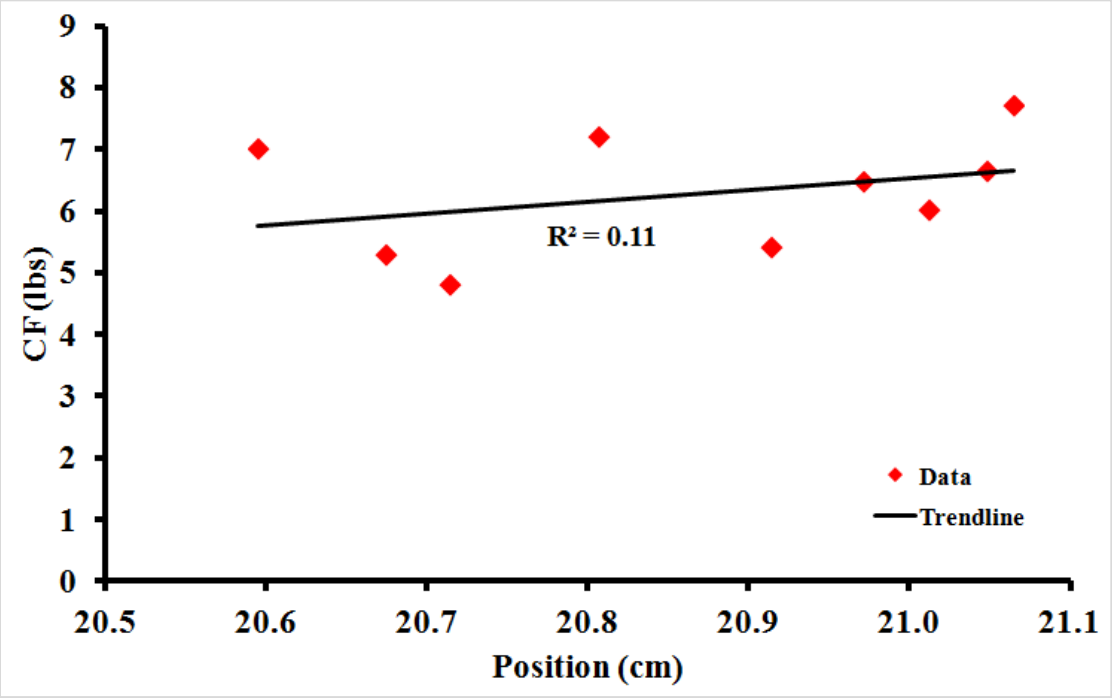

Figure 3-4 - The relationship between PCO position and the CF. No trend was seen between the two variables with R^2 = 0.11.

3.5 Mannequin Evaluation

3.5.1 Purpose

The CPR mannequin study provided a range of forces that seemed feasible on human participants. However, this could not be certain and an evaluation of the CPR mannequin results was performed. The purpose of this study was to apply FM1 to human participants and determine how closely the PF compared to the CF in the CPR mannequin study. Additionally, the PCO was tested to determine the magnitude of force changes during PCO tightening. This provided the means of determining what load cell error was acceptable for the development of a force measurement system. If the PCO force changes were greater than 1%, a load cell with 1% error would be sufficient. If it was less, this may lead to assumptions of whether the difference in force was due to error or the participant wearing the PCO at a different magnitude of force.

3.5.2 Methods

Four male participants who had been wearing a PCO for at least 4 months were recruited by Braceworks to take part in this study. Participants had to have worn the PCO for at least 4 months to ensure they were habituated with the PCO and the magnitude of force they applied to their chest wall. All participants provided informed consent.

To evaluate the findings in the CPR mannequin findings, the participants were required to place the PCO on their chest and tighten it to the magnitude of force they perceived as the CF at the fitting appointment. This was otherwise known as the PF, and was recorded for 10 seconds at 1 Hz. After recording, the participant loosened the PCO to begin a new trial. This process was repeated an additional two times, for a total of three trials.

To determine the magnitude of load cell error required for the force measurement system, three of the four participants were asked to place the PCO on their chest without tightening (one participant was unable to remain for this additional test). The first recording of the PF occurred

in this condition, where no force was being applied by the PCO. The PCO was then tightened in the number of increments required for the participant to reach the CF. Recordings of the PF were acquired at each increment (10 s, 1 Hz). The magnitude of change in PCO forces was represented as a percentage. The PCO force at a specific increment was divided by the preceding increment to obtain a percent change in PCO forces.

3.5.3 Results & Discussion

When the PCO was applied to human participants, the PF magnitudes ranged from 3.72 to 5.96 lbs, with an average of 5.23 (2.97) lbs (Table 3-2). Tightening of the PCO in a stepwise fashion resulted in an average difference of 16.0 (15.7) %. The lowest difference seen was 0.48% and the highest was 58.9%. The lowest difference was the only instance where the difference was less than 1% (Table 3-3).

In the previous CPR mannequin study, it was speculated that the PF would reside in the ranges of 4 to 8 lbs. The results of the mannequin evaluation study revealed that the ranges of the PF were approximately 4 to 6 lbs, falling within the speculated ranges. Therefore, a load cell with a range of 0 to 25 lbs was selected for the development of a force measurement system. The measured differences in force production above 1% between PCO tightening increments suggested a load cell containing 1% error would be sufficient for the purposes of this study.

Table 3-2 - Average and standard deviation of the PF for all four participants.

	Brace Force (lbs)			
	Trial			
Participant	1	2	3	Average (SD)
1	5.21 (2.81)	5.97 (3.13)	6.70 (3.55)	5.96 (3.18)
2	4.43 (2.73)	2.92 (2.81)	3.82 (2.76)	3.72 (2.77)
3	4.66 (3.09)	5.53 (2.64)	5.90 (2.81)	5.36 (2.86)
4	6.57 (2.92)	5.69 (3.24)	5.38 (3.01)	5.88 (3.06)

Table 3-3 - Percent change (including average [SD]) of force for all participants when the PCO was tightened in increments.

Participant	Increment	Force (lbs)	% Change
1	1	3.76	-
	2	3.62	3.63
	3	3.64	0.48
	4	3.95	8.65
	5	4.00	1.26
	6	4.43	10.63
2	1	2.66	-
	2	2.86	7.57
	3	4.55	58.85
	4	5.20	14.41
	5	4.66	10.36
3	1	4.82	-
	2	3.52	26.87
	3	4.44	26.16
	4	4.60	3.57
	5	6.30	36.87
	6	5.55	11.90
	7	6.58	18.49
		Average	16.0 (15.7)

3.6 Load Cell Sensitivity

3.6.1 Purpose

Forces applied by the PCO were at the lower range of the load cell used in FM1. Recalling the normally distributed accuracy of a load cell, the forces may not be reliable at these ranges. Therefore, the purpose of this study was to determine if the load cell was capable of distinguishing different forces at the lower range, and if the location of the applied force had an influence on the repeatability of the magnitudes.

3.6.2 Methods

Determining the load cell sensitivity at lower force magnitudes was performed by placing the load cell onto a scale (maximum 11 lbs). The scale acted as a visual guide to determine how

much force was applied to the load cell. A stand with a screw placed above the load cell provided a controlled force (Figure 3-5). As the screw was turned, the downward movement applied increased force to the load cell. Force data were recorded for four different scenarios: 1) load cell only, 2) load cell on the UCS, 3) both UCS and CS (screw located centrally on pad), and 4) both carbon UCS and CS (screw located on top of load cell). These scenarios were included to determine whether the configuration of FM1 and/or location of the applied forces resulted in differences in measured forces. Force measurements were obtained from 0 to 11 lbs, in 0.5 lb increments, for 10 second durations at each force increment. The 0.5 lb increments were used to produce enough data points to capture a valid relationship between force and voltage outputs at lower forces. Again, ten second durations for data collection were used as the software was limited to a sample rate of 1 Hz. Therefore, ten seconds provided enough data to calculate an appropriate average at each force increment. Average forces for each scenario were then plotted onto a graph for qualitative comparison.

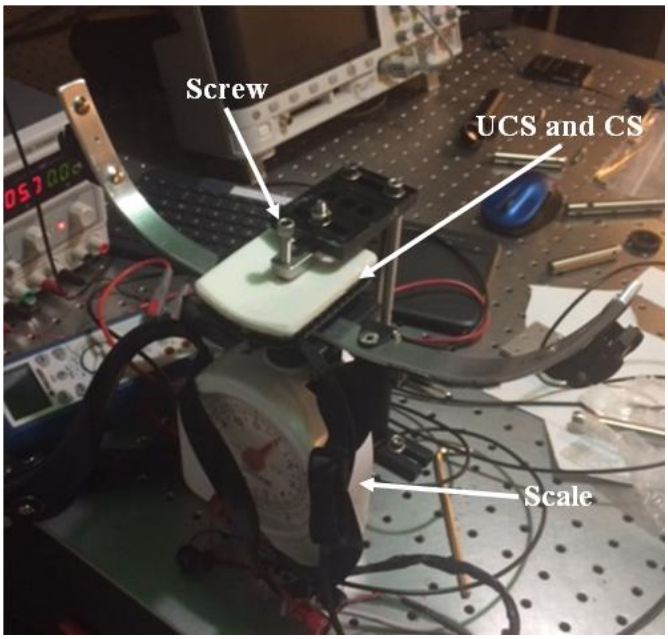

Figure 3-5 – The screw, load cell, and scale design to test the sensitivity of the load cell in different scenarios. The above conditions is scenario 3 (UCS and CS with screw located centrally on pad).

3.6.3 Results & Discussion

The load cell was able to detect small force changes (0.5 lb increments) within the PCO specific range. Force magnitudes were highest when applying forces directly to the load cell (scenario 1 [11.55 lbs] and scenario 2 [11.62 lbs]). Applying the padded CS reduced the response of the load cell in both scenario 3 and 4 by approximately 10% to 20%. The position of the force application also influenced the load cell output, with smaller outputs (~ 7%) occurring when the screw was located away from the load cell (Figure 3-6).

Several flaws with FM1 were identified during this sub-study. First, the location of force application influenced the forces measured by the load cell. The magnitude of force was consistently smaller when a force was applied centrally to the pad versus directly above the load cell (Figure 3-6). This sensitivity of location of force application is problematic for monitoring

changes in the CF and the PF over time associated with treatment interventions, and also for accurate inter-subject comparison purposes. The source of the location sensitivity was speculated to be the non-rigid attachment of the CS to the UCS, which allowed rotational movement of the CS with respect to the UCS. Relative movement between the CS and the UCS may result in lack of complete force transfer to the load cell. Applying this to the PCO, there was a possibility that the position of the apex of the protrusion on the CS could influence the force measurements. Therefore, to address these numerous considerations it was concluded that a new system that remains fixed during PCO tightening and can accommodate the appropriate load cells and shell configuration is required.

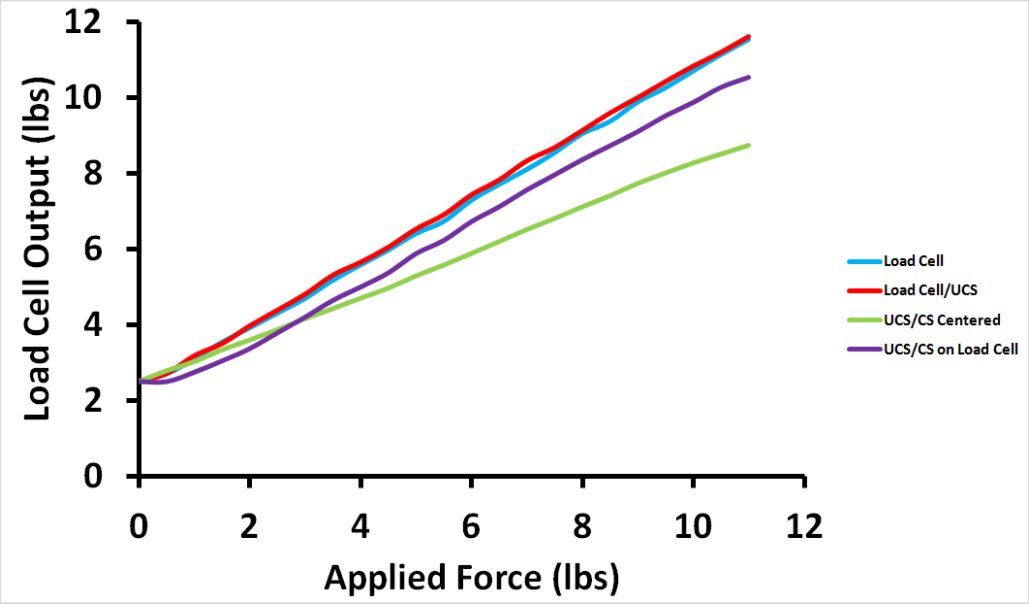

Figure 3-6 - Load cell output for each load cell and position scenario when testing for sensitivity.

3.7 Summary

FM1 was able to successfully provide an approximate range of the PCO forces that would be encountered. This provided the information required to specify a new load cell that contained a mid-range closer to the expected PCO forces. Additionally, with the percent change in PCO forces being larger than 1%, a load cell error of 1% was suitable for the proposed study application. FM1 also presented weaknesses, such as the rotational movement of the CS relative to the UCS. It was concluded that in order to satisfy the first specific aim a new system that considers these flaws needed development.

Chapter Four: Evaluation of Force Measurement System 3

Force Measurement System 3 (FM3) was the final measurement system created primarily by the author of this thesis, with assistance from the study team. FM3 was tested to use for measuring forces applied by the PCO in this study. FM3 is a modification of previous prototype systems, containing adaptations to overcome limitations identified in the previous systems. Force Measurement System 2 [FM2], an earlier prototype version also created by the study team (Appendix A), consisted of a single load cell system which had difficulties accommodating rotational forces. This situation caused exposure to tensile forces on the load cell. Additionally, an LED sensor incorporated into FM2 enabled simultaneous displacement measurements. FM3 was created to accommodate rotational forces. The design included four load cells instead of one. The LED sensor utilized in FM2 was also incorporated in FM3 to allow simultaneous displacement measurement. Details of the construction, calibration, and testing of FM2 are presented in Appendix A. The calibration and evaluation of FM3 and the LED sensor was performed by the author of the thesis.

4.1 Goal of Force Measurement System 3

The goal of this sub-study was to construct and calibrate a new system (FM3) that remained fixed during PCO tightening and accommodated any rotational forces. Additionally, FM3 was tested with the LED sensor to determine if stiffness calculations were accurate, and to ensure the system had the ability to perform while attached to the PCO. FM3 was also evaluated with human participants to obtain preliminary results on how closely participants could follow their CF.

4.2 Construction of Force Measurement System 3

The PCO forces were measured with FM3, which consisted of four uni-axial, compressive load cells (TE Connectivity Ltd® FX1901, 0-25 lbs) placed between the pad and aluminum bar (Figure 4-1).

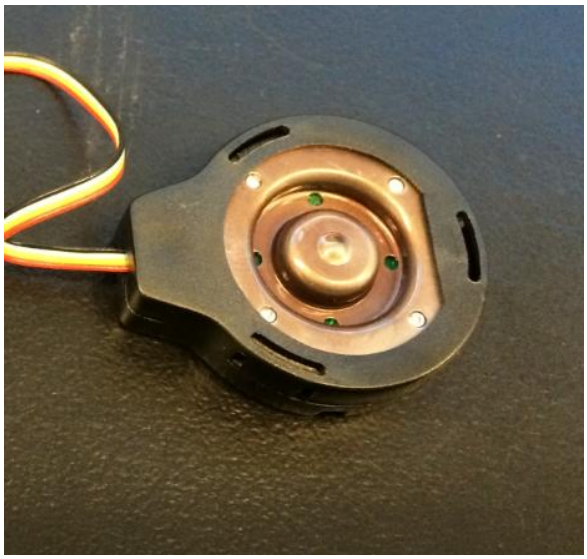

Figure 4-1 – Load cell used in Force Measurement System 3

A force plate, commonly used for measurement of ground reaction forces with motion analysis applications, formed the basis of the FM3 system design. The four load cells were embedded between two three dimensionally (3D) printed surfaces. The 3D surfaces were made from a thermoplastic (Acrylonitrile-Butadiene-Sytrene or ABS) and printed using a LulzBot® Taz 5 3D printing machine (Aleph Objects Inc. ©, Loveland, Colorado). 3D printing was chosen for this application as it is a cheap and efficient solution for producing items required for precise assembly. To obtain an accurate reproduction of the pad of the PCO, it was laser scanned (Desktop 3D Scanner, NextEngine Inc., Santa Monica, California) to obtain a 3D model. Afterwards, the surfaces were constructed with Autodesk Inventor® and Autodesk Mesh Mixer® (Autodesk Inc. ©, Mill Valley, California) to replicate the shape and contours of the pad itself,

providing an optimal fit. This coincides with the load cells as well, which were scanned to fabricate specific insertion points onto one of the surfaces. These insertion points would allow the load cells to insert into this surface, called the backing.

The first "backing" surface was glued to the back of the curved CS of the pad. It was designed to create a flat surface for the attachment of the load cells. The backing surface contained four protruding insertion points, which allowed the load cells to insert into the backing (Figure 4-2 A). These insertion points were developed using the schematics of the load cells to ensure a proper fit when assembled (Figure 4-3). The second "replica" surface was created by forming a positive mould from the negative mould of the CS (Figure 4-2 B). The replica surface performed two functions: 1) provided the second flat surface for embedding of the load cells, and 2) allowed the aluminum bar of the PCO to interact with a surface of a similar contour to the original pad. All four load cells were adhered onto the replica using a steel reinforced epoxy (J-B Weld©, Atlanta, Georgia). Four holes drilled into the replica surface allowed the wires of the load cells to pass through the surface. This design ensured that the load cells would lay as flat as possible on the replica surface. Epoxy cement was not used to attach the load cells onto the backing surface (with insertion points). The multiple insertion sites enabled the system to remain assembled without the need of epoxy on both surfaces (Figure 4-4). This design feature allowed easy access to the screws when substituting the original pad of the PCO with FM3.

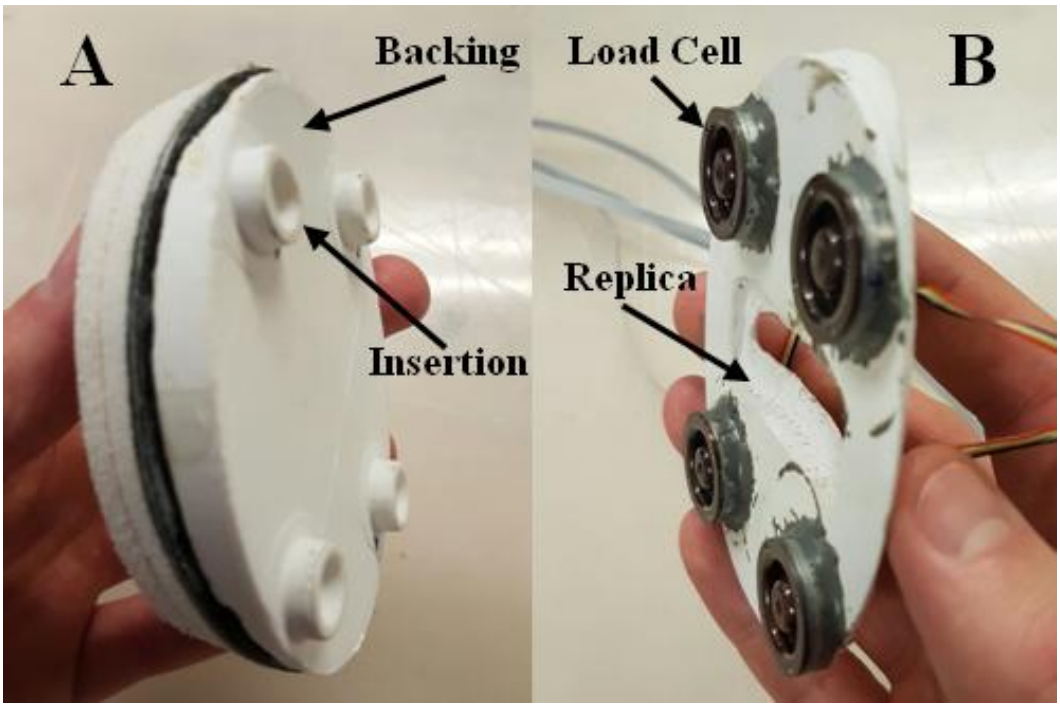

Figure 4-2 - A) The backing surface attached to the pad of the PCO, allowing a flat surface for the incorporation of the load cells on the sites of the four insertion points. B) The replica surface containing the load cells attached with epoxy.

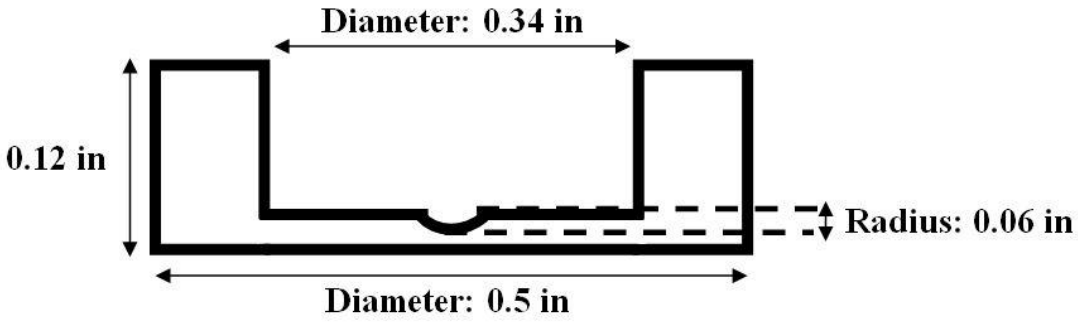

Figure 4-3 – Schematic used to fabricate the insertion points.

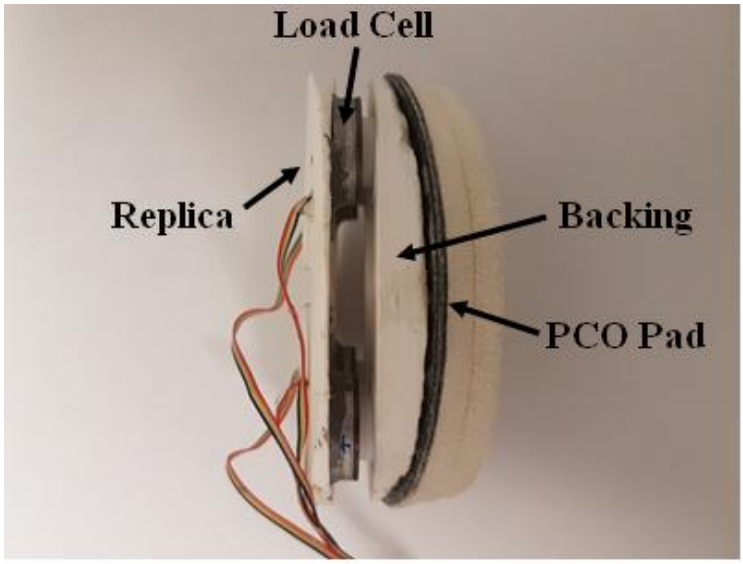

Figure 4-4 – The full assembly of Force Measurement System 3. The load cells on the replica surface inserted into the insertion points contained on the backing surface. The backing surface was glued onto the pad of the PCO.

The LED sensor was mounted onto the end of a wooden board with screws. The wooden board was then bolted to a tripod to ensure the LED sensor could be aligned proximally to the pad of the PCO (Figure 4-5). The tripod contained levels that allowed perpendicular alignment of the LED sensor to the pad of the PCO. An additional reflective surface was implemented to the aluminum bar of the PCO. This surface provided a larger area for the LED sensor to project its light onto (Figure 4-6).

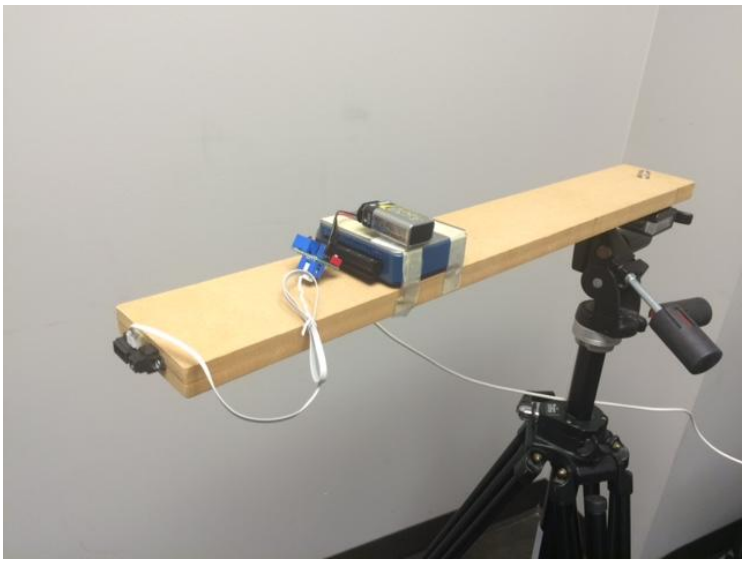

Figure 4-5 – The LED sensor mounted on the wooden board and tripod to allow proximal alignment to the pad of the PCO.

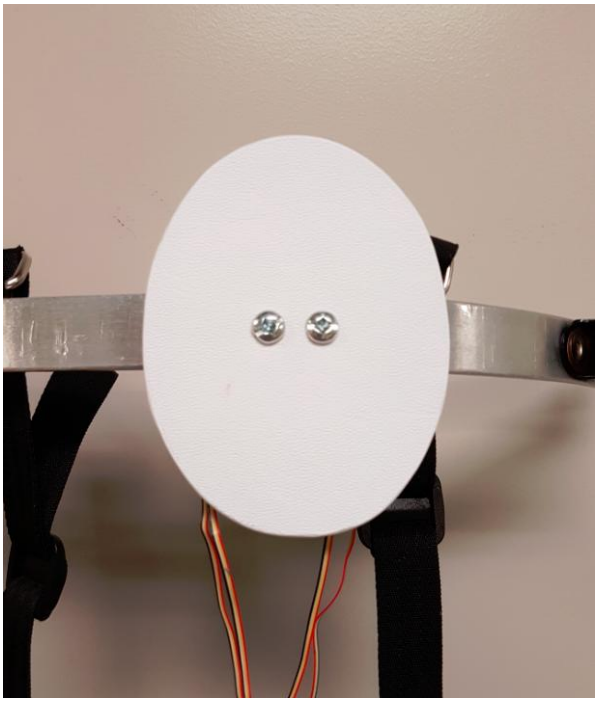

Figure 4-6 – The reflective surface attached anteriorly to the aluminum bar of the PCO. This allowed a larger surface area for the LED sensor to reflect off.

4.3 Load Cell Calibration

4.3.1 Balancing of the Load Cells

The output of FM3 was comprised of the outputs from the four individual load cells. Consequently, a pre-calibration step was required to ensure that the output voltage from each of the four load cells was similar at a certain force (i.e. within 0.02 V). Each load cell has a unique force-voltage relationship. The offset and gain of the voltage output for each load cell was adjusted to ensure that the force-voltage relationships for all four load cells were within the specified acceptable tolerance level. To elaborate, the output of a load cell can be defined as the linear relationship below:

$$V_{out} = AF + B \quad \textbf{(4.1)}$$

where A is the natural gain of the load cell, F is the force applied to the load cell, and B is the natural offset of the load cell. The natural gain and offset of a load cell is unique to itself, thus producing different force-voltage relationships. However, the natural offset of a load cell is generally miniscule and can be ignored. To ensure similar force-voltage relationships between multiple load cells, the natural gain and offset can be adjusted externally producing the following equation:

$$V_{out} = [G(AF)] + \mathrm{O} \quad \textbf{(4.2)}$$

where G is the externally adjusted gain, and O is the externally adjusted offset. With the ability to manipulate G and O, the load cells can be equalized to contain the same parameters (Figure 4-7).

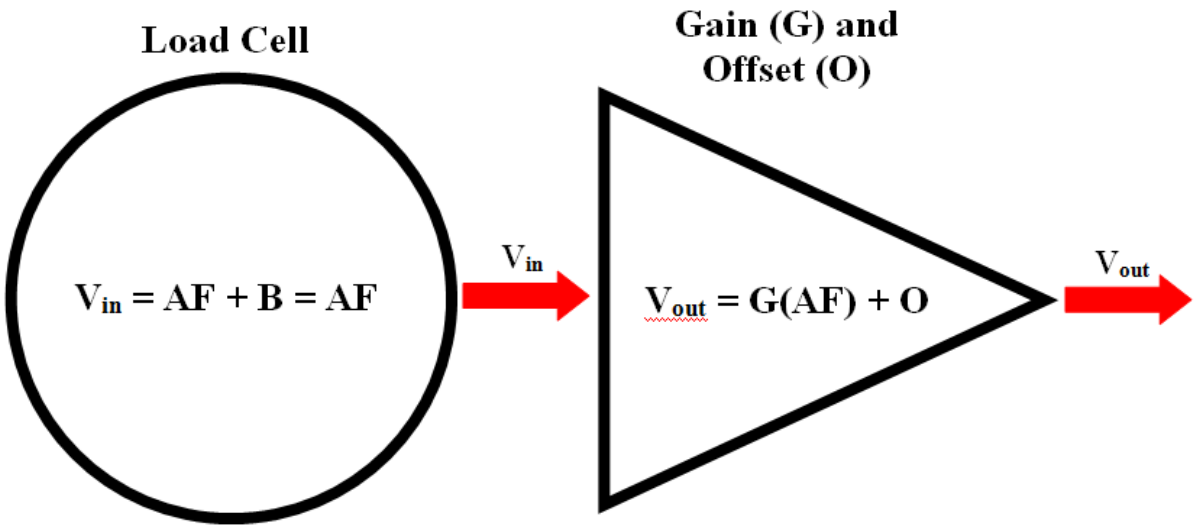

Figure 4-7 – A diagram outlining the process of adjusting the natural load cell gain and offset by manipulating an external gain and offset. This was performed to obtain similar load cell parameters.

The procedure used to balance the load cells involved placing FM3 into a MTS (Bose® 3220-AT) in Zymetrix® at the University of Calgary. To provide stability and full surface contact during load application to FM3, the pad (containing the backing) was placed on a plaster duplicate of the mould used to create the pad. All four load cells (adhered to the replica) were inserted into their specific insertion points. With no forces exposed to the system, the signal offsets for all four load cells were adjusted to obtain a signal output of 0.5 V (± 0.02 V). Afterwards, with all four load cells remaining in their insertion points, a force of 67 N (15 lbs) was applied by the MTS to one load cell at a time (i.e. directly above the specific load cell). The signal gain was adjusted for the corresponding load cell until 15 lbs produced an output of 4.5 V (± 0.02 V). The signal gain contained range from 66.65 kΩ to 115.60 kΩ. A range of 0.5 V to 4.5 V was chosen to ensure the load cell outputs would not reach their minimum and maximum outputs of 0 V and 5 V, respectively. This procedure was repeated for all load cells. Successful

completion of this procedure enabled appropriate summation of all four load cell outputs in order to finalize the calibration of FM3.

4.3.2 Calibration Protocol for Load Cell Calibration

Calibration of FM3 was performed using a custom made indenter. The shaft of the indenter was a rod of cylindrical shape. The base of the indenter consisted of a ½ inch diameter steel ball bearing welded to the cylindrical shaft. The size of the ball bearing was determined based on the size of the load cell. A ½ inch diameter ball bearing provided sufficient surface area to apply forces to the 1 inch diameter load cells. The ball bearing allowed a point pressure to be applied to the curved surface of the replica, whereas a flat surface would have applied an uneven force. Nine points of interest were investigated when applying forces to FM3: The centre of FM3 (Point #1), the four load cells (Points #2-5), and between each of the load cells (Points #6-9) (Figure 4-8).

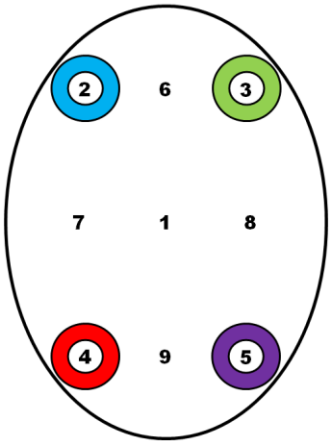

Figure 4-8 - Schematic of the pad and the nine locations (points) of force application when calibrating Force Measurement System 3. Each coloured circle represents a load cell.

For each location on the platform, forces were applied from 0 to 15 lbs in 1.5 lb increments, for a total of ten data points. A custom made Graphic User Interface (GUI) (National Instruments® LabVIEW) was used to numerically display the voltage outputs of all four load cells at a sample

rate of 100 Hz. At each force increment, data acquisition was delayed for 5 seconds to allow stabilization of the system. The displayed voltage outputs of all four load cells were acquired after the 5 seconds. Three consecutive trials of the entire force increment protocol were performed at a point location before changing to another location. The order that the locations were tested was in chronological order. Sums of all four load cell outputs, for all locations, were calculated and averaged at each force increment. Additionally, the individual outputs of each load cell were plotted at each position. This enabled assessment of the contribution of individual load cells to the overall sum of the load cell outputs. Although the load cells were balanced to provide similar outputs, the load cells may receive different forces due to their alignment with the insertion points on the backing surface. The perpendicular alignment of the load cells within the insertion points were performed by visual inspection. Therefore, a slight misalignment may have occurred when assembling FM3. This misalignment may influence the magnitude of compressive force that the load cell receives due to the force transfer occurring at a slight angle. To compensate for any contribution differences, a weighted sum was calculated using the following equation:

$$sum = w_1 l_1 + w_2 l_2 + w_3 l_3 + w_4 l = \sum_{1}^{4} w_i l_i \quad \textbf{(4.3)}$$

where w_i is the weight coefficient for each load cell output l_i. The weight coefficients are the only unknowns, and therefore four equations were required to solve for these four unknowns. Four equations were easily obtained by summing load cell outputs from four different force increments. However, in order to represent the range of measures from various points of load application quantified in the calibration there were a total of ninety equations (9 locations x 10 force increments). The least squares method was used to solve for the over determined system (ninety equations to solve for four unknowns). The sums of the four load cell outputs were

slightly different at every location at a specific applied force increment. However, the goal was to have the values remain as close as possible to the average sum at a specific applied force increment. The least squares method calculated the weights that obtain sums as close to these averages as possible for each of the ninety scenarios. Therefore, it minimized or enhanced the voltage outputs of each load cell to ensure they all had contributions to the sum relative to their individual outputs. The average and standard deviation of the sums for all locations, at each force increment, were plotted on a graph for comparison. The same data set after performing the least squares method was plotted on the same graph. A line of best fit was fit onto the least squares curve to produce an equation that converted the voltage sum of all four load cells to a pound force. This conversion equation was used for calculating the PCO forces in the remaining experiments.

4.3.3 Results of Load Cell Calibration

The independent load cell outputs successfully demonstrated the anticipated characteristics at the nine different force locations. When applying a force above a specific load cell, the greatest voltage output was generated from that specific load cell (Figure 4-9). At 15 lbs, it was expected that the load cell receiving the applied force would contribute approximately 4.5 V associated with the pre-calibration specifications. The outputs from each load cell at each location (# 2-5) under this condition were 4.13 (0.02) V, 4.60 (0.03) V, 4.22 (0.02), and 4.63 (0.08) (Figure 4-9).

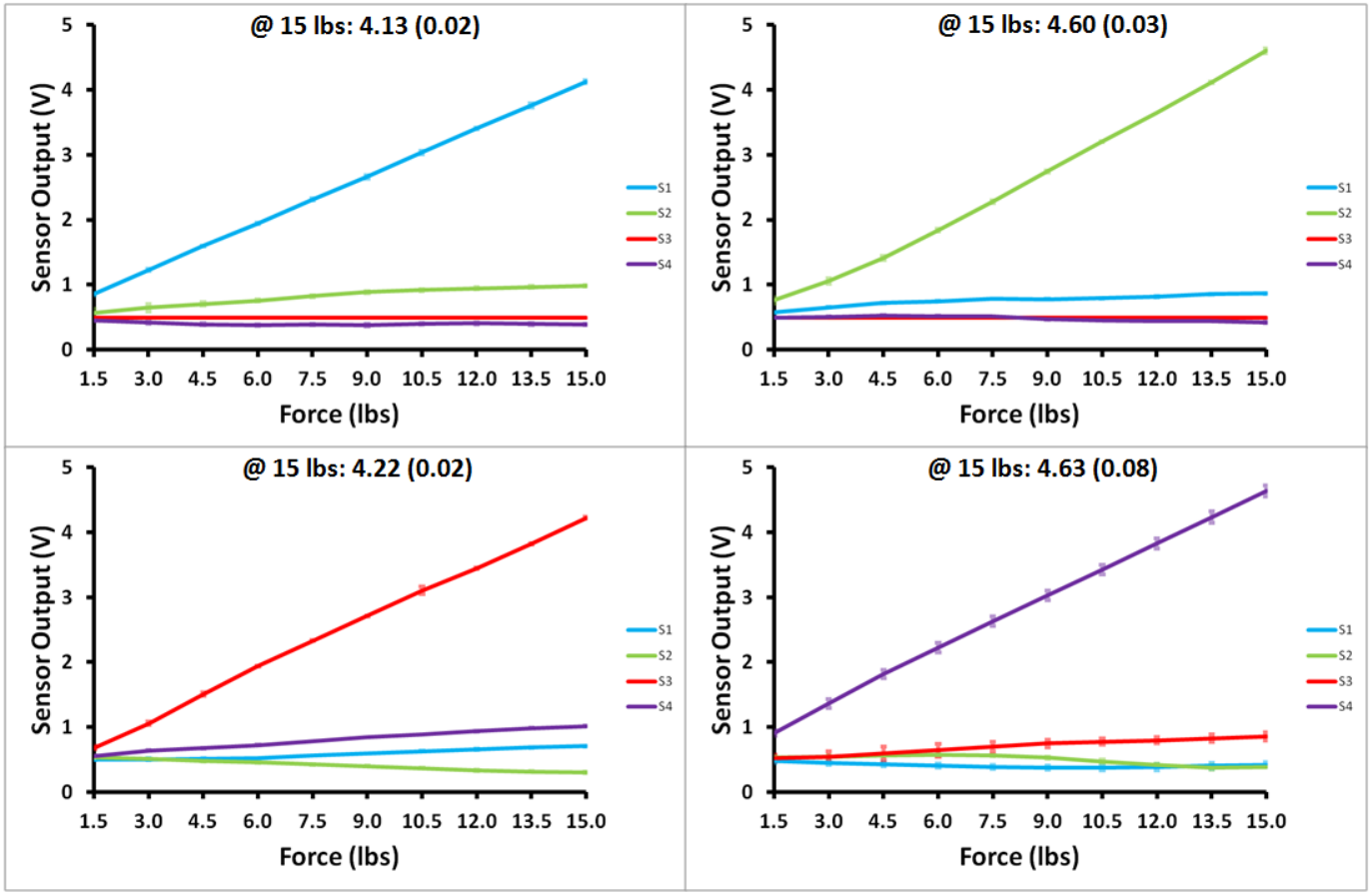

Figure 4-9 - Voltage outputs (and standard deviations) of all four load cells (S1 - S4) when the force application was above each load cell. An 'X' in the top left legend indicates the point of application for the specific graph. The output of the load cell receiving the applied force had the greatest contribution to the sum. The magnitude of the output at 15 lbs is shown for each load cell receiving the applied force.

When applying a force between the load cells, the two load cells closest to the applied force yielded the largest voltage outputs (Figure 4-10). At 15 lbs, it was expected that the sum of the two load cells with largest outputs would be 4.5 V. The summed outputs for force locations 6 to 9 were 2.14 (0.04) V, 5.23 (0.26), 5.06 (0.01) V, and 3.56 (0.06) V (Figure 4-10). Larger sums (~ 40-70 %) were seen when applying a force at the top (5.23 (0.26) V) and bottom (5.06 (0.01) V) of the PCO pad than the left (2.14 (0.04) V) and right (3.56 (0.06) V) of the PCO pad (Figure 4-10). When applying a force in the centre of FM3 (location #1), all four load cells had relatively similar outputs (Figure 4-11). At 15 lbs, the sum of all four load cells was 4.14 (0.05) V (Figure 4-11).

Using the methods of least squares, weighting factors of the load cells were calculated to be w_1 = 1.03, w_2 = 0.92, w_3 = 1.01, and w_4 = 0.93. Implementing the weights into equation (4.3, a new data set containing weighted sums was calculated at each force increment. An increase in variation with increased force was observed for both the original and weighted averages of the load cell sums (Figure 4-12). The variation in the original data ranged from 0.10 V to 1.14 V, with a mean of 0.61 (0.35) V. The variation in the weighted data ranged from 0.09 V to 1.10 V, with a mean of 0.58 (0.34) V. The least squares method was able to slightly decrease this variation by an average of 5.15 (2.14) %. Additionally, a leftward shift in the data occurred after performing the least squared method (Figure 4-12). A line of best fit was overlaid onto the weighted curve with R^2 = 0.99 (Figure 4-12).

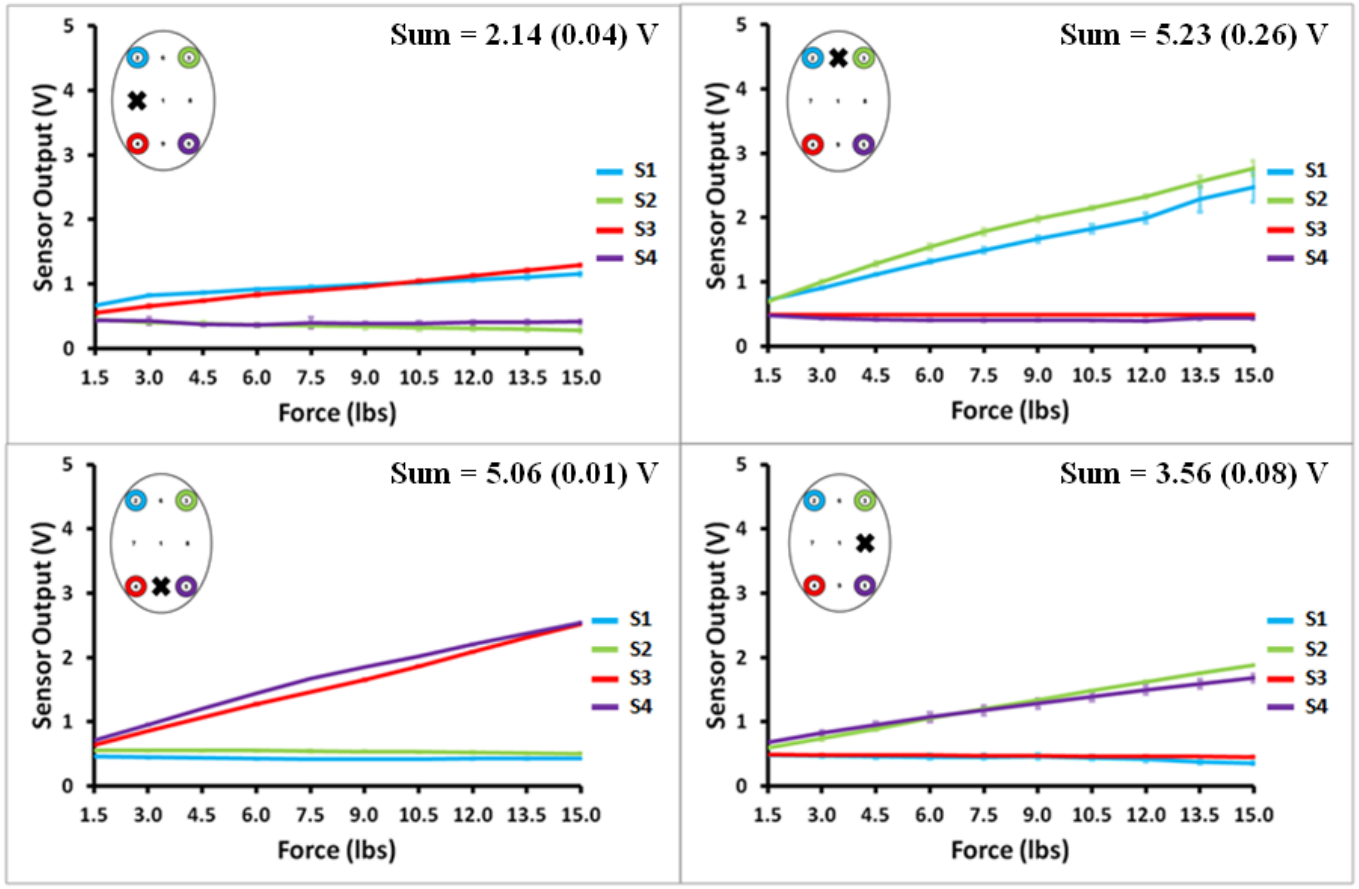

Figure 4-10 - Voltage outputs (and standard deviations) of all four load cells (S1 - S4) when the force application was between the load cells. An 'X' in the top left legend indicates the point of application for the specific graph. At 15 lbs, the sums of the two largest load cell outputs were calculated at each force location. Larger sums (~ 40-70%) were seen when applying a force at the top and bottom of FM3.

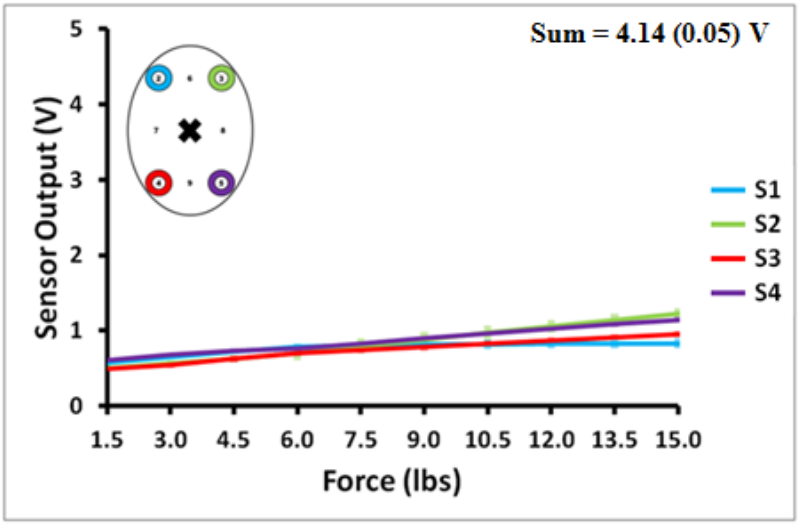

Figure 4-11 - Voltage outputs (and standard deviations) of all four load cells (S1 - S4) when the force application was in the center of the load cells. The sum of all four load cells at 15 lbs was 4.14 (0.05) V.

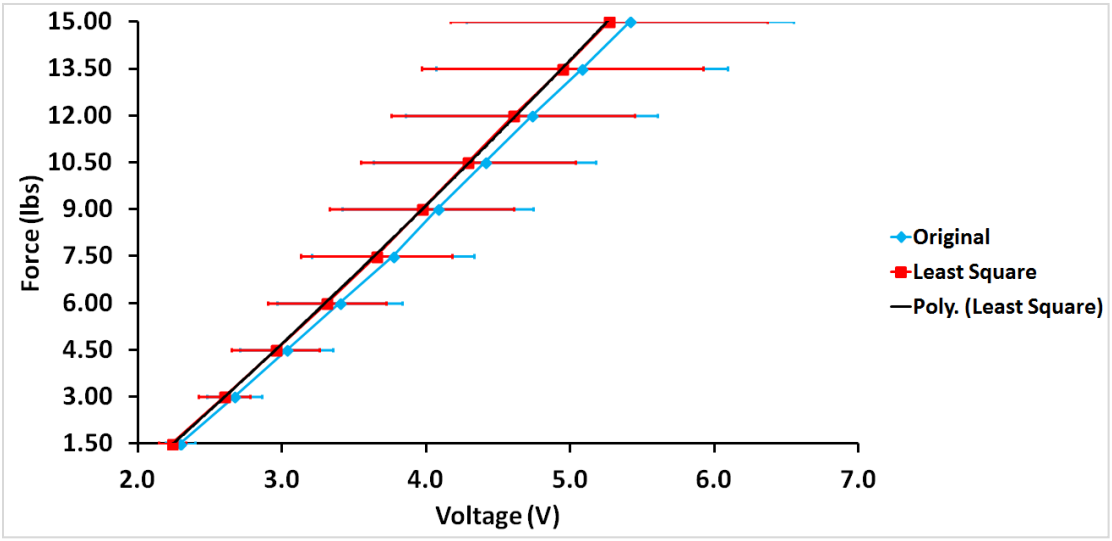

Figure 4-12 - Calibration curve and corresponding standard deviation of Force Measurement System 3. The blue line represents the original data before utilizing the least square method. The red line represents the data after performing the least squares method. The black line is the fitted line on the least square data, used for obtaining the equation that converts voltage to pound force.

4.3.4 Discussion of Load Cell Calibration

The four load cells were able to correctly distinguish the location of force application, as the voltage outputs were largest from the load cells nearest to the applied force. Additionally, the magnitudes from the largest load cell outputs at 15 lbs gave values close to the specifications of the pre-calibrated 4.5 V. However, applying a force at the top and bottom of the pad (locations 6 and 9) produced larger sums than the left and right of the pad (locations 7 and 8). This can most likely be attributed to the curvature of the pad and the mould it resided on (Figure 4-13). The apex of the curved mould ran along the length of the pad and acted as a fulcrum. Therefore, forces applied along this fulcrum (such as in location 6 and 9) provided no rotational moments to FM3 and compressive forces were applied to the load cells. However, forces away from the fulcrum (such as location 7 and 8) would create rotational moments to FM3, causing the forces to transfer to the load cells at an angle. The forces were no longer primarily compressive, influencing the outputs of the compressive load cells. This situation was not considered as a hindrance to the study, as the forces for the calibration were applied in a considerably smaller surface area than a pectus carinatum protrusion.

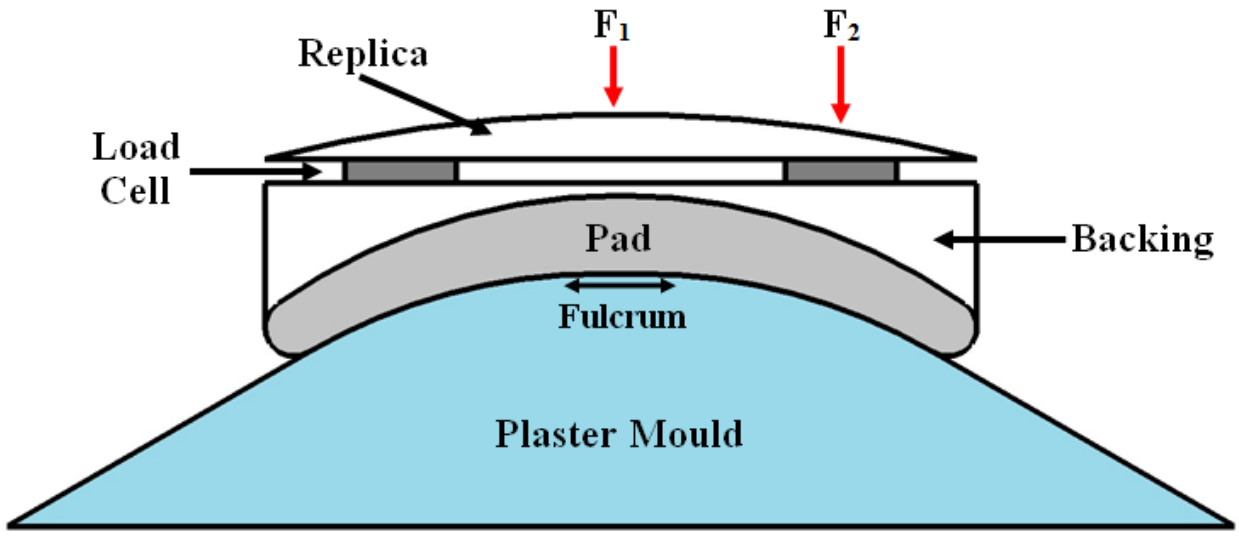

Figure 4-13 – The plaster mould providing the pad with full surface contact when applying loads. The apex of the mould acted as a fulcrum, providing rotational moments to forces that acted away from it (F_2). These rotational moments provided created forces that were no longer primarily compressive, altering the load cell outputs. Forces along the fulcrum (F_1) provided no rotational moments.

The weighting factors of all four load cells were within close proximity to 1, suggesting that the contribution of the load cells were relatively similar and that the force transfer from the insertion points to the load cells were similar. The calibration curve of FM3 showed that as the magnitude of force increased, so did the variation of the output. This was speculated to be caused by the two layers of foam contained in the pad. The two layers contain different durometers to each other, with the stiffer foam lying deep to the flexible foam. When applying increased forces, the force will eventually begin to deform the stiffer foam underneath. The recruitment of this stiffer foam will provide a slight resistance to the applied forces and alter the overall bulk stiffness of the pad. However, random areas of the pad may have greater deformation during each trial. The random areas of the pad that have greater deformation will have relatively higher recruitment of the

stiffer foam, which will alter the bulk stiffness of the pad in a non-uniform manner. The load cells nearest the stiffer areas will contain larger outputs. Therefore, the random recruitment of the stiffer foam during each trial may result in different outputs for all the load cells, thus increasing the variability of the sums.

The approach of applying the least squares methods to the original data enabled the variability of the data to be reduced by approximately 5.15%. This was expected as the goal of the least squares method is to produce weighting factors that optimize the data to produce the smallest error possible. Additionally, the least squares method shifted the calibration curve to the left. This was likely due to the weighting factors. Although all of the weighting factors were close to 1, two of the weighting factors were above 1 (w_1 = 1.03, w_3 = 1.01) and two were below 1 (w_2 = 0.92, w_4 = 0.93). Taking into account the difference of these magnitudes, w_1 and w_3 were closer to 1 and therefore did not have as much influence on the weighted sum as w_2 and w_4. Therefore, when applying the weighted factors into the sum, w_2 and w_4 reduced the magnitude of the corresponding load cell outputs. This results in a reduced overall sum of the load cell outputs, thus shifting the curve leftward.

4.4 LED Sensor Calibration

To calibrate the LED sensor, it was mounted onto a metal stand and placed onto a table containing a ruler with millimeter accuracy. The ruler was clamped to the table to ensure it did not move during data collection. A metal weight was used to act as a reflective surface for the LED sensor (Figure 4-14). White paper was taped to the weight as the LED sensor did not reflect properly on shiny surfaces. The metal weight was aligned with the LED sensor and ruler in a manner which would allow the ruler to read zero when the weight touched the edge of the sensor. Data acquisition began at distance zero on the ruler, and continued recording in 0.5 cm increments up to 15 cm. Afterwards, the metal weight was moved back towards the sensor in 0.5

cm increments. Data collection in between each increment was obtained at 1000 Hz for 1 second using the same custom GUI used to calibrate the load cell. Data at each increment was averaged. Two trials of the entire sequence were performed and then the data was averaged. A line of best fit with the largest R^2 value was fit to these points to create a calibration function. To evaluate the calibration function, the metal weight was placed at random distances from the LED sensor. Using the calibration function, the calculated distance was compared to the real distance. The sensitivity of the LED was also tested by moving the metal weight forward and backward by 1 mm during each random placement to determine if these changes could be detected. Ten trials were performed to evaluate the calibration function and test for the sensitivity of the LED sensor.

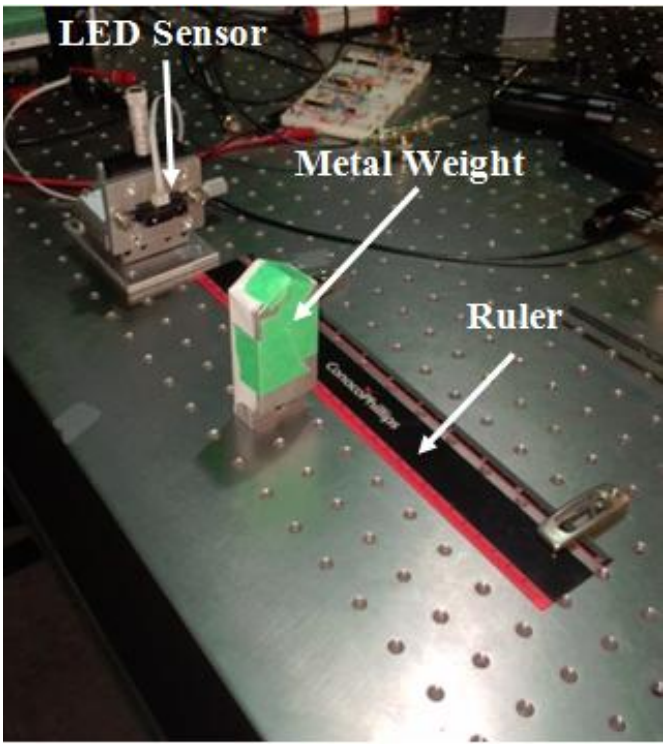

Figure 4-14 – Setup used to calibrate the LED sensor. The LED sensor was mounted onto a metal plate and reflected onto a metal weight covered with white paper. The ruler allowed for known distances of the metal weight.

4.4.1 Results of the LED Sensor Calibration

Two divisions of the LED sensor were found during calibration. These divisions of the LED sensor are referred to as the ascending limb and descending limb (Figure 4-15). The majority of the data points (77%) fell under the descending limb resulting in a conversion equation for that division of data. When evaluating the conversion equation, differences between the observed and calculated values ranges from 0.02 – 0.26 cm, with an average difference of 0.12 cm (0.07) (Table 4-1).

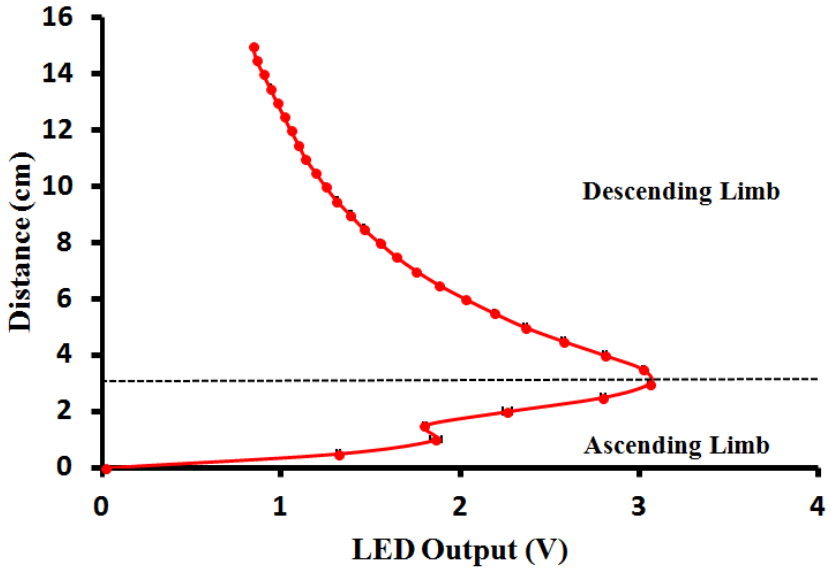

Figure 4-15 - Calibration curve of the LED sensor. Averages between trial one and trial two are plotted with SD bars. Once reaching approximately 4 cm, the voltage began to decrease as distance increased.

Table 4-1 - The difference between the observed and calculated outputs when testing the conversion equation of the LED sensor.

Trial	Distance (cm)		
	Real	Calculated	Absolute Difference
1	11.60	11.47	0.13
2	8.20	8.09	0.11
3	18.80	18.82	0.02
4	13.70	13.44	0.26
5	9.70	9.60	0.10
6	15.10	14.94	0.16
7	6.40	6.33	0.07
8	8.50	8.41	0.09
9	18.00	17.83	0.17
10	10.30	10.21	0.09
		Average (SD)	0.12 (0.07)

Additionally, the LED sensor was sensitive to 1 mm changes. When moving the metal weight 1 mm forward, the difference between the original calculated value and the new calculated value ranged from 0.00 – 0.15 cm with an average of 0.07 (0.06) cm (Table 4-2). A similar result was seen when moving the weight 1 mm backward, with differences ranging from 0.00 – 0.45 cm with an average of 0.15 (0.13) cm (Table 4-3).

Table 4-2 - The difference between the original calculated output and the outputs of the LED sensor when the reflective surface was shifted forward 1 mm.

Trial	Distance (cm)		
	Calculated	1 mm Forward	Absolute Difference
1	11.47	11.47	0.00
2	8.09	7.98	0.10
3	18.82	18.82	0.01
4	13.44	13.44	0.00
5	9.60	9.46	0.14
6	14.94	14.83	0.11
7	6.33	6.26	0.07
8	8.41	8.30	0.11
9	17.83	17.82	0.01
10	10.21	10.05	0.15
		Average (SD)	0.07 (0.06)

Table 4-3 - The difference between the original calculated output and the outputs of the LED sensor when the reflective surface was shifted backward 1 mm.

Trial	Distance (cm)		
	Calculated	1 mm Backward	Absolute Difference
1	11.47	11.67	0.20
2	8.09	8.19	0.11
3	18.82	18.82	0.00
4	13.44	13.71	0.27
5	9.60	9.74	0.14
6	14.94	14.94	0.00
7	6.33	6.46	0.14
8	8.41	8.52	0.11
9	17.83	18.29	0.45
10	10.21	10.31	0.10
		Average (SD)	0.15 (0.13)

4.4.2 Discussion of the LED Sensor Calibration

The calibration of the LED sensor was found to contain two divisions, the ascending limb and the descending limb. The descending limb of the LED sensor was used to obtain the conversion equation for data acquisition. This was due to the descending limb containing the majority of the data points. With the descending limb beginning at an approximate distance of 4 cm from the LED sensor, future studies ensured the LED sensor was placed at least 4 cm away from the reflective surface. The conversion equation for the LED sensor contained small errors (~ 1 mm) when comparing the observed and calculated distances. Additionally, the LED sensor seemed to be capable of detecting millimeter changes in the distance of the metal weight. However, these changes may have been due to the conversion equation errors as the errors were within the 1 mm range. Regardless, the magnitudes of these errors were not large enough to have the ability to influence the subsequent protrusion stiffness calculations.

4.5 Evaluating Force Measurement System 3

Prior to applying FM3 within the PCO and testing this on participants for the full study, it was important to assess two key features that formed the foundation of the study. One study objective was to determine the relationship between the PCO force applied and the corresponding displacement of the PC deformity. This relationship was determined as protrusion stiffness in this study. Second, participants are required to replicate the clinically prescribed force (CF) as closely as possible when wearing the PCO. It is important to understand the baseline variability of the participant applied force (PF) to the PCO, when conducting longitudinal follow-up studies. Consequently, a pilot study was conducted to evaluate FM3 with two SAs:

1) To determine if FM3 could appropriately measure stiffness values.

2) To obtain preliminary data of how closely the participants could follow their clinically prescribed force (CF).

4.5.1 Methods

4.5.1.1 Stiffness Measurements

A mannequin (different model than the CPR mannequin previously used in Section 3.4) was used to act as a surrogate patient with PC. The mannequin was used in replacement of human participants to control the stiffness of the protrusion. Three foams of different stiffness values were fabricated into the shapes of protrusions that could be attached onto the mannequin using double sided tape. The foam stiffness values were characterized subjectively and qualitatively into a hard, medium, and soft stiffness. Using a PCO containing FM3 and the previously calibrated LED sensor force and displacement measurements were obtained for all three foam protrusions. The calibration of the LED sensor revealed two limbs – ascending and descending – in the voltage outputs (refer to Appendix A, Section A.3.) The conversion equation produced for the LED sensor was obtained from the descending limb as it contained the majority of the data points. Therefore, the LED sensor was placed at least 4-6 cm away from the PCO pad to ensure the outputs were within the descending limb. This avoided any LED sensor outputs occurring in the ascending limb, which could lead to errors in the data. A total of five consecutive trials were obtained for one foam protrusion (stiffness value) before switching to a different foam protrusion (stiffness value). A custom made GUI (National Instruments® LabVIEW) was used to collect both force and displacement data simultaneously synchronized at 100 Hz.

The stiffness of the foam protrusion was determined based on the relationship that force is equal to the stiffness multiplied by the displacement of the protrusion. To calculate the stiffness magnitude for a single foam protrusion, a polynomial line of best fit (degree of two) was first calculated for each of the five force and displacement trials. A degree of two was chosen as the force and displacement of the human chest wall was reported to have a non-linear relationship (Gruben et al., 1993). Next, the lines of best fit were plotted onto a force-displacement graph to

produce five curves. A line of best fit with the largest R^2 value was fit onto the five force-displacement curves to obtain an overall force-displacement curve. The derivative of the overall force-displacement curve was obtained, representing the slope of the foam protrusion (i.e. stiffness). This protocol was repeated for all three foams.

4.5.1.2 Clinically Prescribed Force and Participant-Applied Force

Five male participants were recruited by Braceworks to validate the new system (14.6 ± 1.5 yrs). All but one participant had worn the PCO for at least 2 months. All participants provided informed consent to take part in the pilot study.

On the day of testing, the participant initially underwent their original appointment with the clinician to ensure any required adjustments to the PCO were performed. At the beginning of testing, once the PCO was adjusted, the original pad of the PCO was substituted with FM3 to collect both the CF and PF. To obtain the CF, the clinician tightened the PCO to the participant to the magnitude deemed appropriate. With the participant standing against a wall (heels and back touching the wall), the CF was recorded for 10 s at 100 Hz (displacement was not measured when collecting the CF). Only one trial of the CF was performed to closely follow the 'Calgary Protocol', in which the participant is exposed to the CF once in a regular assessment. Multiple trials of the CF were believed to potentially produce a training effect for the participant, allowing them to recall the CF easier. After the CF was collected, the participant was asked to loosen the PCO while it remained on the torso. Next, to acquire the PF, the participant tightened the PCO to their best approximation of the CF. The PF was recorded for 10 s at 100 Hz. The process of the participant loosening the PCO and then tightening again to replicate the CF to the best of their ability was repeated so that a total of five trials of the PF were collected.

Data for both the CF and PF were averaged over the 10 s (100 Hz) interval to obtain an average force per trial. For the five PF trials, the forces were averaged further to obtain a final average

and standard deviation of the PF. This step was not performed with the CF as only one trial was obtained.

4.5.2 Results

When tightening the PCO to the mannequin, the force data was observed to increase with all trials for all three foam protrusions (Figure 4-16). However, in certain trials the displacement data showed signs of movement artefacts during tightening of the PCO. The movement artefact consisted of the foam protrusion moving towards the LED sensor instead of further away (Figure 4-17). These movement artefacts could occur at any time during a trial.

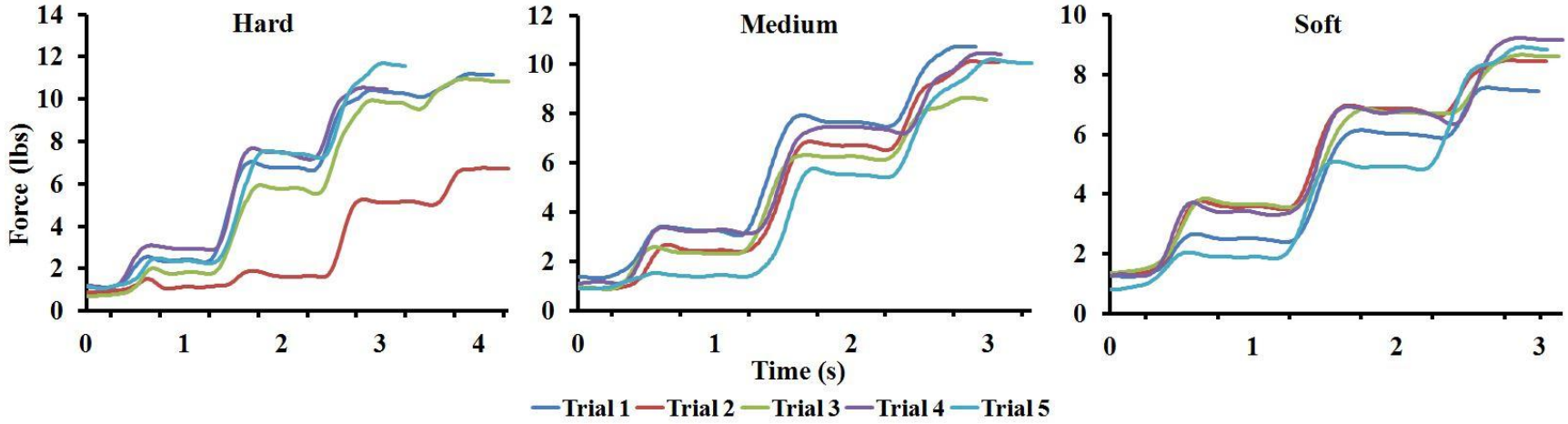

Figure 4-16 – The force data acquired when tightening the PCO on the mannequin. All five trials, for each foam protrusion, are illustrated. The force always increased as the PCO was tightened.

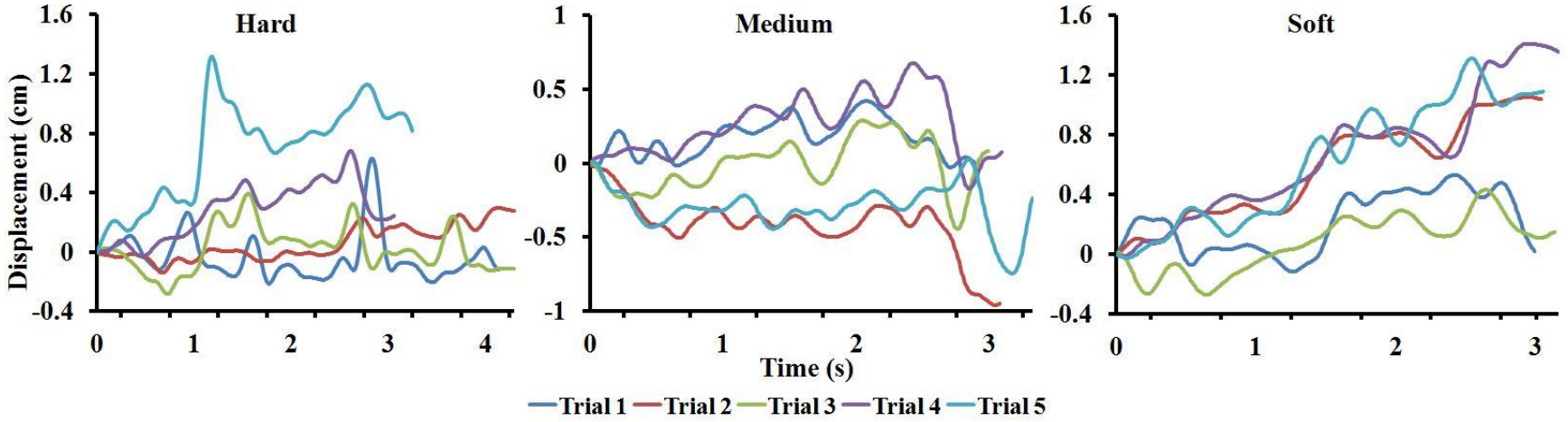

Figure 4-17 - The displacement data acquired when tightening the PCO on the mannequin. All five trials, for each foam protrusion, are illustrated. The displacement data showed movement artefacts within certain trials. For example, Trial 2 (red) using the medium foam protrusion showed that the displacement decreased as the PCO was tightened. These movement artefacts could occur at any point in time during a trial.

Plotting the force and displacement together, two obstacles were observed when reviewing the force-displacement curves of the three foam protrusions. First, it was discovered that the initial displacement of the foam protrusion would frequently reside within the negative ranges for all foams (Figure 4-18). Secondly, the force-displacement curves appeared to have a parabolic shape in certain trials. The inflection point of the parabolas differed between trials, with some occurring midway through data acquisition (Figure 4-18) and others near the end of data acquisition (Figure 4-19).

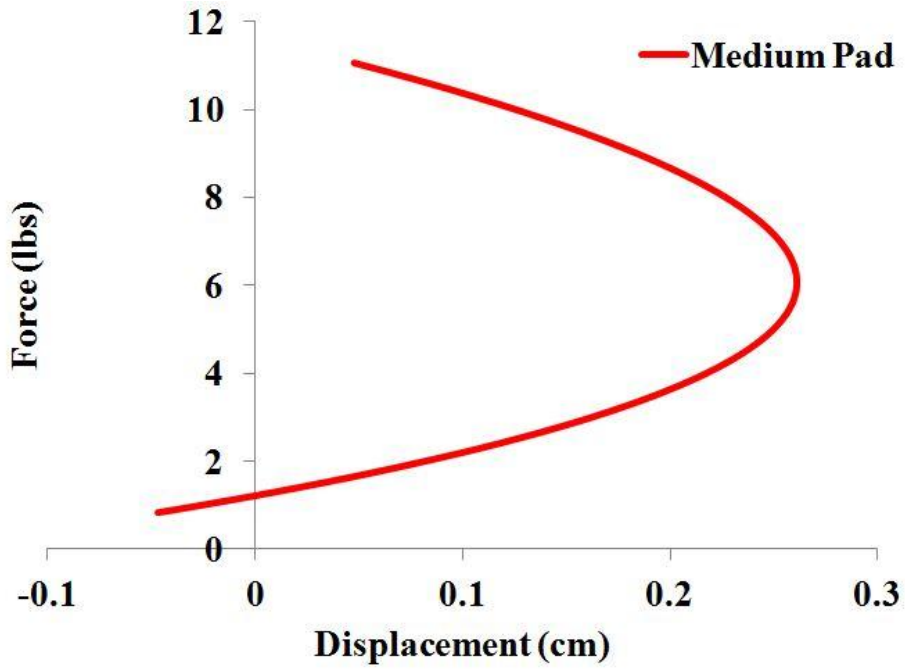

Figure 4-18 – Example of a trial (for the medium foam protrusion) with initial negative displacement. This example also illustrates a parabolic shape where the inflection point occurred midway through data acquisition.

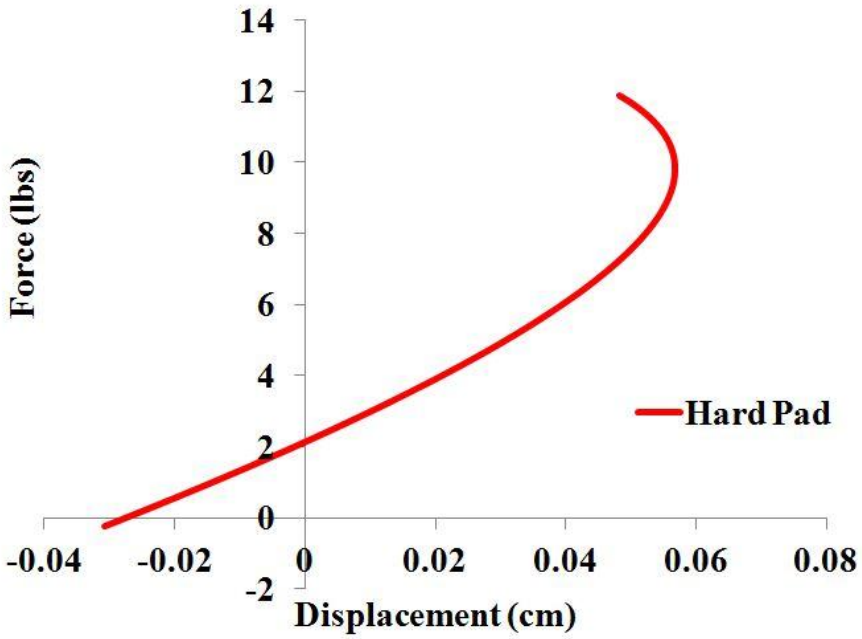

Figure 4-19 – Example of a trial (for the hard foam protrusion) that contained a parabolic shape where the inflection point occurred near the end of data acquisition.

Trials containing these obstacles were "treated" before obtaining the average force-displacement curve. The process of "treating" the trials is discussed in the next section (4.5.3). Before the "treating" process, the average force-displacement curve for the hard, medium, and soft foam protrusions contained an R^2 value of 0.06, 0.00, and 0.42, respectively. The "treating" process excluded trials 1 and 3 from the hard foam protrusion (Figure 4-20), and trials 2, 3, and 5 from the medium foam protrusion (Figure 4-21).

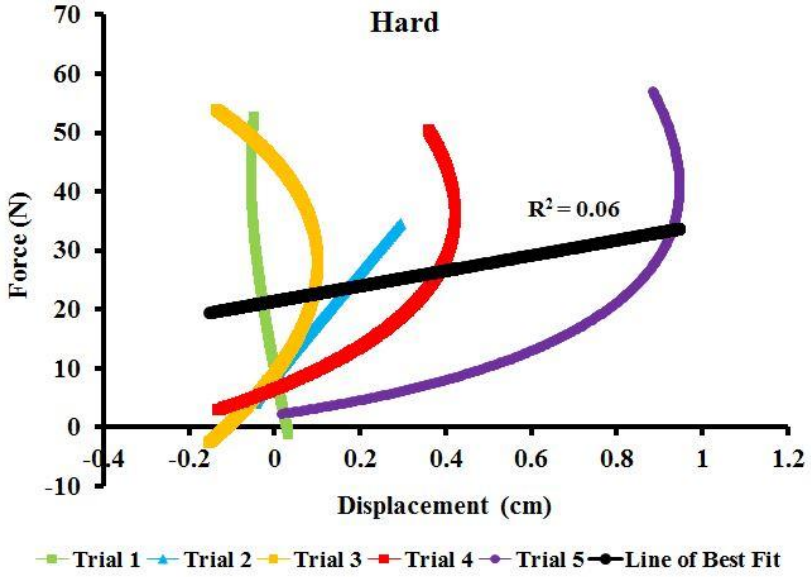

Figure 4-20 – All five trials of the force-displacement curves for the hard foam protrusion. Trials 1 (green) and 3 (orange) were excluded as they contained movement artefacts. A line of best fit contained an R^2 value of 0.06.

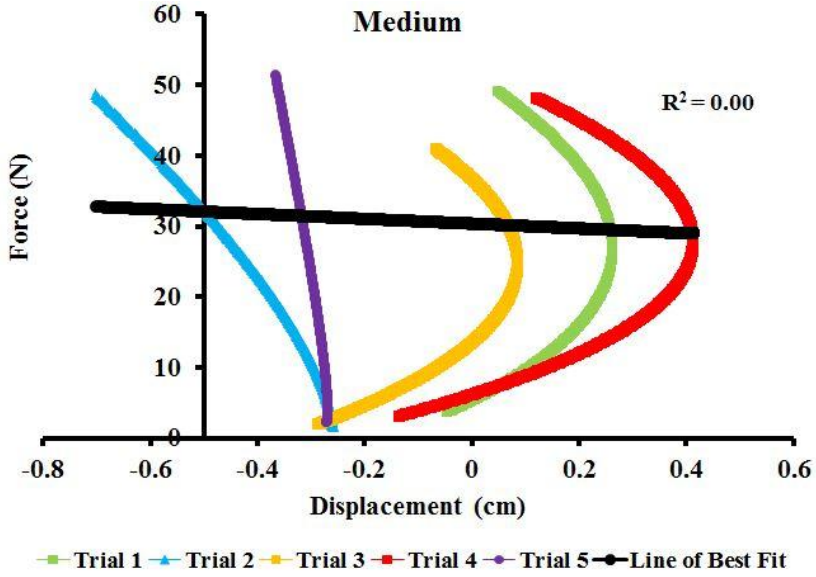

Figure 4-21 - All five trials of the force-displacement curves for the medium foam protrusion. Trials 2 (blue), 3 (orange), and 5 (purple) were excluded as they contained movement artefacts. A line of best fit contained an R^2 value of 0.00.

No trials were excluded from the soft foam (Figure 4-22). Therefore, the numbers of trials remaining for analysis were three, two, and five for the hard, medium, and soft foam protrusion, respectively. After the "treating" process, the stiffness measurements for the hard, medium, and soft foams were determined to be 6.18 kN/m (R^2 = 0.42), 5.88 kN/m (R^2 = 0.53), and 1.45 kN/m (R^2 = 0.48), respectively (Figure 4-23). The average force-displacement curve for all three foam protrusions showed an increase in the R^2 value after the “treating” process (Table 4-4).

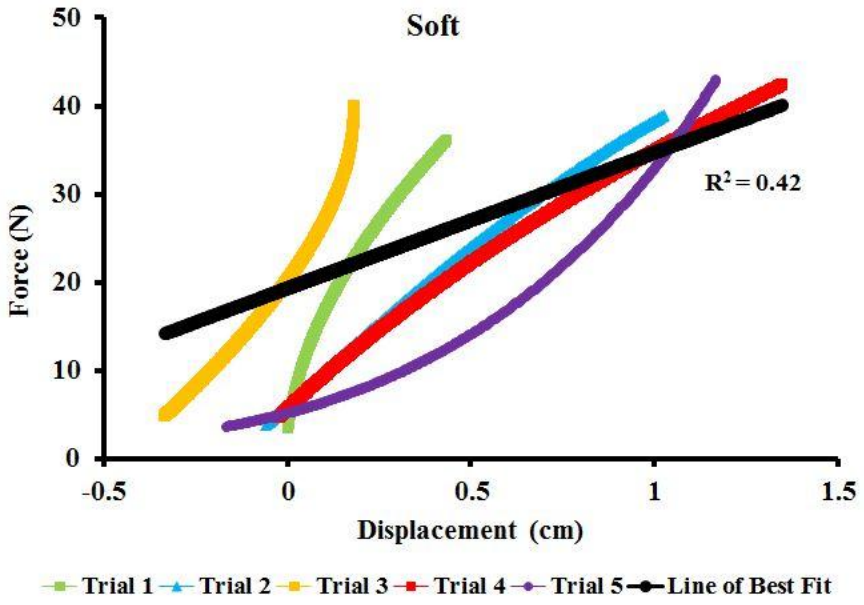

Figure 4-22 - All five trials of the force-displacement curves for the soft foam protrusion. No trials were excluded as they contained no movement artefacts. A line of best fit contained an R^2 value of 0.42.

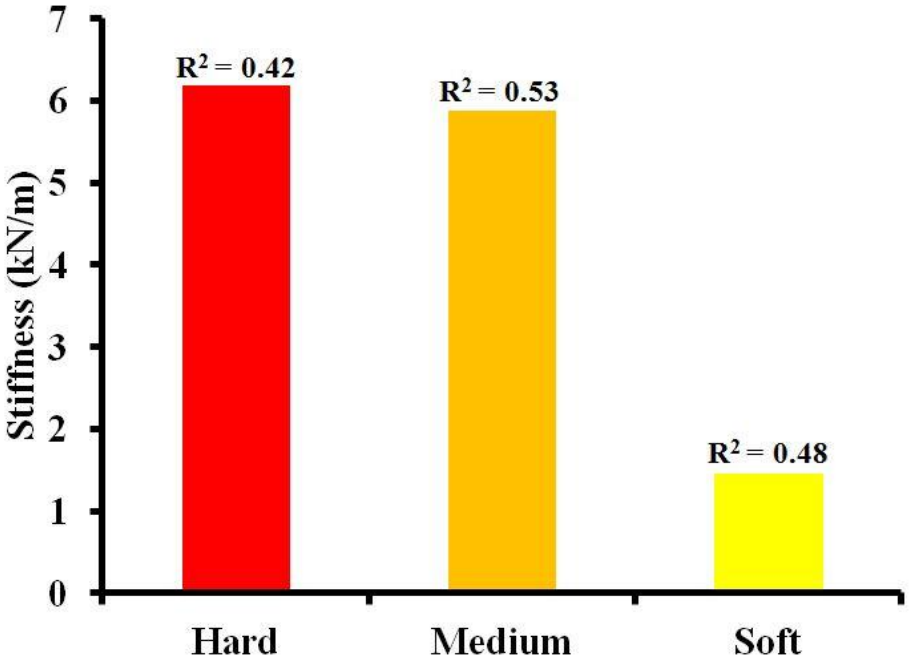

Figure 4-23 – Stiffness magnitudes for the hard, medium, and soft foam protrusion and the corresponding R^2 values for the line of best fit after "treating" the data.

Table 4-4 – R^2 values of the average force-displacement curves before and after the "treating" process.

Foam Protrusion	R^2 Value	
	Before "Treating"	After "Treating"
Hard	0.06	0.42
Medium	0.00	0.53
Soft	0.42	0.48

Using the calibrated PCO on volunteer participants, the force applied by the clinician (CF) using the Calgary Protocol ranged from 3.92 lbs to 6.42 lbs (Figure 4-24), with a mean of 5.21 (0.95) lbs. The results for the individuals in attempting to replicate the CF revealed interesting differences between the participants and the clinician in abilities and approaches to apply forces to the PCO. Firstly, none of the individuals were able to replicate the target CF within 1-2%. The individual applied PF values ranged from 4.30 to 8.91 lbs, with a mean of 6.60 (1.87) lbs. The PF exceeded the CF in all cases. Differences between the PF and the CF ranged from 0.38 to 3.11 lbs, with a mean of 1.39 (1.07) lbs. This translated to all participants ranging from 9.57 to 53.56% above the CF, with a mean of 25.07 (16.98) %. One participant was considered to "over-tighten" the PCO, applying a force 50% greater than the CF (Figure 4-24). Finally, all individuals were successfully able to replicate their PF with high repeatability. Within-participant variation ranged from 0.27 to 1.07 lbs, with a mean of 0.52 (0.33) lbs. This within-participant variation was substantially smaller than the difference between the PF and the CF of 1.39 (1.07) lbs.

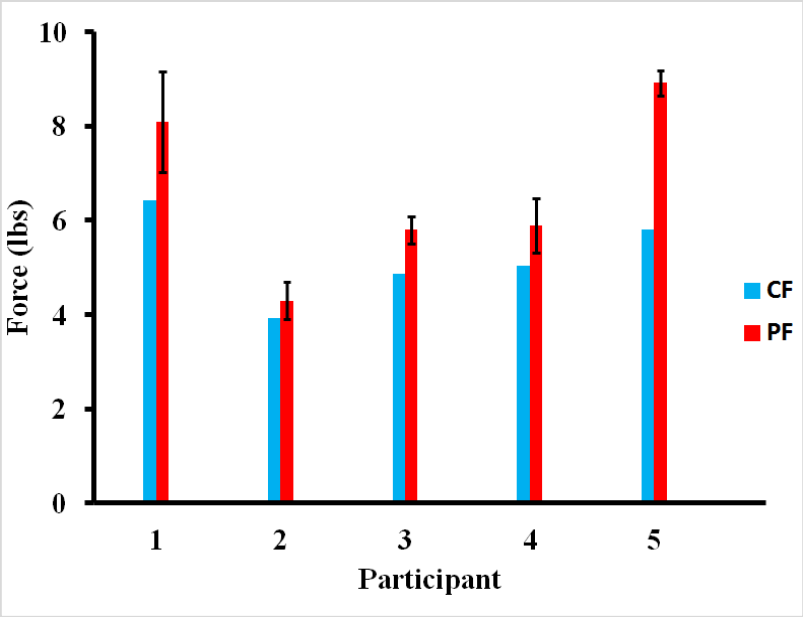

Figure 4-24 - Mean and standard deviation of the clinically prescribed force (CF) and participant-applied force (PF) for each participant.

4.5.3 Discussion

The simultaneous measurements of FM3 and the LED sensor were able to distinguish the stiffness magnitude of each foam protrusion relative to one another. However, these stiffness values were achieved after accommodating for two obstacles found within the data: 1) the initial negative displacement of the foam protrusion, and 2) the parabolic shapes of various force-displacement curves. The force trials provided appropriate data, as the force increased while the PCO was tightened. However, the displacement data showed movement artefacts, thus resulting in the mentioned obstacles. The initial negative displacement was considered to originate from the PCO being loose at the start of data acquisition. With no tension on the straps of the PCO, the pad of the PCO had the ability to shift forward towards the LED sensor. This provided the illusion that the foam protrusion was displacing towards the sensor and not away. To eliminate this obstacle, any initial negative displacements within the force-displacement curves were

removed from the data. The parabolic shapes in various trials were speculated to originate from the rotation of the PCO pad. The foams contained a convex curvature to represent a pectus carinatum (PC) protrusion. As the PCO was tightened, there was potential for the PCO pad to rotate along the apex of the foam protrusion curvature once a sufficient force was achieved to do so. If the LED sensor was reflecting on the end of the pad that rotates towards it, an illusion that the foam protrusion is displacing toward the LED sensor would have been observed. The location of the PCO pad may shift with each trial, thus resulting in different time points where the rotation may begin with the result being the parabolic shape. This obstacle was accommodated for by removing any data past the inflection point of the parabolic shape. For future analysis in this study, if the inflection point began midway through data acquisition the entire trial would be removed. An increase in the R^2 value for the average force-displacement curve was observed when implementing the exclusion criteria to the data of the foam protrusions. The average force-displacement curves with a larger R^2 values were speculated to represent a more valid representation of the foam protrusions. Therefore, these exclusion criteria were used for the remainder of the study when FM3 and the LED sensor were applied to human participants to "treat" the data before analysis.

Using FM3 incorporated into the PCO on participants to measure the CF and the PF, it was observed that the PCO applied force ranges remained within the previously reported data using FM1 (Section 0). With FM1, it was speculated that the PCO forces would range from 4 to 8 lbs. The results of this pilot study demonstrated that both the CF and the PF remained within the speculated range. The CF ranged from 3.92 to 6.42 lbs, and the PF ranged from 4.30 to 8.91 lbs. Additionally, comparing the PF to the CF provided interesting results. All participants applied the PCO at a larger force than the CF. Within this small sample size of participants, it is

interesting that over-tightening by approximately 50% above the CF occurred in one of these individuals. Furthermore, the repeatability of the PF was high; with the variability of the PF being smaller than the difference between the PF and the CF. These repeatability results reinforced the findings that the PF was larger than the CF, as the participants were able to repeatedly produce a force that was greater than the CF. Force feedback is clearly needed to mitigate unintentional excessive force applications.

4.6 Conclusions with Force Measurement System 3

The goal of the first SA was to develop a force measurement system that could measure the PCO forces. The development and evaluation of FM3 has clearly demonstrated that it is a reliable system and can successfully measure PCO forces. These forces have not been previously reported in literature and no attempt has been reported to develop a device to measure these forces. For the first time, an instrumented system will be used to measure PCO forces and displacements throughout the course of treatment. FM3 is the starting point for developing a force measurement system that can provide feedback to both the clinician and the patient. This system will ultimately assist in ensuring that the received CF is being accurately replicated and followed throughout the prescribed treatment leading to improved patient care.

Chapter Five: Methods

FM3 demonstrated to be a successful system in measuring PCO forces and thus satisfied the first SA. With this system in place, this chapter discusses the methods used to address the remaining two SAs: 1) determine relations between the clinically prescribed force (CF) & participant applied force (PF), protrusion stiffness (PS) & PF, and PS & correction rate (CR), and 2) determine the effect of time on PF and PS. These form the primary study of this research.

5.1 Study Participants

Eleven male participants were recruited by Braceworks for the study. Demographics of the participants were obtained (Table 5-1). Informed consent was provided by all the participants. Participants aged 10 to 18 years diagnosed with PC were considered the inclusion criteria for the study. Adolescents were recruited as they are most likely to respond to the PCO protocol. PC is usually corrected surgically at older ages as the protrusion becomes too stiff to compress, and younger children may not be able to comprehend the protocol assigned with the PCO. Inclusion criteria also required the PC protrusion to be located approximately central to the body of the sternum (i.e. chondrogloadiolar), as the PCO is unable to correct the deformity if it is located at the manubrium of the sternum.

Children with PC protrusions not located centrally on the chest (e.g. manubrium), females with more advanced pubertal development (requiring modified version of PCO), Marfan's Syndrome, Ehlers-Danlos Syndrome or other major disorders that affect the mechanics of the thoracic region were excluded from the study. Children with transportation aids (wheelchairs, scooters) were also excluded as participants were required to stand during data collection.

Table 5-1 - Mean and standard deviation of participant demographics.

	Mean	SD
Age (yrs)	14.09	1.38
Height (cm)	169.73	6.92
Weight (kg)	50.73	3.47

5.2 Protocol

Data collection occurred at three time points: 1) the fitting appointment of the PCO, 2) a one month follow-up appointment, and 3) a two month follow-up appointment. The first follow-up appointment, according to the Calgary Protocol, is scheduled two months post fitting. However, in this study, a one month follow-up appointment was included to determine whether a trend could be identified earlier in the course of treatment. Four participants were not included in the two month time point analysis due to time restrictions. Additionally, one participant was not included in the one month time point analysis due to lack of availability of participant. This resulted in a total of 28 data collection periods (11 at the fitting, 10 at the 1 month follow-up, and 7 at the two month follow-up), with some gaps in data for some individuals. Clinically prescribed force (CF) was collected during the fitting appointment only to follow the Calgary Protocol, where the clinician prescribes the force only at the fitting. Participant-applied force (PF), displacement, and anterior-posterior (AP) depth measurements were collected at every time point.

5.2.1 Data Collection

On the testing day, the participant's regular fitting/follow-up appointment with the clinician was performed first. During the appointment, any adjustments and repairs to the PCO were completed to ensure that the PCO fit and maintained proper function. Following the clinician appointment, the AP depth of the participant's torso was measured five times using the standard

clinical measure of calipers (Model 220335, Fillauer©, Chattanooga, Tennessee). Based on the standard clinical technique, the calipers were aligned with the apex of the protrusion. Following the AP depth measurements, the original pad of the PCO was substituted with FM3 (Figure 5-1). A white, plastic surface was attached to the front of the PCO to act as a reflective surface for the LED sensor, allowing displacement measurements of the protrusion to be obtained (Figure 5-1). The participant was positioned standing against a wall in a neutral position (heels and back touching the wall with arms to the side). The participant standing against a wall ensured minimal movement of the torso when tightening the PCO. A tripod containing the LED sensor was placed 6 cm away from the pad, ensuring it was in line with the center of the reflective surface. Levels on the tripod allowed the LED sensor to align approximately perpendicular to the pad (Figure 5-2). Due to the protrusion geometry, the pad was not always parallel with the protrusion. Therefore, perpendicular alignment of the LED sensor was performed qualitatively.

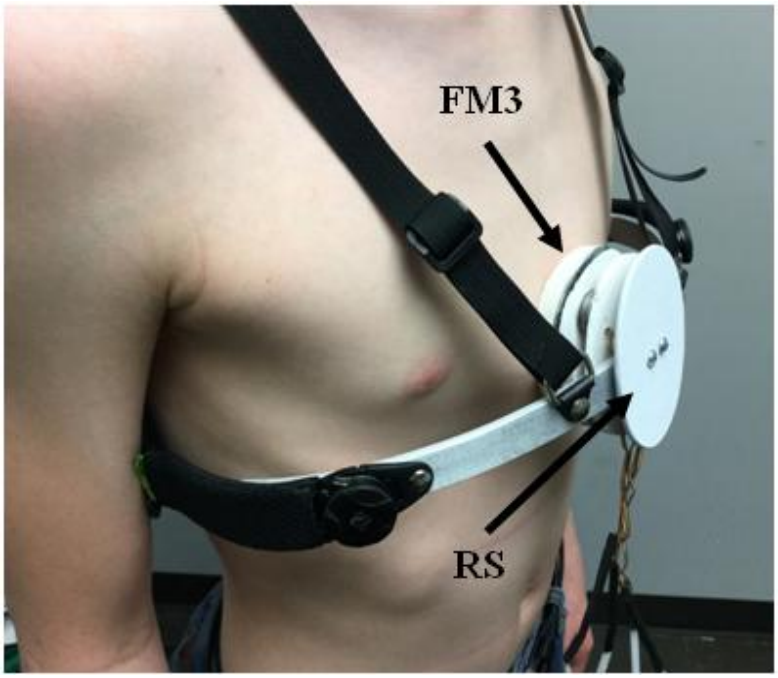

Figure 5-1 - The instrumented pad (FM3) containing the four load cells FM3 and a white, reflective surface for the LED sensor (RS).

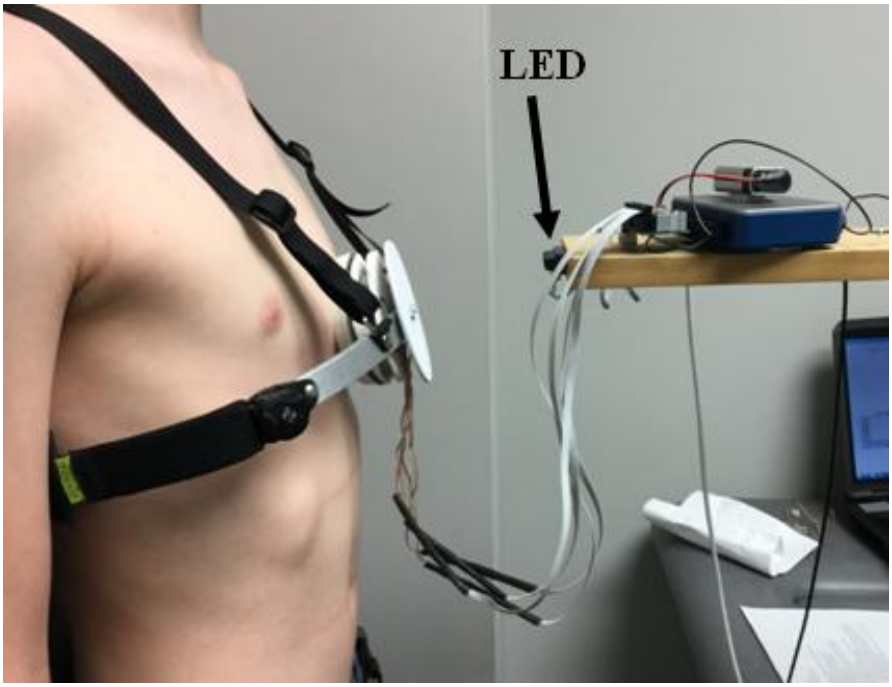

Figure 5-2 - Alignment of the LED sensor to the white, reflective surface on the PCO

CF was the first outcome variable collected (only if it was a fitting appointment). The clinician tightened the PCO to the participant's CF and force data was recorded in the neutral position for one trial (10 s, 100 Hz) using a custom made GUI (National Instruments® LabVIEW). Once completed, the PCO was loosened to begin the simultaneous collection of the PF and protrusion displacement using the same custom made GUI. The collection of the PF and protrusion displacement were synchronized to contain the same sample rate (100 Hz) and duration. The PF and protrusion displacement were acquired over ten trials, which each trial consisting of three phases (Figure 5-3). For the first phase, the participant remained in a neutral position for five seconds to obtain baseline measurements. After five seconds, phase 2 consisted of the participant tightening the PCO to replicate the CF to the best of their ability. The tightening rate of the PCO was controlled by a metronome at a rate of 1 dial turn per second. The controlled tightening rate was to reduce potential influence of loading rate on the predicted stiffness values, as loading

rates have been reported to influence the stiffness measurements of hyaline cartilage (Li, Buschmann, & Shirazi-Adl, 2003; Oloyede et al., 1992). Following phase 2, the third phase required the participant to return to the neutral position for an additional ten seconds to acquire enough data to calculate an average PF. The duration of ten seconds was chosen to take into account any breathing of the individual which may influence the magnitude of PF. The completion of phase 3 ended one trial. Before beginning a new trial, the PCO was loosened.

.

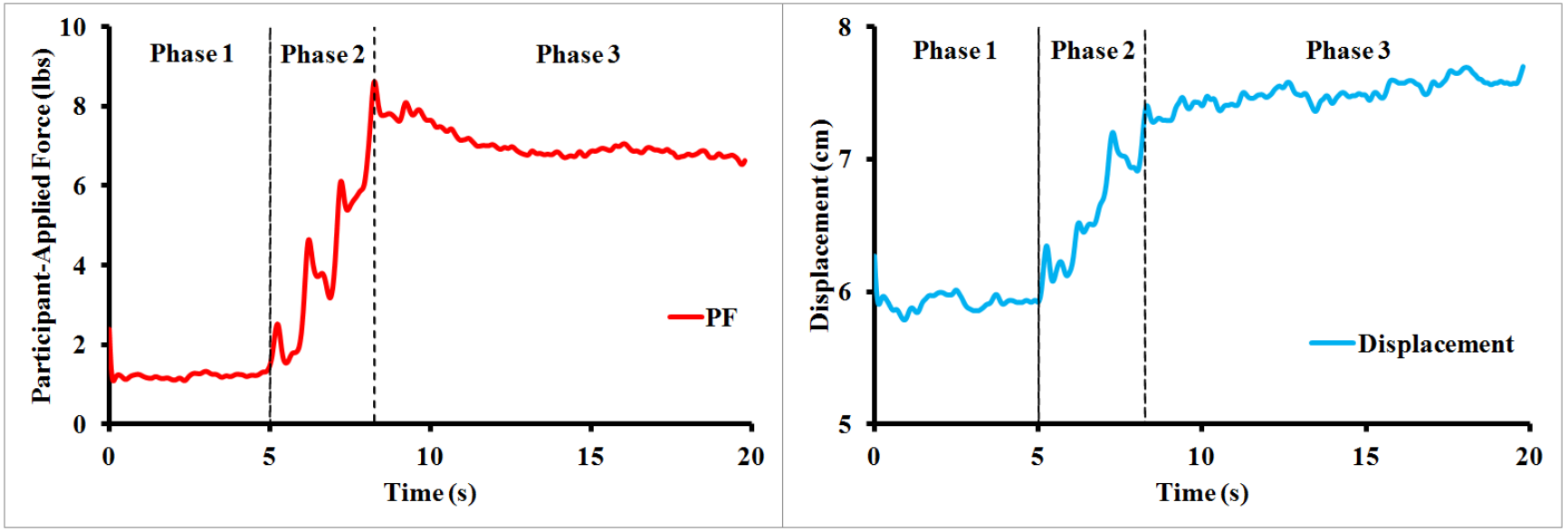

Figure 5-3 - A single trial of the PF (left) and protrusion displacement (right) when performing the three phases. Phase 1 consisted of the participant remaining in a neutral position, Phase 2 the participant tightened the PCO, and Phase 3 the participant returned to a neutral position.

5.3 Data Analysis

The load cell voltage outputs were first summed using the weighted sum equation described in Section 0. Next, the CF and PF were converted into pounds using the conversion equation acquired from the calibration of FM3. The LED sensor voltage outputs were also converted into centimetres using the conversion equation acquired from its calibration (Appendix A, Section A.3.). The CF was calculated by taking an average of the single trial. PF was calculated by averaging the last 10 seconds (phase 3) of load cell data for all trials. CR was calculated as the percent change of AP depth between one time point and its former time point. A CR of 0% represented no change in the AP depth.

PS was calculated in a similar fashion used in Section 4.5.1.1. First, a polynomial line of best fit (degree of two) was obtained for the Phase 2 portion of the data in both the PF and displacement curve (Figure 5-3). A degree of two was chosen as force-displacement curves of the human chest wall were observed to be non-linear (Gruben et al., 1993). This was performed to minimize the fluctuations within the data, speculated to be caused by the rebound of the PCO and chest wall while tightening. Recalling the construction of the PCO, tightening the PCO consists of turning two dials. When tightening the PCO, the chest wall may have the tendency to act like a spring. As the PCO applies an increased force, the chest wall will have the desire to return to its original position in between each dial turn. Therefore, the position of the protrusion will vary between each dial turn. This will consequently impose fluctuations in the force and displacement data. Referring back to the lines of bets fit for the PF and displacement curves, the data points of these two lines were plotted to form a force-displacement curve. This procedure was repeated with all ten trials to obtain a total of ten force-displacement curves. The exclusion criteria mentioned in Section 4.5.3 were applied to the force-displacement curves before obtaining the average force-displacement curve. If more than 5 force-displacement curves were excluded the participant was

removed from the overall analysis for that specific time point. All ten force-displacement curves were then plotted together to obtain a final linear line of best fit. This final line of best fit was the average force-displacement curve of all trials. The stiffness of an object is defined as its ability to resist deformation. In mathematical terms, it is the applied force divided by the displacement that occurred due to the applied force (i.e. slope/derivative of a force-displacement curve). Therefore, the derivative of the average force-displacement curve produced the magnitude of the protrusion stiffness.

5.4 Statistical Analysis

A paired t-test was used to determine if the PF was different from the CF at each time point (H1). Normality to perform the paired t-test was checked using Q-Q Plots. A Generalized Estimating Equation (GEE) and pairwise comparison using the methods of GENLIN in SPSS v 22.0 were used to answer the remainder of our hypotheses. The GEE is used to estimate the parameters of a generalized linear model, which corresponds to the strength of a relationship between two variables. For this study, the GEE estimated the strength of the relationship between the protrusion stiffness (PS) and participant-applied force (PF) (H3), and PS and correction rate (CR) (H4). The pairwise comparisons performed were similar to the mixed repeated measure analysis of variance (rANOVA). However, a mixed rANOVA was not used as this method was unable to take into consideration any missing data at time points. By using GENLIN, any missing data was accounted for. The pairwise comparisons were used to determine if PF and PS changed over time (H2 and H5, respectively). Additionally, normality of the data is not a limiting factor to the GENLIN method and therefore was not required to be checked. All hypotheses were tested at a significance level of 0.05.

Chapter Six: Results

Overall, the 28 collection periods showed that the majority of participants (75%) tightened the PCO to a magnitude different from their CF (Table 6-1). The results of the fitting appointment, with data for all eleven participants, revealed that six participants had tightened the PCO to a significantly different PF from their CF ($p \leq 0.05$). Of these six individuals, half over-tightened the PCO, ranging from 0.77 - 2.23 lbs (16.98 – 64.46%) and a mean of 1.51 (0.73) lbs (38.39 [16.40]%) above the CF. The other three tightened the PCO with less force than prescribed, ranging from 0.75 - 0.95 lbs (15.9 – 25.09%) and a mean of -0.83 (0.10) lbs (21.15 [19.77]%) under the CF. Interestingly, the one month follow-up time point revealed an increase (50%) in the number of participants with differences between the CF and PF. Of the ten participants at the one month follow-up, nine applied a PF that was significantly different from the CF ($p \leq 0.05$). Seven participants had tightened the PCO with too much force, ranging from 0.46 - 4.61 lbs (11.34 – 130.46%) with a mean of 2.00 (1.72) lbs (54.75 [18.99]%) above the CF. The remaining two participants had tightened the PCO to a force below the CF, ranging from 0.42 - 0.93 lbs (11.13 – 19.61%) with a mean of -0.68 (0.36) lbs (15.37 [5.41]%) under the CF. A similar pattern was observed at the two month follow-up. Of the seven participants at the two month follow-up, six individuals were observed to tighten the PCO to a significantly different magnitude than the CF ($p \leq 0.05$). However, no participants were found to tighten the PCO under the CF. All six participants tightened the PCO excessively, ranging from 0.94 - 5.01 lbs (27.03 – 141.80%) with a mean of 3.05 (1.62) lbs (95.62 [22.66]%) above CF.

Table 6-1 - Mean differences (PF-CF [lbs] and in percent) and standard deviations (tested at α = 0.05) of the clinically prescribed force and participant applied force, at each time point. Significant values are highlighted in grey. Time point 1 is the fitting appointment, time point 2 is the one month follow-up, and time point 3 is the two month follow-up.

Paired Samples Test									
		Paired Differences							
					95% Confidence Interval of the Difference				
Time	ID	Mean Difference (PF-CF)	Std. Deviation	Std. Error Mean	Lower	Upper	Mean Difference (%)	Std. Deviation (%)	Sig. (2-tailed)
1	1	0.47	1.11	0.35	1.26	-0.32	13.40	31.39	0.21
	2	-0.03	0.30	0.10	0.19	-0.25	-0.77	7.60	0.78
	3	2.23	0.76	0.24	2.77	1.69	64.46	21.97	0.00
	4	-0.79	0.89	0.28	-0.15	-1.43	-22.45	25.26	0.02
	5	-0.31	0.59	0.19	0.11	-0.73	-14.00	26.73	0.13
	6	-0.95	0.20	0.06	-0.81	-1.09	-25.09	5.35	0.00
	7	0.18	0.74	0.23	0.71	-0.34	4.99	19.88	0.46
	8	1.55	0.54	0.17	1.93	1.17	33.72	11.74	0.00
	9	0.77	0.62	0.20	1.21	0.32	16.98	13.64	0.00
	10	0.04	0.36	0.11	0.30	-0.22	1.08	10.23	0.74
	11	-0.75	1.06	0.34	0.01	-1.51	-15.90	22.49	0.05
2	1	4.61	0.85	0.27	5.22	4.00	130.46	24.12	0.00
	2	0.46	0.54	0.17	0.85	0.07	11.34	13.50	0.02
	3	0.91	0.58	0.18	1.33	0.49	26.22	16.86	0.00
	4	4.21	1.09	0.35	4.99	3.43	119.33	31.11	0.00
	6	-0.42	0.17	0.05	-0.30	-0.55	-11.13	4.56	0.00
	7	-0.21	0.50	0.16	0.15	-0.57	-5.53	13.57	0.22
	8	1.39	0.56	0.18	1.78	0.99	30.18	12.11	0.00
	9	0.55	0.62	0.20	0.99	0.10	12.14	13.75	0.02
	10	1.88	0.46	0.15	2.21	1.55	53.55	13.14	0.00
	11	-0.93	0.29	0.09	-0.72	-1.14	-19.61	6.15	0.00
3	1	5.01	1.51	0.48	6.09	3.93	141.80	42.81	0.00
	2	1.32	0.51	0.16	1.69	0.96	32.85	12.68	0.00
	3	0.94	0.43	0.14	1.25	0.63	27.03	12.54	0.00
	4	4.22	0.73	0.23	4.74	3.70	119.74	20.53	0.00
	5	3.73	0.35	0.11	3.97	3.48	170.29	15.83	0.00
	6	3.09	0.60	0.19	3.53	2.66	82.02	16.04	0.00
	7	0.41	0.60	0.19	0.84	-0.01	11.22	16.20	0.06

Considering the effect of time on the PF, there was no difference in the PF between the fitting appointment and one month follow-up (mean 0.93 lbs (SEM = 0.79), p = 0.40) (Table 6-2). However, as time progressed an additional month, the PF at the two month follow-up was significantly different from both the fitting appointment (mean 2.36 lbs (SEM = 0.79), p < 0.01) and the one month follow-up time point (mean 1.43 lbs (SEM = 0.73), p = 0.02) [Table 6-2]). Examining the overall trend of the PF over time, the PF showed an increase with time (Figure 6-1). Bearing in mind that the CF was a constant throughout the study, the increase in PF over time resulted in the PF deviating further from the CF; increasing the difference as treatment progressed (Figure 6-2).

Table 6-2 - Pairwise comparison of the PF over time (tested at α = 0.05). All significant values are highlighted in grey. Time point 1 is the fitting appointment, time point 2 is the one month follow-up, and time point 3 is the two month follow-up.

Pairwise Comparisons							
						95% Wald Confidence Interval for Difference	
Time (I)	Time (J)	Mean Difference (I-J)	Std. Error	df	Bonferroni Sig.	Lower	Upper
1	2	-0.93	0.62	1	0.40	-2.41	0.55
	3	-2.36	0.62	1	0.00	-3.83	-0.88
2	1	0.93	0.62	1	0.40	-0.55	2.41
	3	-1.43	0.54	1	0.02	-2.71	-0.14
3	1	2.36	0.62	1	0.00	0.88	3.83
	2	1.43	0.54	1	0.02	0.14	2.71

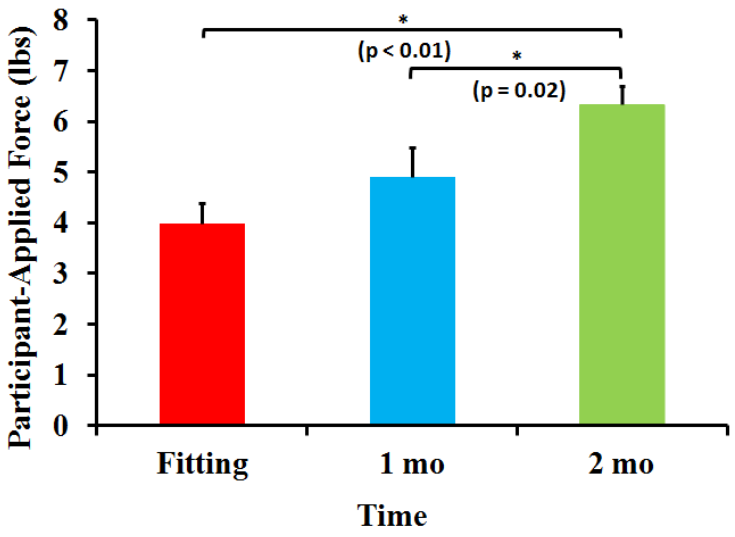

Figure 6-1 - PF over time. A general trend was demonstrated where the PF increased over time.

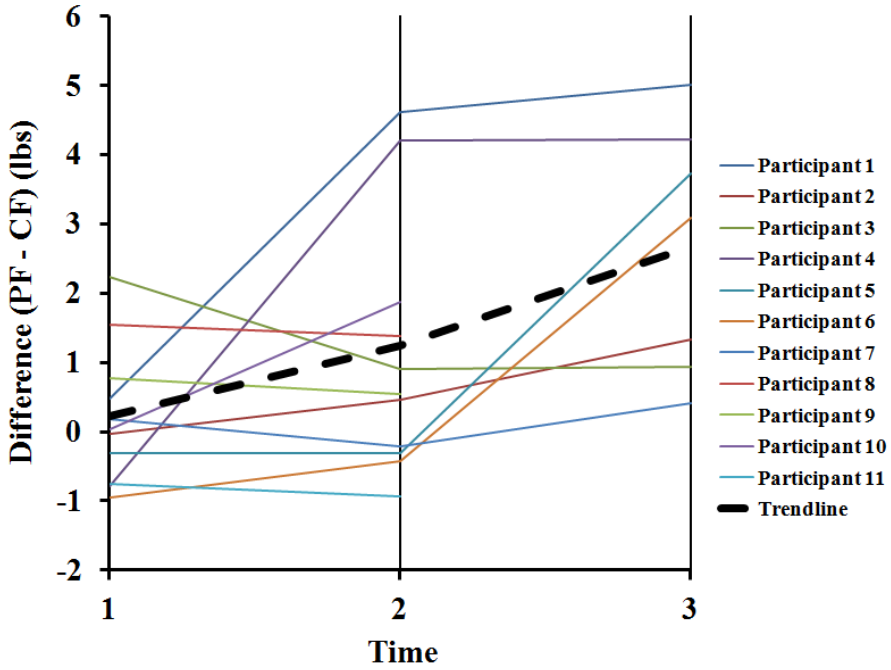

Figure 6-2 - Mean difference (PF - CF) over time. The coloured lines represent each participant; the black dotted line represents the mean difference (PF-CF) at each time point. Time point 1 is the fitting appointment, time point 2 is the one month follow-up, and time point 3 is the two month follow-up.

Additionally, the PF was observed to increase with PS, thus forming a positive relationship (2.29 (SEM = 0.61), $p < 0.01$ [Table 6-3]). This positive relationship was illustrated when plotting the PF and PS at all three time points. Applying a line of best fit on the plots, R^2 values were determined for the fitting appointment, 1 month follow-up appointment, and 2 month follow-up appointment ($R^2 = 0.58$, $R^2 = 0.17$, and $R^2 = 0.17$, respectively [Figure 6-3]).

Table 6-3 - Results of the GEE for PS (kN/m) and the PF (lbs) (testing at $\alpha = 0.05$). A significant positive relationship (grey) was determined.

Parameter Estimates							
			95% Wald Confidence Interval		Hypothesis Test		
Parameter	B	Std. Error	Lower	Upper	Wald Chi-Square	df	Sig.
(Intercept)	1.796	.8640	.102	3.489	4.319	1	.038
PS	2.287	.6089	1.094	3.480	14.109	1	.000
(Scale)	2.390						

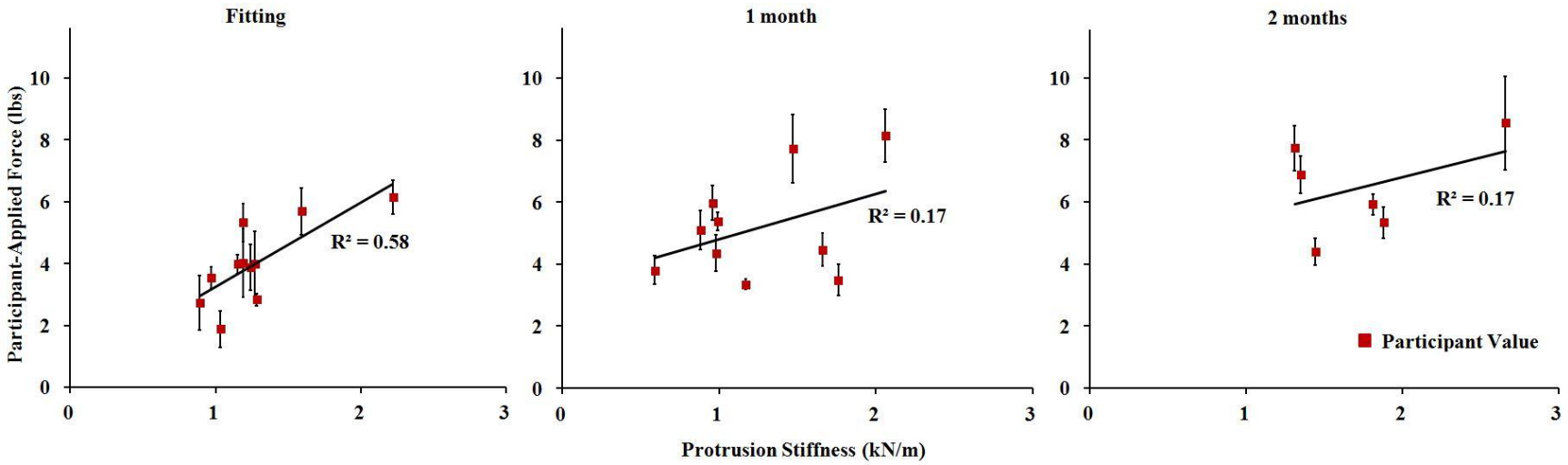

Figure 6-3 - Illustration of the relationship between PS and PF over time. The fitting appointment, 1 month follow-up appointment, and 2 month follow-up appointment showed a positive trend with $R^2 = 0.58$, $R^2 = 0.17$, and $R^2 = 0.17$, respectively. One participant was removed from the 2 month analysis as more than five PS trials were considered unsuitable for analysis.

Conversely, examining the relationship between the CR and the PS showed that no relationship existed (-0.70 (SEM = 1.14), p = 0.54 [Table 6-4]). No potential trends were seen when plotting the CR with PS at the 1 month follow-up appointment and 2 month follow-up appointment. Applying a line of best fit to both plots, the R^2 values for the 1 month follow-up appointment and 2 month follow-up appointment were 0.03 and 0.02, respectively (Figure 6-4).

Table 6-4 - Results of the GEE for PS (kN/m) and CR (testing at α = 0.05). No relationship was found between the two variables.

Parameter Estimates							
			95% Wald Confidence Interval		Hypothesis Test		
Parameter	B	Std. Error	Lower	Upper	Wald Chi-Square	df	Sig.
(Intercept)	3.573	1.7871	.070	7.075	3.996	1	.046
PS	-.698	1.1368	-2.926	1.530	.377	1	.539
(Scale)	4.466						

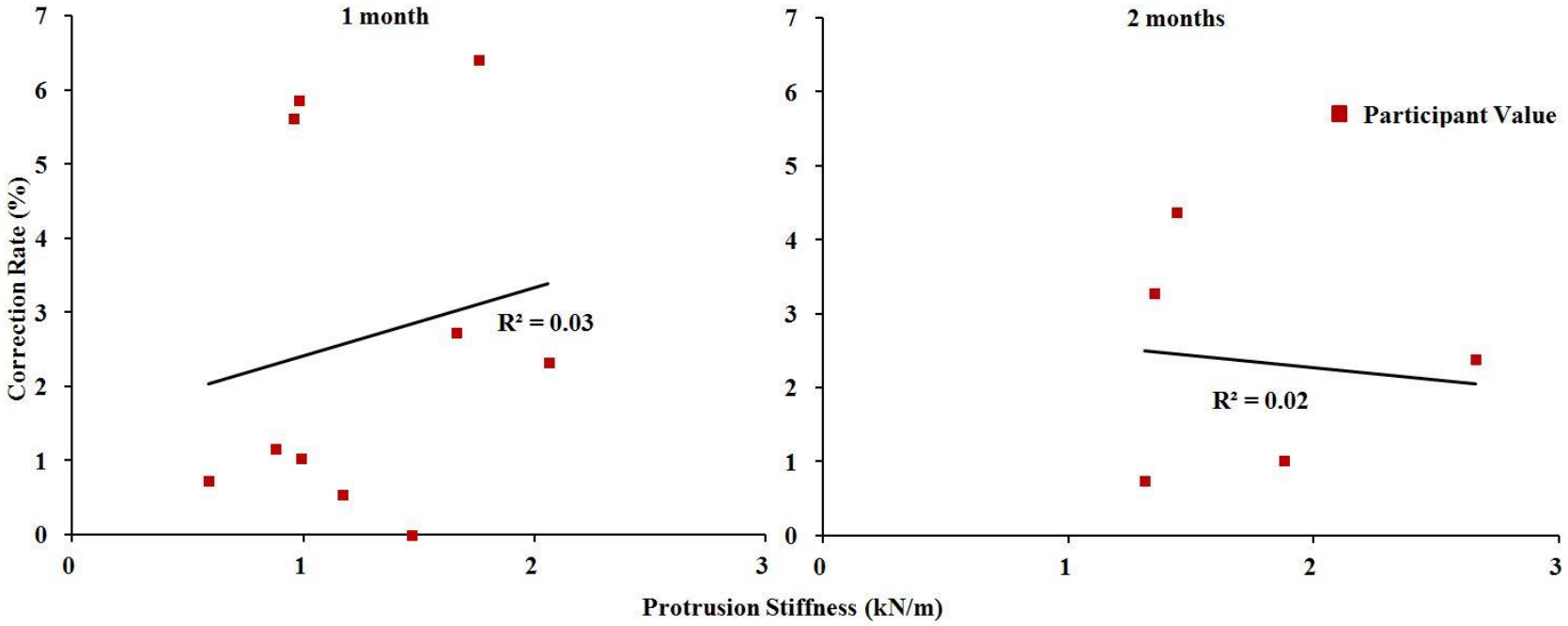

Figure 6-4 - Illustration of the relationship between PS and CR. No trends were seen with R^2 being close to zero. One participant was removed from the 2 month analysis as more than five PS trials were considered unsuitable for analysis.

Lastly, when exploring the effect of time on the PS, the PS at the two month follow-up appointment was significantly larger than the PS at the 1 month follow-up appointment (0.36 kN/m (SEM = 0.13 kN/m, p = 0.02 [Table 6-5]). No other significant differences were observed. The mean PS at the fitting appointment, one month follow-up appointment, and two month follow-up appointment were 1.27 (SEM = 0.11) kN/m, 1.26 (SEM = 0.14) kN/m, and 1.62 (SEM = 0.17) kN/m, respectively [Figure 6-5]). The magnitudes of the PS ranged from 0.59 – 2.66 kN/m.

Table 6-5 - Pairwise comparison of the PS (kN/m) over time (tested at α = 0.05). A significant difference (grey) in PS was found between the 1 month and 2 month follow-up appointment.

Pairwise Comparisons							
						95% Wald Confidence Interval for Difference	
(I) Time	(J) Time	Mean Difference (I-J)	Std. Error	df	Bonferroni Sig.	Lower	Upper
1	2	.0047	.19289	1	1.000	-.4571	.4665
	3	-.3524	.19634	1	.218	-.8224	.1177
2	1	-.0047	.19289	1	1.000	-.4665	.4571
	3	-.3571	.13120	1	.019	-.6712	-.0430
3	1	.3524	.19634	1	.218	-.1177	.8224
	2	.3571	.13120	1	.019	.0430	.6712

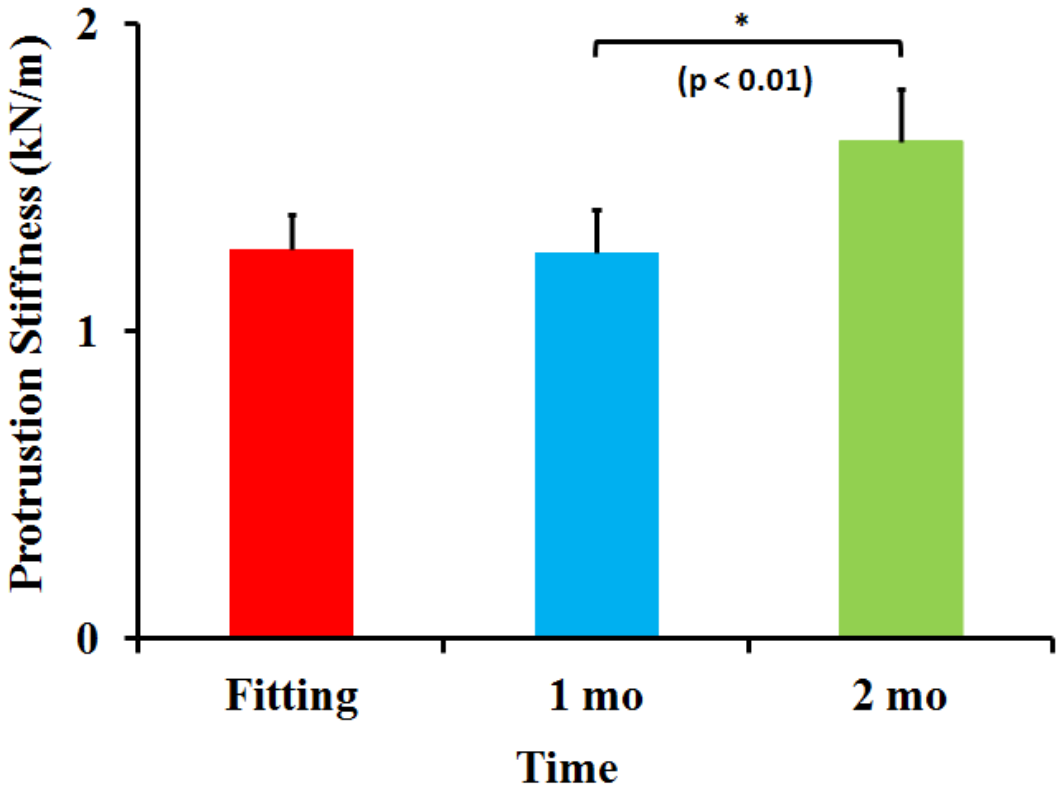

Figure 6-5 – PS (with SEM bars) over time. A significant difference was found in the PS between the 1 month and 2 month follow-up appointment. No trend was found over time.

Chapter Seven: Discussion

The gold standard of treatment for PC has shifted from surgical methods to the PCO. These PCOs all have a similar goal to provide a constant force to the sternal protrusion to correct the deformity. An abundance of PCO literature has shown that this method of treatment is successful (Haje & Bowen, 1992; Kang et al., 2014; Kravarusic et al., 2006; R. T. Lee et al., 2013; Lopez et al., 2013; Martinez-ferro et al., 2016). However, research has yet to quantify the PCO forces acting on this deformity or characterize the stiffness and potential change in stiffness of the protrusion during treatment. Quantifying the forces of the PCO has been reported to be an essential aspect of treatment and remains to be investigated (Harrison et al., 2016). The purpose of this exploratory study was to determine what magnitudes of forces are being prescribed to the patient, and whether the patient is able to correctly follow this prescribed force over two months. Additionally, we sought to characterize the protrusion by measuring its stiffness during treatment, and how this stiffness and potential changes in stiffness with treatment may influence the magnitude of PCO forces and correction rate of the deformity.

7.1 Participant-Applied Force

The majority of participants were observed to tighten the PCO at a significantly different force than what they were prescribed. This finding supported the first hypothesis (H1), which stated that the PF would be different from the CF over two months. However, the magnitudes of some of these differences were minimal and may not be clinically significant. For example, one participant over-tightened the PCO by 0.77 lbs (16.98%) at the fitting appointment, which may not be a sufficiently large difference to cause any harm to the chest wall. In scoliosis bracing mean thoracic forces have been reported ranging from 58.1 N and 66 N (13.1 lbs and 15 lbs) (Chase et al., 1989; Van den Hout et al., 2002). PCO force magnitudes were not observed to reside at these high magnitudes, with the largest force being 8.55 lbs (Figure 6-3). However,

scoliosis braces correct a larger structure and transmit forces through a larger surface area. Therefore, larger corrective forces up to 15 lbs may be reasonable. The PCO is designed to correct a smaller structure and to transmit forces through a smaller surface area. Therefore, there is a possibility that some PFs were sufficiently large to provide injury. However, this study was not designed to investigate this aspect and it is beyond the scope of this study to definitely state the level of force associated with injury. Further investigation is required to determine what force magnitudes result in injury.

PFs at the two month follow-up were significantly different between both the fitting appointment and 1 month follow-up. These results agree with our hypothesis (H2) suggesting the PF will change over time. A trend was observed in which the PF increased during the course of treatment (Figure 6-1). There are multiple possibilities to explain this observation. Firstly, the PS was determined to have a positive relationship with PF. Therefore, as the PS increased, the PF also increased to produce the same magnitude of protrusion displacement. Secondly, it is possible that the participants could not remember the CF over time. If the participant was unable to recall the CF, they may have over-tightened the PCO to ensure that they were receiving an adequate corrective force. Thirdly, participants may have become comfortable or acclimatized with the PCO over time and may have develop a routine that drifts away from the CF. Individuals could have obtained the provoking thought of over-tightening the PCO to correct the deformity at a faster rate as they became proficient with the PCO. Another possible explanation is a habituation effect. In this case, the patient could have obtained an increase in pain tolerance over time with the PCO. Habituation to pain has been shown in research, specifically with cryokinetic training in athletes. With repeated cryokinetic training sessions, individuals developed a higher tolerance to cold (Carman & Knight, 1992). In reference to the PCO, repetitive force applications could

allow the chest wall to adapt, resulting in higher pain tolerance to the PCO forces. These rationales are merely speculations and require further research to determine whether there is evidence to support or refute any of these possibilities.

7.2 Protrusion Stiffness

The majority of predicted protrusion stiffness values were within a range (means of 1.27, 1.26, and 1.62 kN/m) that was lower than the previously reported ranges of chest wall stiffness from 5 kN/m to 40 kN/m (Gruben et al., 1993). This is a reasonable outcome as costal cartilages have been reported to become less stiff when entering adolescence (Guo et al., 2007). Additionally, these values fell within the proximity of the soft foam protrusion (1.45 kN/m) previously reported in Section 4.5.2. The PS was observed to significantly increase after the 1 month follow-up appointment, agreeing with the study hypothesis H5. This finding does not support the results in previous literature stating that costal cartilage stiffening rarely occurs during adolescence (Guo et al., 2007). However, individuals receiving treatment for PC are exposed to constant forces on their chest wall. Therefore, the costal cartilages are consistently under compression due to the PCO forces. Constant PCO forces applied to the costal cartilages may subsequently result in chondrocyte apoptosis (Trias, 1961). The death of these chondrocytes may lead to calcification of the costal cartilages, thus increasing the stiffness (Hashimoto et al., 1998). This phenomenon may begin to initiate after 2 months of treatment. Additional studies are required to determine if costal cartilages begin to calcify earlier when exposed to the PCO treatment.

CR did not show a relationship with PS, therefore not supporting study hypothesis H4. In scoliosis bracing, CR was influenced by the stiffness of the spine but also a multitude of other factors such as the type of scoliotic curve, the properties of the tissues transmitting the force, and the patient compliance in wearing the brace (Van den Hout et al., 2002). In PC bracing, although

the CR may not be affected by the stiffness of the protrusion, other factors may potentially influence CR such as the patient compliance or the geometry of the protrusion. Patient compliance has been reported as a key factor for successful treatment (Kang et al., 2014). Generally, more rapid correction occurs in an individual wearing the PCO as prescribed in comparison to an individual wearing the PCO inconsistently. The geometry of the protrusion may also influence the alignment of the pad relative to the protrusion, consequently affecting the magnitudes and locations of compressive forces. This latter speculation requires further investigation. Clearly, both patient compliance and geometry of the protrusion should be considered for future studies when quantifying CR.

The PF was observed to contain a positive relationship with the PS. This result supported the study hypothesis H3. This finding may be partially attributed to different comfort levels of the participant. If two individuals with different PS values applied the same magnitude of force to their protrusion, the chest wall of the individual with the lower PS will undergo a larger displacement. This larger displacement of the chest wall may restrict the breathing capacity of the individual and result in a requirement to lower the amount of applied force. The individual with the larger PS may be able to maintain regular breathing patterns and continue wearing the PCO with the same force magnitude. Additionally, the participants may use their protrusion displacement as a guide to the amount of PCO force they require. To elaborate, some patients may observe the displacement of their protrusion as they tighten the PCO. To obtain the same displacement (i.e. flatten their protrusion), those with a larger PS would require a larger magnitude of force. Further investigation is required to conclusively address these speculations. However, the R^2 values for the positive trend were low for the 1 month follow-up and 2 month follow-up appointments ($R^2 = 0.17$). As with the CR, the PF may be influenced by other factors,

such as pain tolerance. If an individual has a naturally greater pain tolerance, they may tighten the PCO to a greater magnitude of force. Furthermore, the PF may be altered by the positioning of the PCO, as the shape of the protrusion is not always symmetrical. Similar to the geometry of the protrusion, the angle at which the PCO applies a force may change resulting in altered applied compressive forces. These altered forces have been reported in scoliosis bracing, where thoracic forces have changed due to different positioning of the brace (Van den Hout et al., 2002).

7.3 Limitations

There were several limitations in this study that must be considered. The first limitation was the total sample size of 11 participants, with 7 participants completing the entire study with 3 time points of data collection spaced at one month intervals. This sample size was likely not large enough to produce sufficient statistical power, and more participants should be recruited. Unfortunately, no estimated sample size could be calculated as the statistical methods used (GENLIN) currently contain no method of sample size calculation. The protocol used also has potential flaws, including the metronome, measurement of displacement, and placement of the PCO on the protrusion. The metronome is an indirect method to control the loading rate of the PCO and opens the possibility to user error, as participants may not be able to perform equal turns on the boa straps. Although the metronome provides a timing control, the straps themselves may be producing different loading rates for every turn. The measurement of displacement may be influenced by the placement of the PCO and the slight variations of its movements when being tightened. The LED sensor depends on the reflective surface to measure the displacement of the protrusion. Consequently, any abnormal movements of the PCO or the participant may cause the reflective surface to shift and impose movement artefacts into the data. Identifying participant compliance was potentially a confounding factor that may limit the interpretation of

the data collected in this study. It was assumed that the participant wore the PCO as prescribed during the treatment phase (~ 23 hrs/day). If the participant did not wear the PCO as prescribed this may have affected the CR, as well as the PF if any training effect is present.

7.4 Future Work

This exploratory study has been able to produce a range of new research questions that must be considered in future work. Currently, it would be ideal to recruit additional participants to obtain a more statistically powerful data set for the current study. A data set with more participants could compensate for those individuals with missing data. Therefore, other statistical methods could be used, such as a rANOVA. Using a rANOVA would allow the estimation of the sample size to obtain a certain magnitude of statistical power. Longitudinal studies following the complete treatment should be considered to determine what changes may occur at durations longer than 2 months. This could improve the current protocol, specifically determining when the maintenance phase should be initiated, and why the protrusion does not have the tendency to reappear after treatment. Studies regarding the costal cartilages at a cellular level may provide answers to these questions; to determine what changes (if any) take place within the costal cartilage during treatment.

An improved method to measure stiffness may provide more reliable and accurate results. The current methodology to measure displacement contains flaws that could be absolved with constrained methods. The LED sensor is capable of producing movement artefacts caused by the shifts in body position, or rotations of the reflective surface. Using equipment such as a linear voltage displacement transducer may reduce or remove these effects.

The CR may also be determined more robustly than with just simple AP depth measurements using calipers. 3D topography scans of the protrusion during treatment would allow quantification of the thoracic region as a whole, and development of anatomical indices to track

correction over time. Additionally, the geometrical shape of the protrusion could be obtained through 3D modelling that would allow comparison of custom geometric properties of the protrusion, chest wall and torso with the PF or the CR. This will provide the ability to correlate any geometrical changes of the protrusion with the PF or CR.

Finally, the current force measurement system (FM3) is limited to measuring PCO forces within a clinical setting. However, developing a new system with low-profile sensors that can measure forces outside of the clinic in real time could provide a significant improvement in the treatment of PC. This could be a possibility by substituting the current load cells in FM3 with two tensile force sensors on the boa straps of the PCO. The tension measured within the straps may relate to the magnitude of force provided by the pad. A pilot study has been published with this goal in mind, using a device capable of recording brace pressures and temperatures (Harrison et al., 2016). The ability to measure PCO forces outside of the clinic creates the possibility of determining patient compliance, and also providing real time feedback. Determining the patient compliance will remove one of the major limiting factors in most PC literature to date, which is the duration the patient wears the brace. Understanding compliance with brace force and protrusion displacement will enable more accurate conclusions and rationale for interpreting any differences in correction rates. Lastly, real time force acquisition may assist in developing a device that can provide real time feedback to both the clinician and the patient. With the technology to determine the CF, real time feedback would allow the patient to maintain a force within the CF range. The clinician may also have access to this data to determine if the patient is following the CF, or if the brace is being worn according to the protocol. Furthermore,

The Calgary Protocol may also be improved by combining a more accurate method of measuring PS with a real time feedback device to measure PCO forces. This would provide the clinicians

the ability to individualize patient care. Recalling the Calgary Protocol, it is a guideline to inform patients on the length of time the PCO should be worn. This protocol could be individualized for every patient depending on their PS. There is a possibility that not every patient is required to wear the PCO for 23 hour per day for efficient correction, or that the patient does not qualify for PCO correction due to a high PS. Additionally, the current Calgary Protocol does not monitor the CF over treatment. The possibility exists where the PF may increase due to the chest wall characteristics changing. Therefore, the CF may also alter over the course of treatment due to these changes. It is recommended that future studies obtain the CF over time to determine if the differences between the PF and CF remain or if the CF also increases with the PF over time.

7.5 Conclusions

The first SA of this study was to develop a force measurement system to quantify PCO forces and protrusion. With the addition of an LED sensor, simultaneous displacement measurements were achieved to calculate PS. This system provided the means to satisfy the remaining two SAs: 1) determine relations between: CF and PF, PS and PF, and PS and CR, and 2) determine the effect of time on PF and PS. It was found that the majority of participants applied the PCO at a different force than the CF, agreeing with the first study hypothesis H1. Furthermore, the PF was observed to increase over time, agreeing with the hypothesis H2. This increase in the PF over time may have been caused by the increase in PS after two months, due to the positive relationship they contained. This positive relationship between PF and PS agreed with our third hypothesis H3. However, no relationship was determined between the CR and PS, thus contradicting our fourth hypothesis H4. In addition, the increase in PS over time agreed our fifth hypothesis H5.

The current findings show potential in determining what magnitudes of forces are required for efficient correction and if any individual characteristics influence these forces and correction

rates. Furthermore, the study has opened the door to a variety of research questions that require investigation to further develop the PCO and associated protocol. This information may provide the means required to develop an improved PCO and provide clinicians with better assessment tools, as well as standardized guidance for the treatment of PC. Additionally, the development of an advanced force measurement system that can measure PCO forces outside of the clinic may provide patients with real-time feedback, ensuring the PCO is worn within the range of the CF.

References

Ateş, O., Karakuş, O. Z., Hakgüder, G., Olguner, M., & Akgür, F. M. (2013). Pectus carinatum: the effects of orthotic bracing on pulmonary function and gradual compression on patient compliance. *European Journal of Cardio-Thoracic Surgery*, *44*(3), e228-32. https://doi.org/10.1093/ejcts/ezt345

Cahill, B. J. L., Lees, G. M., & Robertson, H. T. (1984). A summary of preoperative and postoperative cardiorespiratory performance in patients undergoing pectus excavatum and carinatum repair. *Journal of Pediatric Surgery*, *19*(4), 430–433.

Canavese, F., & Dimeglio, A. (2013). Normal and abnormal spine and thoracic cage development. *World Journal of Orthopedics*, *4*(4), 167–174. https://doi.org/10.5312/wjo.v4.i4.167

Carman, K. W., & Knight, K. L. (1992). Habituation to cold-pain during repeated cryokinetic sessions. *Journal of Athletic Training*, *27*(3), 223–30. Retrieved from http://www.pubmedcentral.nih.gov/articlerender.fcgi?artid=1317250&tool=pmcentrez&rendertype=abstract

Chase, A. P., Bader, D. L., & Houghton, G. R. (1989). The biomechanical effectiveness of the boston brace in the management of adolescent idiopathic scoliosis. *Spine*, *14*(6), 636–642.

Cobben, J. M., Oostra, R.-J., & van Dijk, F. S. (2014). Pectus excavatum and carinatum. *European Journal of Medical Genetics*, *57*(8), 414–417. https://doi.org/10.1016/j.ejmg.2014.04.017

Colozza, S., & Bütter, A. (2013). Bracing in pediatric patients with pectus carinatum is effective and improves quality of life. *Journal of Pediatric Surgery*, *48*(5), 1055–9. https://doi.org/10.1016/j.jpedsurg.2013.02.028

Davis, J. T., & Weinstein, S. (2004). Repair of the pectus deformity: Results of the Ravitch

approach in the current era. *The Annals of Thoracic Surgery*, *78*(2), 421–426. https://doi.org/10.1016/j.athoracsur.2004.03.011

Dearden, L. C., Bonucci, E., & Cuicchio, M. (1974). An investigation of ageing in human costal cartilage. *Cell and Tissue Research*, *152*(3), 305–337. https://doi.org/10.1007/BF00223953

Desmarais, T. J., & Keller, M. S. (2013). Pectus carinatum. *Current Opinion in Pediatrics*, *25*(3), 375–381. https://doi.org/10.1097/MOP.0b013e3283604088

Fonkalsrud, E. W. (2008). Surgical correction of pectus carinatum: lessons learned from 260 patients. *Journal of Pediatric Surgery*, *43*(7), 1235–1243. https://doi.org/10.1016/j.jpedsurg.2008.02.007

Fonkalsrud, E. W., & Anselmo, D. M. (2004). Less extensive techniques for repair of pectus carinatum: The undertreated chest deformity. *Journal of the American College of Surgeons*, *198*(6), 898–905. https://doi.org/10.1016/j.jamcollsurg.2004.02.016

Forman, J. L., del Pozo de Dios, E., Dalmases, C. A., & Kent, R. W. (2010). The contribution of the perichondrium to the structural mechanical behavior of the costal-cartilage. *Journal of Biomechanical Engineering*, *132*(9), 1–5. https://doi.org/10.1115/1.4001976

Forman, J. L., & Kent, R. W. (2014). The effect of calcification on the structural mechanics of the costal cartilage. *Computer Methods in Biomechanics and Biomedical Engineering*, *17*(2), 94–107. https://doi.org/10.1080/10255842.2012.671307

Golladay, E. S. (2003). *Pectus carinatum and other deformities of the chest wall*. (R. G. Azizkhan & T. R. Weber, Eds.), *Operative pediatric surgery*. New York, NY: McGraw-Hill.

Gruben, K. G., Guerci, A. D., Halperin, H. R., Popel, A. S., & Tsitlik, J. E. (1993). Sternal force-displacement relationship during cardiopulmonary resuscitation. *Journal of Biomechanical*

Engineering, *115*(2), 195–201. https://doi.org/10.1109/10.771188

Guo, B., Liao, D., Li, X., Zeng, Y., & Yang, Q. (2007). Age and gender related changes in biomechanical properties of healthy human costal cartilage. *Clinical Biomechanics (Bristol, Avon)*, *22*(3), 292–297. https://doi.org/10.1016/j.clinbiomech.2006.10.004

Haje, S. A., & Bowen, J. R. (1992). Preliminary results of orthotic treatment of pectus deformities in children and adolescents. *Journal of Pediatric Orthopaedics*, *12*(6), 795–800.

Haje, S. A., Harcke, H. T., & Bowen, J. R. (1999). Growth disturbance of the sternum and pectus deformities: Imaging studies and clinical correlation. *Pediatric Radiology*, *29*(5), 334–341. https://doi.org/10.1007/s002470050602

Harrison, B., Stern, L., Chung, P., Etemadi, M., Kwiat, D., Roy, S., … Martinez-Ferro, M. (2016). MyPectus: First-in-human pilot study of remote compliance monitoring of teens using dynamic compression bracing to correct pectus carinatum. *Journal of Pediatric Surgery*, *51*(4), 608–611. https://doi.org/10.1016/j.jpedsurg.2015.11.007

Hashimoto, S., Ochs, R. L., Rosen, F., Quach, J., McCabe, G., Solan, J., … Lotz, M. (1998). Chondrocyte-derived apoptotic bodies and calcification of articular cartilage. *Proceedings of the National Academy of Sciences of the United States of America*, *95*(6), 3094–3099. https://doi.org/10.1073/pnas.95.6.3094

Kang, D.-Y., Jung, J., Chung, S., Cho, J., & Lee, S. (2014). Factors affecting patient compliance with compressive brace therapy for pectus carinatum. *Interactive Cardiovascular and Thoracic Surgery*, *19*(6), 1–4. https://doi.org/10.1093/icvts/ivu280

Kimpara, H., Iwamoto, M., Watanabe, I., Miki, K., Lee, J. B., Yang, K. H., & King, A. I. (2006). Effect of assumed stiffness and mass density on the impact response of the human chest using a three-dimensional FE model of the human body. *Journal of Biomechanical*

Engineering, *128*(5), 772–776. https://doi.org/10.1115/1.2264394

Kravarusic, D., Dicken, B. J., Dewar, R., Harder, J., Poncet, P., Schneider, M., & Sigalet, D. L. (2006). The calgary protocol for bracing of pectus carinatum: A preliminary report. *Journal of Pediatric Surgery*, *41*(5), 923–6. https://doi.org/10.1016/j.jpedsurg.2006.01.058

Laasanen, M. S., Töyräs, J., Korhonen, R. K., Rieppo, J., Saarakkala, S., Nieminen, M. T., … Jurvelin, J. S. (2003). Biomechanical properties of knee articular cartilage. *Biorheology*, *40*(1–3), 133–40. Retrieved from http://www.ncbi.nlm.nih.gov/pubmed/12454397

Lacquet, L. K., Morshuis, W. J., & Folgering, H. T. (1998). Long-term results after correction of anterior chest wall deformities. *Journal of Cardiovascular Surgery*, *39*(5), 683–688.

Lam, C. R., & Taber, R. E. (1971). Surgical treatment of pectus carinatum. *Archives of Surgery*, *103*(2), 191–194.

Lau, A., Oyen, M. L., Kent, R. W., Murakami, D., & Torigaki, T. (2008). Indentation stiffness of aging human costal cartilage. *Acta Biomaterialia*, *4*(1), 97–103. https://doi.org/10.1016/j.actbio.2007.06.008

Lee, R. T., Moorman, S., Schneider, M., & Sigalet, D. L. (2013). Bracing is an effective therapy for pectus carinatum: Interim results. *Journal of Pediatric Surgery*, *48*(1), 184–90. https://doi.org/10.1016/j.jpedsurg.2012.10.037

Lee, S. Y., Lee, S. J., Jeon, C. W., Lee, C. S., & Lee, K. R. (2008). Effect of the compressive brace in pectus carinatum. *European Journal of Cardio-Thoracic Surgery*, *34*(1), 146–149. https://doi.org/10.1016/j.ejcts.2008.04.012

Li, L. P., Buschmann, M. D., & Shirazi-Adl, A. (2003). Strain-rate dependent stiffness of articular cartilage in unconfined compression. *Journal of Biomechanical Engineering*, *125*(2), 161–168. https://doi.org/10.1115/1.1560142

Lopez, M., Patoir, A., Varlet, F., Perez-Etchepare, E., Tiffet, T., Villard, A., & Tiffet, O. (2013). Preliminary study of efficacy of dynamic compression system in the correction of typical pectus carinatum. *European Journal of Cardio-Thoracic Surgery : Official Journal of the European Association for Cardio-Thoracic Surgery*, *44*(5), e316-9. https://doi.org/10.1093/ejcts/ezt425

Mackie, E. J., Ahmed, Y. A., Tatarczuch, L., Chen, K. S., & Mirams, M. (2008). Endochondral ossification: How cartilage is converted into bone in the developing skeleton. *International Journal of Biochemistry and Cell Biology*, *40*(1), 46–62. https://doi.org/10.1016/j.biocel.2007.06.009

Martinez-ferro, M., Fraire, C., & Bernard, S. (2008). Dynamic compression system for the correction of pectus carinatum. *Seminars in Pediatric Surgery*, *17*(3), 194–200.

Martinez-ferro, M., Munzon, G. B., Fraire, C., Abdenur, C., Chinni, E., Strappa, B., & Ardigo, L. (2016). Non-surgical treatment of pectus carinatum with the FMF ® Dynamic Compressor System. *Journal of Visualized Surgery*, *2*(3), 1–8. https://doi.org/10.21037/jovs.2016.02.20

Mattice, J., Lau, A., Oyen, M., & Went, R. (2006). Spherical indentation load-relaxation of soft biological tissues. *Journal of Materials Research*, *21*(8), 2003–2010. https://doi.org/10.1557/JMR.2006.0243

Oloyede, A., Flachsmann, R., & Broom, N. D. (1992). The dramatic influence of loading velocity on the compressive response of articular cartilage. *Connective Tissue Research*, *27*(4), 211–224. https://doi.org/10.3109/03008209209006997

Park, C. H., Kim, T. H., Haam, S. J., Jeon, I., & Lee, S. (2014). The etiology of pectus carinatum involves overgrowth of costal cartilage and undergrowth of ribs. *Journal of Pediatric Surgery*, *49*(8), 1252–8. https://doi.org/10.1016/j.jpedsurg.2014.02.044

Park, C. H., Kim, T. H., Haam, S. J., & Lee, S. (2013). Does overgrowth of costal cartilage cause pectus carinatum? A three-dimensional computed tomography evaluation of rib length and costal cartilage length in patients with asymmetric pectus carinatum. *Interactive Cardiovascular and Thoracic Surgery*, *17*(1), 757–63. https://doi.org/10.1093/icvts/ivt321

Rejtarová, O., Slízová, D., Smoranc, P., Rejtar, P., & Bukac, J. (2004). Costal cartilages - A clue for determination of sex. *Biomedical Papers of the Medical Faculty of the University Palacky, Olomouc, Czechoslovakia*, *148*(2), 241–243.

Ruan, J., El-Jawahri, R., Chai, L., Barbat, S., & Prasad, P. (2003). Prediction and analysis of human thoracic impact responses and injuries in cadaver impacts using a full human body finite element model. *Stapp Car Crash Journal*, *47*, 299–321.

Sandoz, B., Badina, A., Laporte, S., Lambot, K., Mitton, D., & Skalli, W. (2013). Quantitative geometric analysis of rib, costal cartilage and sternum from childhood to teenagehood. *Medical and Biological Engineering and Computing*, *51*(9), 971–979. https://doi.org/10.1007/s11517-013-1070-5

Shamberger, R., & Welch, K. (1987). Surgical correction of pectus carinatum. *Journal of Pediatric Surgery*, *22*(1), 48–53. https://doi.org/10.1016/S0022-3468(87)80014-3

Sigalet, D. L., Montgomery, M., & Harder, J. (2003). Cardiopulmonary effects of closed repair of pectus excavatum. *Journal of Pediatric Surgery*, *38*(3), 380–385. https://doi.org/10.1053/jpsu.2003.50112

Stephenson, J. T., & Du Bois, J. (2008). Compressive orthotic bracing in the treatment of pectus carinatum: The use of radiographic markers to predict success. *Journal of Pediatric Surgery*, *43*(10), 1776–1780. https://doi.org/10.1016/j.jpedsurg.2008.03.049

Trias, A. (1961). Effect of persistent pressure on the articular cartilage. *The Journal of Bone and*

Joint Surgery, *43 B*(2), 376–386.

Tucker, M. A., Andrew, M. F., Ogle, S. J., & Davison, J. G. (1989). Age-associated change in pain threshold measured by transcutaneous neuronal electrical stimulation. *Age and Ageing*, *18*(4), 241–6. https://doi.org/10.1093/ageing/18.4.241

Van den Hout, J., Van Rhijn, L., Van den Munckhof, R., & Van Ooy, a. (2002). Interface corrective force measurements in Boston brace treatment. *European Spine Journal*, *11*(4), 332–335. https://doi.org/10.1007/s00586-001-0379-1

Welch, K., & Vos, A. (1973). Surgical correction of pectus carinatum (pigeon breast). *Journal of Pediatric Surgery*, *8*(5), 659–667.

Wong, K. E., Gorton, G. E., Tashjian, D. B., Tirabassi, M. V, & Moriarty, K. P. (2014). Evaluation of the treatment of pectus carinatum with compressive orthotic bracing using three dimensional body scans. *Journal of Pediatric Surgery*, *49*(6), 924–7. https://doi.org/10.1016/j.jpedsurg.2014.01.024

Woodrow, K., Friedman, G., Siegelaub, A., & Collen, M. (1972). Pain tolerance: Differences according to age, sex and race. *Psychosomatic …*, *34*(6), 548–556. https://doi.org/10.1097/00006842-197211000-00007

APPENDIX

A. FORCE MEASUREMENT SYSTEM 2

A.1. Purpose

From the sub-studies performed with FM1 (Chapter Three:), the load cell specifications required for the creation of Force Measurement System 2 (FM2) were obtained. In addition, flaws discovered with FM1 were taken into account when creating FM2. To have the ability to calculate protrusion stiffness, an LED sensor (refer to Section 4.4) was incorporated into FM2 to simultaneously measure displacements of the protrusion. The purpose of this sub-study was to develop adapters to implement the load cell into the PCO, calibrate the load cell, and evaluate FM2 and the LED sensor on human participants. FM2 was developed by the study team, and calibration and evaluation was performed by the author of the thesis.

A.2. Construction of Force Measurement System 2

Measuring forces with FM2 involved a single uni-axial, compressive load cell (TE Connectivity Ltd® FX1901, 0-25 lbs [Figure A-1]) that was positioned between the pad and aluminum bar of the PCO using two custom made aluminum adapters.

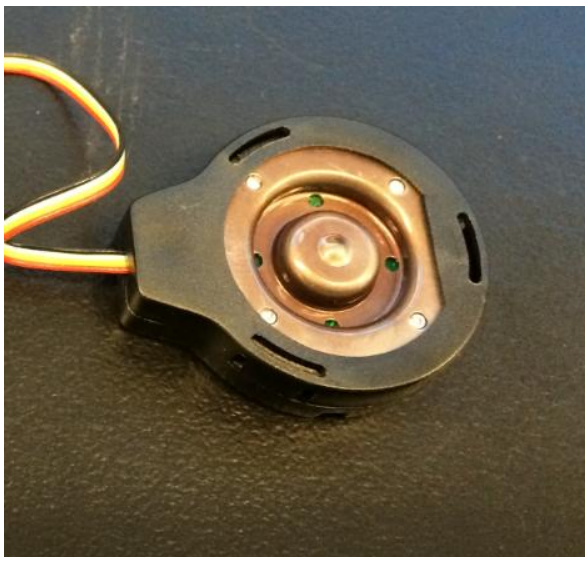

Figure A-1 - Load cell used for Force Measurement System 2.

The first adapter (A1) was designed to insert into the load cell and provide a surface to screw the load cell into the aluminum bar via two threaded holes (Figure A-2). The second adapter (A2) was a flat, square inch surface containing a threaded hole in the center for a screw to insert. The flat surface was the second attachment site for the load cell, while the threaded hole was the attachment site for the pad (Figure A-3). The load cell was adhered onto both adapters with a steel reinforced epoxy (J-B Weld®) to create a single unit (Figure A-4).

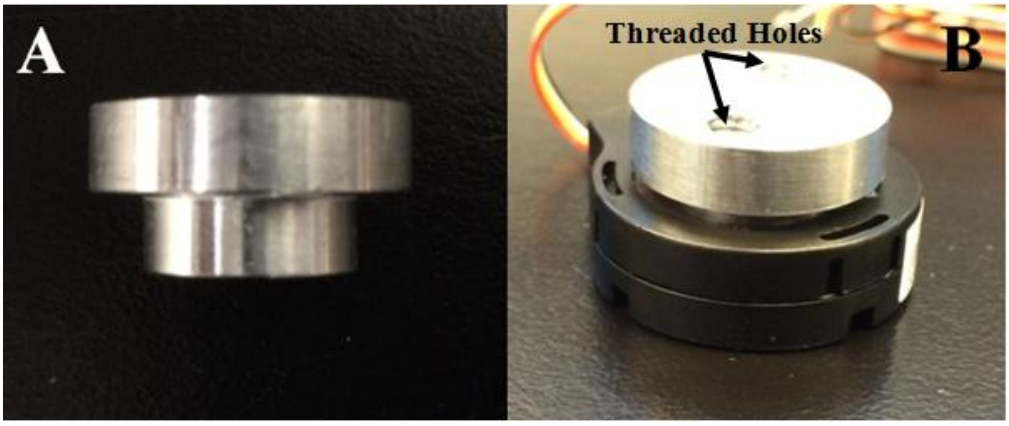

Figure A-2 - A) Adapter 1 and B) A1 slotted into the load cell to allow full surface area contact. The threaded holes can be seen that allowed attachment to the aluminum bar of the PCO.

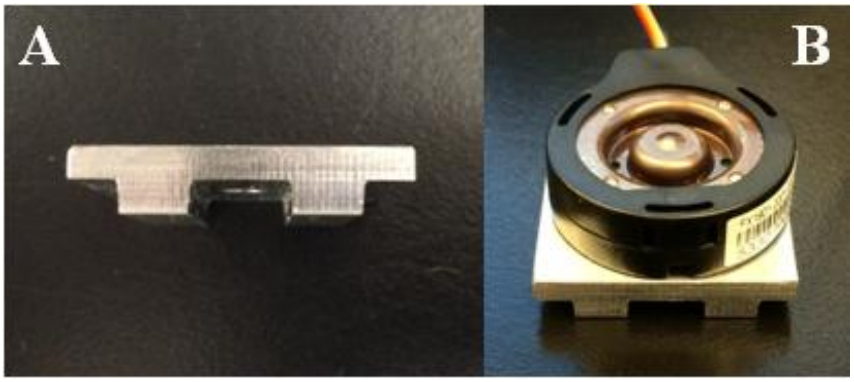

Figure A-3 - A) Adapter 2 and B) The load cell placed onto A2 to act as a flat surface on the curved pad of the PCO.

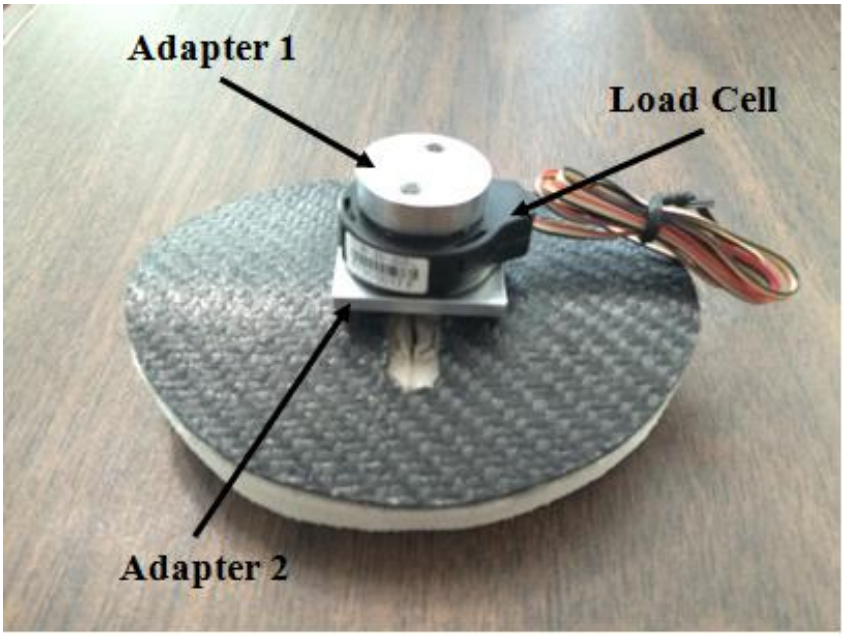

Figure A-4 – The full assembly of FM2 on the pad of the PCO. Both adapters were adhered to the load cell with epoxy to create a single unit.

A.3. Calibration of FM2

A calibration of FM2 was completed to obtain a relationship between the voltage outputs of the load cell and the magnitude of force (in lbs) while within the PCO. Before performing the calibration, a PC simulation was conducted using a scale (MyWeigh© Ultraship R1 80) to ensure applied forces were known. The fabricated protrusion to mimic PC was a dental plaster copy of the mould used to construct the pad of the PCO. This allowed the pad of the PCO to have full surface area contact during calibration. The mould was attached to the scale with double sided tape and rotated orthogonally to the table surface (Figure A-5). The PCO, containing FM2, was then aligned with the mould on the scale. Specific force increments could not be obtained due to the nature of the PCO. Unfortunately, tightening of the PCO was unreliable and force magnitudes could alter with different trials. Therefore, forces were incrementally increased until an approximate force of 20 lbs was achieved. A total of 14 trials were performed to obtain

several data points that could thoroughly cover the PCO outputs between 0 and 20 lbs. During each trial, data was collected (3 s, 100 Hz) at each force increment using a custom made GUI (National Instruments® LabVIEW). Data at each force increment was averaged. All data points from every trial were plotted onto a scatter plot to obtain a line of best fit with the largest R^2 value. The equation of this line was used to convert the voltage outputs of the load cell into a pound force. This equation was evaluated by placing the PCO onto the calibration system and tightening the PCO to a random magnitude for ten trials. Afterwards, the differences between the observed and calculated values were calculated.

Figure A-5 - Moulding of the template used to produce the pad of the PCO attached to the scale. The mould allowed full surface area contact of the pad when tightening the PCO.

A.3.1. Results of the Load Cell Calibration

Calibration of the load cell produced a quadratic function with $R^2 = 0.92$ (Figure A-6). When evaluating the equation, differences between the observed and calculated PCO forces ranged from 0.56 – 3.51 lbs, with an average difference of 2.18 lbs (0.89) (Table A-1).

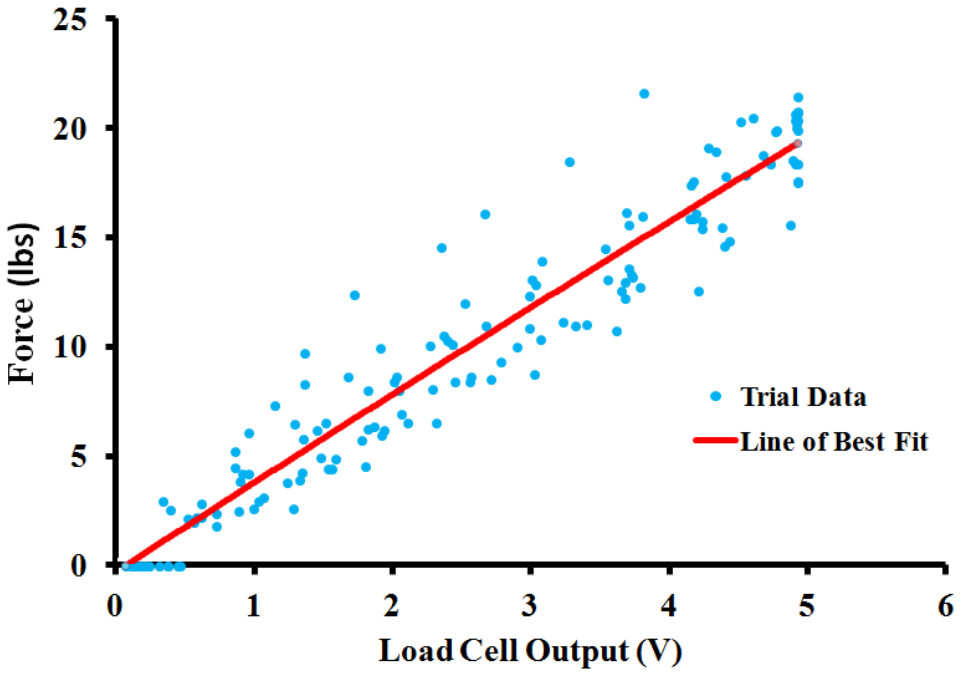

Figure A-6 - Calibration curve of Force Measurement System 2. The red line represents the quadratic equation used to convert voltage outputs to pounds ($R^2 = 0.92$).

Table A-1 - The difference between the observed and calculated outputs when testing the conversion equation of FM2.

Trial	Observed Force (lbs)	Calculated Force (lbs)	Absolute Difference (lbs)
1	6.70	4.58	2.12
2	3.59	5.44	1.85
3	11.82	10.33	1.49
4	2.41	3.87	1.46
5	5.46	8.97	3.51
6	5.58	3.51	2.07
7	18.40	14.89	3.51
8	5.26	4.70	0.56
9	1.98	5.00	3.02
10	5.10	7.31	2.21
		Average (SD)	2.18 (0.89)

A.3.2. Discussion of the Load Cell Calibration

The calibration of FM2 was regarded as acceptable considering the unpredictable environment of the padded PCO. When evaluating the conversion equation for FM2, the differences found between the observed and calculated values were speculated to be from the random placements of the PCO pad on the moulding. When tightening the PCO, the pad may be placed in a different position, thus altering the overall alignment of the PCO. The contact conditions between the mould and PCO would cause the force transfer to the load cell to differ in direction. This limiting factor could not be controlled and was therefore deemed suitable for the study.

A.4. Evaluating Force Measurement System 2

A.4.1. Study Participants

Four male participants diagnosed with PC had been recruited for this pilot study. Participants could be at any stage of treatment with the PCO. All participants provided informed consent to participate in the study.

A.4.2. Methods

The participants first underwent their regular fitting/follow-up appointment with the clinician. Therefore, if the PCO was not fitting properly, or if it was damaged, the clinician could resolve these issues before data collection. When the appointment was completed, the participant's pad was substituted for the instrumented pad (FM2). Afterwards, the participant was positioned standing against a wall with their heels and back touching the wall, in a posture called the neutral position. A calibrated LED sensor (as found in Section 4.4) was attached to a wooden board and placed in line with the center of the pad approximately 4-6 cm away. This ensured the LED sensor would measure distances within the descending limb. With the aid of levels on the tripod, the board was adjusted to align the LED sensor perpendicularly to the pad. The participant was then instructed to tighten the PCO to their comfortable level (PF). The PF and displacement were acquired simultaneously (20 s, 100 Hz) while the PCO was tightened by the participant. The length of data acquisition was 20 s to guarantee that the participant could tighten the PCO to the PF. Therefore, once the participant completed tightening the PCO, the remainder of time consisted of the participant standing in neutral position. After data acquisition, the PCO was loosened to begin a new trial. A total of four trials were performed. Force and displacement data were plotted for qualitative analysis to determine if FM2 could detect increases in PCO forces, and if the LED sensor could detect the displacement of the protrusion as the PCO was tightened.

A.4.3. Results

When tightening the PCO, force data had the tendency to return to the original magnitude (when the PCO was not tightened) with most trials. There were little or no signs of the PF increasing while the PCO was tightened (Figure A-7). The displacement of the protrusion, measured by the LED sensor, increased during tightening of the PCO, with the exception of Participant 4 (Figure A-8). Fluctuations in the both the force and displacement data were noticed while tightening the PCO.

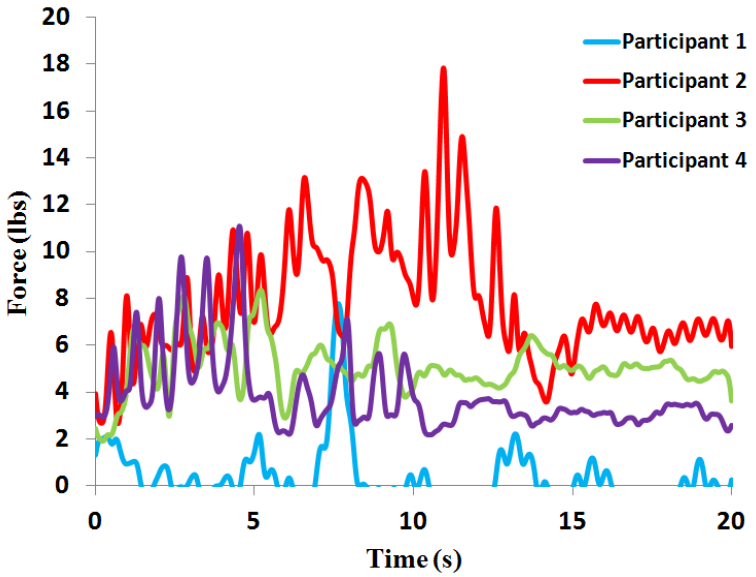

Figure A-7 - Forces from all participants when tightening the PCO. There was little or no increase in force magnitude when compared to the PCO forces before tightening.

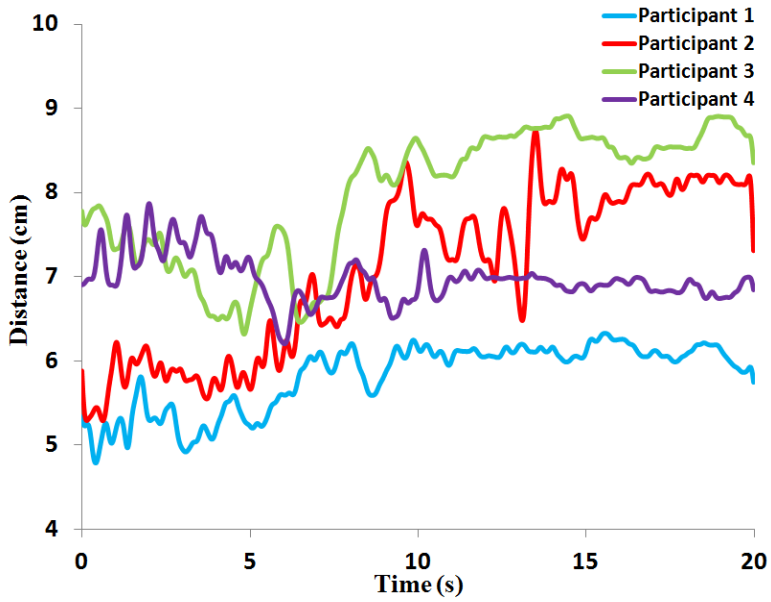

Figure A-8 - Distance of the reflective surface during tightening of the PCO, representing the displacement of the protrusion.

A.4.4. Discussion

FM2 clearly shows signs of error when applied to a human participant. The data illustrates the inability of FM2 to properly measure an increase in the PF while the PCO is tightened. The cause of this was believed to originate from tensile forces being applied to the sensor due to rotational movements of the pad. These tensile forces would mitigate any compressive forces that simultaneously occurred when tightening the PCO. Recalling the design of FM2, the load cell was adhered to both aluminum adapters (A1 and A2). It was speculated that if the pad was exposed to a large moment (i.e. the primary force application was closer to the edge of the pad) A1 - embedded between the aluminum bar and load cell - may rotate in a manner that pulls on the load cell instead of pushing. To resolve this issue, a force measurement system with four load cells was considered. Separating the four load cells into each corner of the pad would allow them to distribute the forces among themselves, as they provide a larger base for the applied forces. If

any applied forces occurred along the perimeter of the pad (producing a moment), the load cells along that perimeter could detect the compressive forces while the others would have little or no contribution to the final output.

The LED sensor appeared to detect the displacement of the protrusion as the PCO was tightened. One participant was seen to show no displacement. This may have simply been due to the protrusion not displacing during tightening. There were no reported issues with the current setup of the LED sensor, and therefore no changes were needed.

Lastly, fluctuations in the both the force and displacement data were observed. This was potentially due to the PCO rebounding while being tightened. Additionally, any breathing from the participant will expand and retract the chest wall. This will alter the tightness of the PCO and the displacement of the protrusion.

B. COPYRIGHT PERMISSIONS

ELSEVIER LICENSE
TERMS AND CONDITIONS
May 30, 2017

This Agreement between Tomasz Bugajski ("You") and Elsevier ("Elsevier") consists of your license details and the terms and conditions provided by Elsevier and Copyright Clearance Center.

License Number	4092700295761
License date	Apr 19, 2017
Licensed Content Publisher	Elsevier
Licensed Content Publication	Thoracic Surgery Clinics
Licensed Content Title	The Anatomy of the Ribs and the Sternum and Their Relationship to Chest Wall Structure and Function
Licensed Content Author	Geoffrey M. Graeber,Muhammad Nazim
Licensed Content Date	Nov 1, 2007
Licensed Content Volume	17
Licensed Content Issue	4
Licensed Content Pages	17
Start Page	473
End Page	489
Type of Use	reuse in a thesis/dissertation
Portion	figures/tables/illustrations
Number of figures/tables/illustrations	1
Format	electronic
Are you the author of this Elsevier article?	No
Will you be translating?	No
Order reference number	
Original figure numbers	Figure 6
Title of your thesis/dissertation	Dynamic Bracing of Pectus Carinatum: A Quantitative Analysis
Expected completion date	May 2017
Estimated size (number of pages)	100
Elsevier VAT number	GB 494 6272 12

Requestor Location

Total 0.00 CAD

Terms and Conditions

INTRODUCTION

1. The publisher for this copyrighted material is Elsevier. By clicking "accept" in connection with completing this licensing transaction, you agree that the following terms and conditions apply to this transaction (along with the Billing and Payment terms and conditions established by Copyright Clearance Center, Inc. ("CCC"), at the time that you opened your Rightslink account and that are available at any time at http://myaccount.copyright.com).

GENERAL TERMS

2. Elsevier hereby grants you permission to reproduce the aforementioned material subject to the terms and conditions indicated.

3. Acknowledgement: If any part of the material to be used (for example, figures) has appeared in our publication with credit or acknowledgement to another source, permission must also be sought from that source. If such permission is not obtained then that material may not be included in your publication/copies. Suitable acknowledgement to the source must be made, either as a footnote or in a reference list at the end of your publication, as follows:

"Reprinted from Publication title, Vol /edition number, Author(s), Title of article / title of chapter, Pages No., Copyright (Year), with permission from Elsevier [OR APPLICABLE SOCIETY COPYRIGHT OWNER]." Also Lancet special credit - "Reprinted from The Lancet, Vol. number, Author(s), Title of article, Pages No., Copyright (Year), with permission from Elsevier."

4. Reproduction of this material is confined to the purpose and/or media for which permission is hereby given.

5. Altering/Modifying Material: Not Permitted. However figures and illustrations may be altered/adapted minimally to serve your work. Any other abbreviations, additions, deletions and/or any other alterations shall be made only with prior written authorization of Elsevier Ltd. (Please contact Elsevier at permissions@elsevier.com). No modifications can be made to any Lancet figures/tables and they must be reproduced in full.

6. If the permission fee for the requested use of our material is waived in this instance, please be advised that your future requests for Elsevier materials may attract a fee.

7. Reservation of Rights: Publisher reserves all rights not specifically granted in the combination of (i) the license details provided by you and accepted in the course of this licensing transaction, (ii) these terms and conditions and (iii) CCC's Billing and Payment terms and conditions.

8. License Contingent Upon Payment: While you may exercise the rights licensed immediately upon issuance of the license at the end of the licensing process for the transaction, provided that you have disclosed complete and accurate details of your proposed use, no license is finally effective unless and until full payment is received from you (either by publisher or by CCC) as provided in CCC's Billing and Payment terms and conditions. If full payment is not received on a timely basis, then any license preliminarily granted shall be deemed automatically revoked and shall be void as if never granted. Further, in the event that you breach any of these terms and conditions or any of CCC's Billing and Payment terms and conditions, the license is automatically revoked and shall be void as if never granted. Use of materials as described in a revoked license, as well as any use of the materials beyond the scope of an unrevoked license, may constitute copyright infringement and publisher reserves the right to take any and all action to protect its copyright in the materials.

9. Warranties: Publisher makes no representations or warranties with respect to the licensed material.

10. Indemnity: You hereby indemnify and agree to hold harmless publisher and CCC, and their respective officers, directors, employees and agents, from and against any and all claims arising out of your use of the licensed material other than as specifically authorized pursuant to this license.

11. No Transfer of License: This license is personal to you and may not be sublicensed, assigned, or transferred by you to any other person without publisher's written permission.

12. No Amendment Except in Writing: This license may not be amended except in a writing signed by both parties (or, in the case of publisher, by CCC on publisher's behalf).

13. Objection to Contrary Terms: Publisher hereby objects to any terms contained in any purchase order, acknowledgment, check endorsement or other writing prepared by you, which terms are inconsistent with these terms and conditions or CCC's Billing and Payment terms and conditions. These terms and conditions, together with CCC's Billing and Payment terms and conditions (which are incorporated herein), comprise the entire agreement between you and publisher (and CCC) concerning this licensing transaction. In the event of any conflict between your obligations established by these terms and conditions and those established by CCC's Billing and Payment terms and conditions, these terms and conditions shall control.

14. Revocation: Elsevier or Copyright Clearance Center may deny the permissions described in this License at their sole discretion, for any reason or no reason, with a full refund payable to you. Notice of such denial will be made using the contact information

provided by you. Failure to receive such notice will not alter or invalidate the denial. In no event will Elsevier or Copyright Clearance Center be responsible or liable for any costs, expenses or damage incurred by you as a result of a denial of your permission request, other than a refund of the amount(s) paid by you to Elsevier and/or Copyright Clearance Center for denied permissions.

LIMITED LICENSE

The following terms and conditions apply only to specific license types:

15. **Translation**: This permission is granted for non-exclusive world **English** rights only unless your license was granted for translation rights. If you licensed translation rights you may only translate this content into the languages you requested. A professional translator must perform all translations and reproduce the content word for word preserving the integrity of the article.

16. **Posting licensed content on any Website**: The following terms and conditions apply as follows: Licensing material from an Elsevier journal: All content posted to the web site must maintain the copyright information line on the bottom of each image; A hyper-text must be included to the Homepage of the journal from which you are licensing at http://www.sciencedirect.com/science/journal/xxxxx or the Elsevier homepage for books at http://www.elsevier.com; Central Storage: This license does not include permission for a scanned version of the material to be stored in a central repository such as that provided by Heron/XanEdu.

Licensing material from an Elsevier book: A hyper-text link must be included to the Elsevier homepage at http://www.elsevier.com . All content posted to the web site must maintain the copyright information line on the bottom of each image.

Posting licensed content on Electronic reserve: In addition to the above the following clauses are applicable: The web site must be password-protected and made available only to bona fide students registered on a relevant course. This permission is granted for 1 year only. You may obtain a new license for future website posting.

17. **For journal authors:** the following clauses are applicable in addition to the above:

Preprints:

A preprint is an author's own write-up of research results and analysis, it has not been peer-reviewed, nor has it had any other value added to it by a publisher (such as formatting, copyright, technical enhancement etc.).

Authors can share their preprints anywhere at any time. Preprints should not be added to or enhanced in any way in order to appear more like, or to substitute for, the final versions of articles however authors can update their preprints on arXiv or RePEc with their Accepted

Author Manuscript (see below).

If accepted for publication, we encourage authors to link from the preprint to their formal publication via its DOI. Millions of researchers have access to the formal publications on ScienceDirect, and so links will help users to find, access, cite and use the best available version. Please note that Cell Press, The Lancet and some society-owned have different preprint policies. Information on these policies is available on the journal homepage.

Accepted Author Manuscripts: An accepted author manuscript is the manuscript of an article that has been accepted for publication and which typically includes author-incorporated changes suggested during submission, peer review and editor-author communications.

Authors can share their accepted author manuscript:

- immediately
    - via their non-commercial person homepage or blog
    - by updating a preprint in arXiv or RePEc with the accepted manuscript
    - via their research institute or institutional repository for internal institutional uses or as part of an invitation-only research collaboration work-group
    - directly by providing copies to their students or to research collaborators for their personal use
    - for private scholarly sharing as part of an invitation-only work group on commercial sites with which Elsevier has an agreement
- After the embargo period
    - via non-commercial hosting platforms such as their institutional repository
    - via commercial sites with which Elsevier has an agreement

In all cases accepted manuscripts should:

- link to the formal publication via its DOI
- bear a CC-BY-NC-ND license - this is easy to do
- if aggregated with other manuscripts, for example in a repository or other site, be shared in alignment with our hosting policy not be added to or enhanced in any way to appear more like, or to substitute for, the published journal article.

Published journal article (JPA): A published journal article (PJA) is the definitive final record of published research that appears or will appear in the journal and embodies all value-adding publishing activities including peer review co-ordination, copy-editing, formatting, (if relevant) pagination and online enrichment.

Policies for sharing publishing journal articles differ for subscription and gold open access articles:

Subscription Articles: If you are an author, please share a link to your article rather than the full-text. Millions of researchers have access to the formal publications on

ScienceDirect, and so links will help your users to find, access, cite, and use the best available version.

Theses and dissertations which contain embedded PJAs as part of the formal submission can be posted publicly by the awarding institution with DOI links back to the formal publications on ScienceDirect.

If you are affiliated with a library that subscribes to ScienceDirect you have additional private sharing rights for others' research accessed under that agreement. This includes use for classroom teaching and internal training at the institution (including use in course packs and courseware programs), and inclusion of the article for grant funding purposes.

Gold Open Access Articles: May be shared according to the author-selected end-user license and should contain a CrossMark logo, the end user license, and a DOI link to the formal publication on ScienceDirect.

Please refer to Elsevier's posting policy for further information.

18. **For book authors** the following clauses are applicable in addition to the above: Authors are permitted to place a brief summary of their work online only. You are not allowed to download and post the published electronic version of your chapter, nor may you scan the printed edition to create an electronic version. **Posting to a repository:** Authors are permitted to post a summary of their chapter only in their institution's repository.

19. **Thesis/Dissertation**: If your license is for use in a thesis/dissertation your thesis may be submitted to your institution in either print or electronic form. Should your thesis be published commercially, please reapply for permission. These requirements include permission for the Library and Archives of Canada to supply single copies, on demand, of the complete thesis and include permission for Proquest/UMI to supply single copies, on demand, of the complete thesis. Should your thesis be published commercially, please reapply for permission. Theses and dissertations which contain embedded PJAs as part of the formal submission can be posted publicly by the awarding institution with DOI links back to the formal publications on ScienceDirect.

Elsevier Open Access Terms and Conditions

You can publish open access with Elsevier in hundreds of open access journals or in nearly 2000 established subscription journals that support open access publishing. Permitted third party re-use of these open access articles is defined by the author's choice of Creative Commons user license. See our open access license policy for more information.

Terms & Conditions applicable to all Open Access articles published with Elsevier:

Posting or linking by commercial companies for use by customers of those companies.